

**PARAMETRIC INVESTIGATION AND OFF-DESIGN  
SIMULATION OF LOW TEMPERATURE ORGANIC RANKINE  
CYCLE FOR RESIDENTIAL APPLICATIONS**

*Thesis*

*Submitted in partial fulfilment of the requirements for the Degree of*

**DOCTOR OF PHILOSOPHY**

By

**SUHAS UPADHYAYA**

**(155036 ME15F12)**



DEPARTMENT OF MECHANICAL ENGINEERING  
NATIONAL INSTITUTE OF TECHNOLOGY KARNATAKA,  
SURATHKAL, MANGALORE-575025

May 2021

**PARAMETRIC INVESTIGATION AND OFF-DESIGN  
SIMULATION OF LOW TEMPERATURE ORGANIC RANKINE  
CYCLE FOR RESIDENTIAL APPLICATIONS**

*Thesis*

*Submitted in partial fulfillment of the requirements for the Degree of*

**DOCTOR OF PHILOSOPHY**

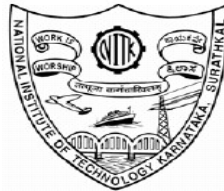
By

**SUHAS UPADHYAYA  
(155036 ME15F12)**

Under the Guidance of

**Dr. VEERSHETTY GUMTAPURE**

Associate Professor



DEPARTMENT MECHANICAL ENGINEERING  
NATIONAL INSTITUTE OF TECHNOLOGY KARNATAKA,  
SURATHKAL, MANGALORE -575025

May 2021

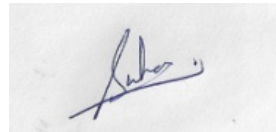
## DECLARATION

I hereby declare that the Research Thesis entitled “**PARAMETRIC INVESTIGATION AND OFF-DESIGN SIMULATION OF LOW TEMPERATURE ORGANIC RANKINE CYCLE FOR RESIDENTIAL APPLICATIONS**” which is being submitted to the **National Institute of Technology Karnataka, Surathkal** in partial fulfilment of the requirements for the award of the Degree of **Doctor of Philosophy in Mechanical Engineering** is a *bonafide report of the research work carried out by me*. The material contained in this Research Thesis has not been submitted to any other Universities or Institutes for the award of any degree.

Register Number: **155036 ME15F12**

Name of the Research Scholar: **SUHAS UPADHYAYA**

Signature of the Research Scholar:

A rectangular box containing a handwritten signature in blue ink. The signature appears to be 'Suhas' followed by a flourish.

Department of Mechanical Engineering

Place: NITK, Surathkal

Date: 07/06/2021

## **C E R T I F I C A T E**

This is to certify that the Research Thesis entitled “**PARAMETRIC INVESTIGATION AND OFF-DESIGN SIMULATION OF LOW TEMPERATURE ORGANIC RANKINE CYCLE FOR RESIDENTIAL APPLICATIONS**” submitted by **Mr. SUHAS UPADHYAYA (Register Number: 155036 ME15F12)** as the record of the research work carried out by him, *is accepted as the Research Thesis submission* in partial fulfilment of the requirements for the award of the degree of **Doctor of Philosophy**.

**Research Guide**

**Dr. Veershetty Gumtapure**

**Associate Professor**

**Department of Mechanical Engineering,**

**NITK Surathkal**

**Chairman-DRPC**

**Date:**

## **ACKNOWLEDGEMENT**

I would like to extend my gratitude to Dr. Veershetty Gumtapure, Associate Professor, Mechanical Engineering, National Institute of Technology Karnataka (NITK), Surathkal who has been a great pillar of support and strength. I would like to thank him for his guidance and encouragement throughout my research work.

I would like to thank my Research Progress Assessment Committee members Dr. Anish S and Dr. Nagendrappa H, for their valuable inputs and suggestions.

I would like to thank Prof. Shrikantha. S. Rao, Head of the Mechanical Engineering and all the members of faculty, Mechanical Engineering, NITK for their support throughout this research work.

I would also like to thank all my friends and fellow research scholars whose support helped me to complete this thesis.

Last but not least, this would not have been possible without constant encouragement of my family and my colleagues at GMR Energy for pursuing higher studies. I would like to thank them for their love and support.

## ABSTRACT

The energy demand across the world is increasing rapidly as a result of massive urbanization and industrialization. This is coupled with scarcity of traditional energy sources and severe environmental issues such as global warming and climate change. In order to counter this problem, there is a sense of urgency to explore alternative sources of energy. In this regard, harnessing the renewable energies and waste heat recovery are considered as potential solutions that can effectively address these issues. The organic Rankine cycle is proved to be reliable technology that can efficiently convert these low to medium-grade heat sources into useful power.

The ORC power block consists of a pump which is used for pumping the working fluid to the desired pressure. This pressurized fluid is then passed on to the evaporator where heat addition takes place. The pressurized vapor passes through the expander, where the actual expansion of the working fluid takes place and the pressure drops. Finally, the vapor condenses in the condenser to complete the cycle. In ORC systems, the enthalpy drop across the expanders is less. Net work output per unit mass of the working fluid is small in ORC plants. In order to achieve higher power output (greater than  $10 \text{ kW}_e$ ), mass flow rate of working fluids has to increase. This will increase the size and cost of the ORC system. Therefore, it is reasonable to adopt small capacity ORC systems ( $1\text{-}5 \text{ kW}_e$ ).

The present study focussed in detail the overall system performance in terms of thermal and exergy efficiencies. Moreover, major components constituting the ORC system such as evaporator and expander are assessed. A thermodynamic model for ORC system was developed based on laws of mass and energy conservation. Using this model, ORC thermal and exergy efficiencies were evaluated for four different working fluids; R245fa, R123, Isobutane and R134a. Sensitivity analysis was performed using key thermodynamic parameters including expander inlet temperature, expander inlet pressure, condensation temperature and pinch point temperature difference (PPTD) to study its effect on net work output, mass flow rate, thermal and exergy efficiencies. Optimization of the system was also performed using genetic algorithm. The system was optimized to maximize cycle exergy efficiency. Parametric analysis was carried out to investigate the impact of evaporator pressure, condensation pressure, superheat, dead state temperature and PPTD on the system performance. Thermo-hydraulic model of plate heat

exchanger evaporator was used to study the effect of evaporator pressure, PPTD and superheat on evaporator area. The effect of expansion ratio, shaft speed and expander inlet temperature on mass flow rate, work output and efficiency of open-drive scroll expander was studied using validated semi-empirical model. Finally, cost analysis and exergoeconomic optimization of 1 kW<sub>e</sub> driven solar ORC system was performed to compare the cost of solar ORC with solar PV in India and to determine the minimum cost of electricity respectively.

Optimization results showed that the highest thermal efficiency (7.1%) and exergy efficiency (45.53%) at lowest expander inlet pressure (3.66 bar) was attained with R123. This was followed by R245fa with thermal efficiency of 7.04% and exergy efficiency of 44.98% at expander inlet pressure of 6.07 bar. R245fa was preferred for this study as it is a zero ODP fluid and also has a lower specific volume compared to R123. Sensitivity analysis showed that, expander inlet pressure showed the highest degree of sensitiveness for all working fluids. Detailed exergy analysis of ORC components was performed to identify the location and to assess the magnitude of exergy losses occurring within the ORC system. Exergy analysis of 1 kW<sub>e</sub> ORC system showed that, evaporator accounted for the maximum exergy loss. 41% of the total exergy loss occurred in the evaporator. It was also observed that evaporator pressure had significant effect on both energy and exergy efficiencies of the ORC. Significant reduction in evaporator area (75.87%) and cost (63.59%) was observed when evaporator pressure was increased from 4 to 10 bar. Heat exchanger area decreased by 89.65% and evaporator cost was reduced by 74.86% when PPTD was increased from 2 to 14 °C. It was also observed from the model that the cost increases whereas the pressure drop decreases with increase in plate width and plate spacing. The trade off point for plate width was at 0.0065 m, where the evaporator cost was found to be 1166 USD (Rs 87,450) and frictional pressure drop was 2.03 kPa. In case of plate spacing, it was at 0.003 m, where the evaporator cost was 1210 USD (Rs 90,750) and frictional pressure drop was 1.27 kPa. Parametric investigation of scroll expander showed that the scroll expander should be operated in a range close to its adapted expansion ratio to achieve maximum efficiency. It was also revealed that increasing expander inlet temperature led to increase in thermal energy dissipation. This leads to the deterioration in efficiency of the expander. The economic analysis showed that the capital cost of small scale ORC systems is very high (Rs 7,42,500) compared to equivalent solar PV system (Rs 85,000) in India. Exergoeconomic optimization showed that minimum electricity cost of 3.9 Rs/kWh could be attained at maximum evaporator pressure of 13.9 bar.

**Keywords:** *Organic Rankine cycle (ORC), Energy and Exergy analysis, Plate heat exchanger, scroll expander, Semi-empirical model, Exergoeconomic analysis*



## TABLE OF CONTENTS

<b>ABSTRACT</b>	<b>I</b>
<b>TABLE OF CONTENTS</b>	<b>IV</b>
<b>LIST OF TABLES</b>	<b>XII</b>
<b>NOMENCLATURE</b>	<b>XIII</b>
<b>CHAPTER 1</b>	<b>1</b>
<b>INTRODUCTION</b>	<b>1</b>
1.1 Need for alternative source of energy .....	1
1.2 Available energy conversion technologies for DPG systems .....	5
1.2.1 Kalina cycle .....	5
1.2.2 Supercritical CO <sub>2</sub> Brayton cycle .....	6
1.2.3 Organic Rankine cycle .....	7
1.3 Selection of ORC working fluid .....	10
1.4 Expansion device .....	14
1.4.1 Scroll expanders .....	15
1.4.2 Screw expanders .....	16
1.4.3 Reciprocating piston expanders .....	17
1.4.4 Rotary vane expander .....	18
1.4.5 Turbo-expanders (axial flow and radial inflow turbines) .....	18
1.5 Various configurations of ORC systems .....	19
1.5.1 Biomass combined heat and power (CHP) .....	19
1.5.2 Solar power cycles .....	20
1.5.3 Geothermal .....	21
1.5.4 Waste heat recovery .....	21

1.6 Organization of the thesis .....	22
<b>CHAPTER 2</b>	<b>24</b>
<b>LITERATURE REVIEW</b>	<b>24</b>
2.1 Exergy analysis of ORC systems .....	24
2.2 Optimization of ORC systems .....	29
2.3 Review of components in ORC system .....	35
2.3.1 Evaporator .....	35
2.3.2 Expander.....	38
2.4 Research objectives.....	40
2.5 Motive and scope of the present work .....	41
2.6 Methodology .....	42
<b>CHAPTER 3</b>	<b>44</b>
<b>ENERGY AND EXERGY ANALYSIS OF MICRO ORGANIC RANKINE CYCLE SYSTEM</b>	<b>44</b>
3.1 System description .....	46
3.2 Thermodynamic model of ORC system.....	47
3.3 Parametric analysis .....	50
3.3.1 Expander inlet temperature .....	50
3.3.2 Expander inlet pressure .....	53
3.3.3 Effect of Pinch point temperature difference .....	56
3.3.4 Effect of condensation temperature.....	59
3.4 Sensitivities of system parameters .....	62
3.5 Genetic Algorithm optimization for selection of working fluid .....	65
3.6 Exergy analysis of ORC system.....	68

3.7 Effect of key thermodynamic parameters on cycle exergy efficiency and rate of exergy destruction.....	74
3.7.1 Effect of evaporation pressure.....	75
3.7.2 Effect of superheating .....	76
3.7.3 Effect of condenser pressure .....	77
3.7.4 Effect of dead state temperature.....	79
3.7.5 Effect of evaporator pinch point temperature difference (PPTD).....	81
3.8 Chapter closure .....	82
<b>CHAPTER 4</b>	<b>84</b>
<b>PARAMETRIC STUDY OF PLATE HEAT EXCHANGER EVAPORATOR FOR ORGANIC RANKINE CYCLE SYSTEMS</b>	<b>84</b>
4.1 Plate heat exchanger design .....	85
4.2 Evaporator sub-model.....	87
4.2.1 Single phase.....	87
4.2.2 Two phase.....	88
4.3 Effect of thermodynamic parameters on evaporator area and cost.....	91
4.3.1 Evaporator pressure.....	91
4.3.2 Pinch point temperature difference .....	94
4.3.3 Expander inlet temperature .....	96
4.4 Effect of geometrical parameters on pressure drop and evaporator cost .....	98
4.5 Chapter closure .....	99
<b>CHAPTER 5</b>	<b>100</b>
<b>PARAMETRIC INVESTIGATION OF OPEN-DRIVE SCROLL EXPANDER FOR ORGANIC RANKINE CYCLE SYSTEMS</b>	<b>100</b>
5.1 Semi-empirical model description .....	100

5.2 Parametric analysis .....	107
5.2.1 Effect of expansion ratio .....	107
5.2.2 Effect of shaft speed.....	110
5.2.3 Effect of inlet temperature.....	113
5.3 Chapter closure .....	115
<b>CHAPTER 6</b>	<b>116</b>
<b>COST ANALYSIS AND EXERGO-ECONOMIC OPTIMIZATION OF SOLAR DRIVEN ORGANIC RANKINE CYCLE SYSTEM</b>	<b>116</b>
6.1 Economic analysis of solar ORC system .....	116
6.1.1 Exergoeconomic optimization of 1 kW <sub>e</sub> ORC system .....	118
6.2 Chapter closure .....	123
<b>CHAPTER 7</b>	<b>124</b>
<b>CONCLUSIONS AND SCOPE OF FUTURE WORK</b>	<b>124</b>
7.1 Conclusions.....	124
7.2 Scope of future work.....	127
<b>REFERENCES</b>	<b>128</b>
<b>APPENDIX A</b>	<b>139</b>
MATHEMATICAL MODELLING CODE.....	139
A.1 Mathematical code to calculate energy and exergy efficiency of the ORC cycle using R245fa as the working fluid .....	139
A.2 Mathematical code of plate heat exchanger evaporator to estimate the surface area of the heat exchanger using Han Lee Kim correlations.....	143
A.3 Mathematical code for semi-empirical model of open-drive scroll expander.....	155
A.4 Mathematical code for exergoeconomic optimization of solar driven ORC system .....	159

<b>LIST OF PUBLICATIONS</b>	<b>165</b>
<b>BIODATA</b>	<b>166</b>

## LIST OF FIGURES

Figure 1.1: Data showing the share of each energy production technology in world energy consumption (OECD/IEA 2019) .....	1
Figure 1.2: Schematic diagram of the Kalina cycle process (Ogriseck 2009).....	5
Figure 1.3: Schematic diagram of closed cycle brayton cycle .....	6
Figure 1.4: Schematic diagram of ORC power block.....	7
Figure 1.5: Various configurations and technologies available in organic Rankine cycle....	8
Figure 1.6: Schematic diagram of ORC cycle (a) Basic (b) with recuperator.....	9
Figure 1.7: T-s diagram of wet, dry and isentropic fluids .....	11
Figure 1.8: (a) Moving scroll (b) Fixed scroll (Wu et al. 2015).....	15
Figure 1.9: Diagram of mode of operation of the scroll expander (Quoilin et al. 2013).....	15
Figure 1.10: Diagram of a single screw expander (Shen et al. 2018).....	16
Figure 1.11: Diagram of a twin screw expander (Papes et al. 2015).....	17
Figure 1.12: Schematic diagram of reciprocating type piston expander (Oudkerk et al. 2015) .....	17
Figure 1.13: Vane-type air motor used as an expander (Qiu et al. 2011).....	18
Figure 1.14: 3D geometry of (a) Axial turbine (b) Radial turbine (Alshammari et al. 2018) .....	19
Figure 1.15: (a) Biomass fired ORC based cooling heating and power (CHP) system (b) T-s diagram of the CHP system (Qiu et al. 2012).....	20
Figure 1.16: Schematic diagram of compound parabolic collector (CPC) driven ORC system (Wang et al. 2014) .....	21
Figure 1.17: Schematic representation of a geothermal ORC system (Quoilin et al. 2013)	22
Figure 2.1: Research methodology of the present study.....	43
Figure 3.1: Schematic demonstration of a low temperature ORC system.....	46
Figure 3.2: Temperature-entropy (T-s) diagram of R245fa.....	47
Figure 3.3: Effect of expander inlet temperature on net work output.....	51
Figure 3.4: Effect of expander inlet temperature on working fluid mass flow rate.....	51
Figure 3.5: Effect of expander inlet temperature on enthalpy difference across the expander .....	52
Figure 3.6: Effect of expander inlet temperature on thermal efficiency.....	52

Figure 3.7: Effect of expander inlet temperature on exergy efficiency .....	53
Figure 3.8: Effect of expander inlet pressure on net work output .....	54
Figure 3.9: Effect of expander inlet pressure on working fluid mass flow rate .....	54
Figure 3.10: Effect of expander inlet pressure on enthalpy difference across the expander	55
Figure 3.11: Effect of expander inlet pressure on thermal efficiency .....	55
Figure 3.12: Effect of expander inlet pressure on exergy efficiency.....	56
Figure 3.13: Effect of pinch point temperature difference on net work output.....	57
Figure 3.14: Effect of pinch point temperature difference on working fluid mass flow rate .....	57
Figure 3.15: Effect of pinch point temperature difference on enthalpy difference across the expander.....	58
Figure 3.16: Effect of pinch point temperature difference on thermal efficiency .....	58
Figure 3.17: Effect of pinch point temperature difference on exergy efficiency.....	59
Figure 3.18: Effect of condensation temperature on net work output .....	60
Figure 3.19: Effect of condensation temperature on working fluid mass flow rate .....	60
Figure 3.20: Effect of condensation temperature on enthalpy difference across the expander .....	61
Figure 3.21: Effect of condensation temperature on thermal efficiency .....	61
Figure 3.22: Effect of condensation temperature on exergy efficiency.....	62
Figure 3.23: Schematic diagram indicating the genetic algorithm process .....	66
Figure 3.24: Exergy loss distribution in ORC components.....	73
Figure 3.25: Effect of evaporation pressure on thermal and exergy efficiency.....	75
Figure 3.26: Effect of evaporation pressure on component irreversibilities.....	76
Figure 3.27: Effect of degree of superheat on thermal and exergy efficiency.....	77
Figure 3.28: Effect of degree of superheat on component irreversibilities .....	78
Figure 3.29: Effect of condenser pressure on thermal and exergy efficiency .....	78
Figure 3.30: Effect of condenser pressure on component irreversibilities .....	79
Figure 3.31: Effect of dead state temperature on exergy efficiency.....	80
Figure 3.32: Effect of dead state temperature on component irreversibilities.....	80
Figure 3.33: Effect of PPTD on thermal and exergy efficiency .....	81
Figure 3.34: Effect of PPTD on component Irreversibilities.....	82

Figure 4.1: Three zone plate heat exchanger evaporator model .....	85
Figure 4.2: Main dimensions of the plate heat exchanger (Konstantinos and Sotirios, 2017)...	86
Figure 4.3: Effect of evaporator pressure on net work output .....	93
Figure 4.4: Effect of evaporator pressure on evaporator area and cost .....	93
Figure 4.5: Effect of pinch point temperature difference on net work output.....	95
Figure 4.6: Effect of pinch point temperature difference on evaporator area and cost .....	95
Figure 4.7: Effect of expander inlet temperature on net work output.....	97
Figure 4.8: Effect of expander inlet temperature on evaporator area and cost .....	97
Figure 4.9: Effect of plate width on evaporator cost and frictional pressure drop .....	98
Figure 4.10: Effect of plate spacing on evaporator cost and frictional pressure drop .....	99
Figure 5.1: Conceptual diagram of scroll expander model.....	102
Figure 5.2: Effect of expansion ratio on mass flow rate of the working fluid.....	108
Figure 5.3: Effect of expansion ratio on shaft power .....	109
Figure 5.4: Effect of expansion ratio on expander efficiency.....	110
Figure 5.5: Effect of shaft speed on mass flow rate of the working fluid .....	111
Figure 5.6: Effect of shaft speed on shaft power .....	112
Figure 5.7: Effect of shaft speed on expander efficiency .....	112
Figure 5.8: Effect of inlet temperature on mass flow rate .....	113
Figure 5.9: Effect of inlet temperature on shaft power.....	114
Figure 5.10: Effect of inlet temperature on expander efficiency .....	114
Figure 5.11: Effect of inlet temperature on heat loss to ambient.....	115
Figure 6.1: Schematic diagram of solar driven ORC system .....	117



## LIST OF TABLES

Table 1.1: Power rating of DPG systems.....	3
Table 1.2: Region wise electricity generation from renewable energy in 2018 (OECD/IEA 2019).....	3
Table 1.4: List of commonly used ORC fluids categorized based on heat source temperature .....	13
Table 1.5: Various types of prime movers used in ORC systems .....	14
Table 3.1: Properties of the selected ORC working fluids (Wang et al. 2013) .....	45
Table 3.2: Design conditions of ORC system.....	48
Table 3.3: Sensitivity analysis of net power output, thermal efficiency and exergy efficiency for R245fa .....	63
Table 3.4: Sensitivity analysis of net power output, thermal efficiency and exergy efficiency for R123 .....	64
Table 3.5: Sensitivity analysis of net power output, thermal efficiency and exergy efficiency for Isobutane .....	64
Table 3.6: Sensitivity analysis of net power output, thermal efficiency and exergy efficiency for R134a .....	64
Table 3.7: Input data for GA optimization .....	67
Table 3.8: Optimization results of ORC system for all working fluids.....	68
Table 3.9: Thermophysical properties of R245fa .....	69
Table 3.10: Input parameters for energy and exergy analysis (Galloni et al. 2015).....	71
Table 3.11: Energy analysis.....	72
Table 3.12: Results obtained from exergy analysis of ORC system .....	73
Table 3.13: Properties of water and R245fa at each thermodynamic state.....	74
Table 4.1: Inputs to the model.....	87
Table 4.2: Effect of evaporator pressure.....	91
Table 4.3: Effect of pinch point temperature difference.....	94
Table 4.4: Effect of expander inlet temperature .....	96
Table 5.1: Inputs to the semi empirical model.....	107
Table 6.1: Cost of major components of the solar ORC plant in India as per price quotations.....	116

Table 6.2: Cost of 1 kW <sub>p</sub> solar PV system (Ahsan et al. 2016).....	117
Table 6.3: Upper and lower bounds for GA optimization .....	122
Table 6.4: Exergoeconomic optimization results .....	122

## NOMENCLATURE

### Abbreviations

EES	Engineering Equation Solver
GWP	Global Warming Potential
ICC	Initial Capital Cost (Rs)
LMTD	Logarithmic Mean Temperature Difference (°C)
ODP	Ozone Depletion Potential
OM	Operation and Maintenance Cost (Rs)
ORC	Organic Rankine Cycle
PPTD	Pinch Point Temperature Difference (°C)
TCC	Total Capital Cost (Rs)

### Symbols

A	Area of the heat exchanger (m <sup>2</sup> )
A <sub>f</sub>	Amortization factor
b	Plate spacing (m)
C	Specific heat (kJ/kg °C)
C <sub>e</sub>	Electricity cost rate (Rs/kWh)
D <sub>h</sub>	Hydraulic diameter (m)
e	Specific exergy (kJ/kg)
Ė	Rate of exergy (kW)
Ė <sub>x</sub>	Rate of exergy (kW)
G	Mass velocity (kg/m s)
h	Specific enthalpy (kJ/kg)
i	Interest rate (%)
I	Irreversibility (kW)

$h_{fg}$	Enthalpy of vaporization (kJ/kg)
$k$	Thermal conductivity (W/m °C)
$L$	Length of the plate (m)
$\dot{m}$	Mass flow rate of the fluid across the expander (kg/s)
$M_1$	Mass flow rate of the working fluid (kg/s)
$M_2$	Mass flow rate of the heat transfer fluid (kg/s)
$n$	Number of years
$N$	Rotational speed (rpm)
$P$	Pressure (Pa)
$P_{co}$	Corrugation pitch (mm)
$q''$	Average heat flux (W/m <sup>2</sup> )
$\dot{Q}$	Heat transfer rate (kW)
$r_{v,in}$	Built in volume ratio
$t$	Plate thickness (m)
$T$	Temperature (°C)
$U$	Overall heat transfer coefficient (W/m <sup>2</sup> °C)
$UA$	Heat transfer coefficient (W/ °C)
$v$	Specific volume (m <sup>3</sup> /kg)
$w$	Plate width (m)
$\dot{W}$	Power (W)
$x$	Vapor quality
$\dot{Z}_x$	Cost rate (Rs/h)

### Greek Symbols

$\alpha$	Convective heat transfer coefficient (W/m <sup>2</sup> °C)
$\beta$	Chevron angle (Degree)
$\gamma$	Isentropic exponent
$\Delta$	Difference or change
$\epsilon$	Effectiveness of scroll expander
$\eta$	Efficiency

$\mu$	Viscosity (kg/m s)
$\rho$	Density (kg/m <sup>3</sup> )
$\tau$	Torque (N m)

### Subscripts

1,2,3,4,5,6,7,8	Thermodynamic states
ad	adapted
amb	ambient
calc	calculated
col	collector
cond	condenser
cr	critical
eq	equivalent
evp	evaporator
ex	exhaust
exg	exergy
exp	expander
f	fluid phase
g	vapor phase
hf	hot fluid
i	inlet
int	internal
in	input
is	isentropic
leak	leakage
loss	losses
max	maximum
meas	measured
min	minimum
nom	nominal

o	dead state
pl	plate
pp	pump
r	refrigerant
rej	rejection
s	swept
sh	shaft
sp	single phase
su	supply
sup	superheated
t	expander
th	thermal
thr	throat
tp	two phase
w	envelope or wall
wf	working fluid
ws	water side

### **Non-dimensional numbers**

Bo	Boiling number
f	Friction factor
$Ge_1, Ge_2, Ge_3, Ge_4$	Constants in Han, Lee and Kim correlations
Nu	Nusselt number
Pr	Prandtl number
Re	Reynolds number

## CHAPTER 1

### INTRODUCTION

#### 1.1 Need for alternative source of energy

Energy demand is increasing around the world because of rapid urbanization and industrialization. The current energy production and consumption pattern has led to significant emissions of carbon dioxide (CO<sub>2</sub>), oxides of nitrogen (NO<sub>x</sub>) and oxides of sulphur (SO<sub>x</sub>). These pollutants have a negative effect on the environment leading to global warming and climate change (Quoilin et al. 2013). This has forced the policy makers to adopt green technologies and increase the share of renewable energy in total energy consumption basket (Landelle et al. 2017).

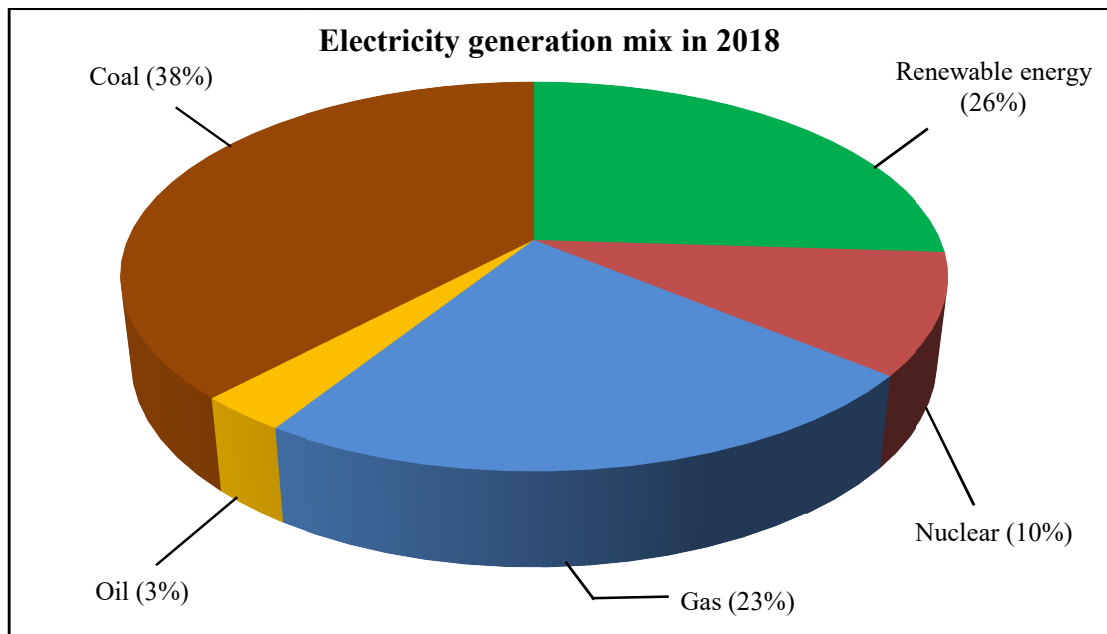


**Figure 1.1:** Data showing the share of each energy production technology in world energy consumption (OECD/IEA 2019)

Energy generation from renewable energy sources constituted 26% of the overall electricity generation in the world in 2018, as shown in Figure 1.1. India has committed to increase its renewable energy share to 40% of the total energy consumption by 2030 (United Nations Framework Convention on Climate Change (UNFCCC) 2016).

International Energy Agency (IEA) presented a sustainable alternative called '2DS' in 2014. 2DS offered a vision to create an energy system that reduced CO<sub>2</sub> emissions and to restrict global temperature rise within 2 °C by 2050. This however, requires that the future energy systems should be smart, integrated, well distributed, and policy makers should give more thrust towards renewable energy generation. In the case of centralized power generation (CPG), there are transmission and distribution losses associated with it. In addition to this, CPG requires large investment cost for electrification of remote areas. The official data from Ministry of power, Government of India shows that the aggregate technical and commercial losses (AT&C) at all-India level were at 18.7% in 2018-19. This can be reduced to a great extent by using DPG or on-site power generation systems. There are close to 1.6 billion people around the world, living in remote areas without access to electricity. It is almost impossible to create a transmission infrastructure to connect every household to central grid (Rahbar et al. 2017; Tchanche et al. 2011). Distributed (on-site) power generation (DPG) is a better option, which is directly connected to the distribution network or to the customer site. This results in the reduction in transmission and distribution losses. DPG systems can also use any renewable energy source such as solar, wind, geothermal and waste heat recovery (Aboelwafa et al. 2018). Table 1.1 (Ackermann et al. 2001) shows power ratings of DPG systems.

Global energy demand is increasing at a rapid pace, powered by a strong global economy and higher heating and cooling needs in some parts of the world. Driven by higher electricity demand, global energy-related CO<sub>2</sub> emissions increased 1.7% to a record high of 33.1 Gt CO<sub>2</sub> in 2018.

**Table 1.1:** Power rating of DPG systems

<b>Category</b>	<b>Power rating</b>
Distributed micro power generation	1 W to 5 kW
Distributed small power generation	5 kW to 5 MW
Distributed medium power generation	5 MW to 50 MW
Distributed large power generation	50 MW to 500 MW

Although emissions from all fossil fuels rose, the power sector accounted for almost two-thirds of the growth in emissions. China, India and the United States of America (USA) accounted for 85% of net carbon emission increase (OECD/IEA 2019). In 2018, renewable energy generation grew by 7%, accounting for 26% of global demand for electricity as indicated in Table 1.2.

**Table 1.2:** Region wise electricity generation from renewable energy in 2018 (OECD/IEA 2019)

<b>Region</b>	<b>Renewable- based energy Generation in 2018 (TWh)</b>	<b>Growth rate (2017-18) (%)</b>
United States	744	4.1
China	1854	10.9
India	291	10.6
Europe	1462	8.5
Rest of the world	2449	4
Total	6800	7.1

Despite this, more than 5% of India’s population (1.4 crore households approximately) do not have access to electricity (IEA et al. 2019). In India, generation from renewable energy includes small Hydro Projects, Biomass Gasifier, Biomass Power, Urban & Industrial Waste Power, Solar and Wind Energy. In 2019-20, renewable energy



generation increased by 9.12% and thermal energy generation decreased by 2.75%. At present, renewable energy constitutes around 24.5% of the total installed capacity. Therefore, there is a need to identify alternative technologies to increase the share of renewable energy generation to 40% by the end of next decade. DPG systems of 1-5 kW<sub>e</sub> capacity using renewable energy are best suited to achieve 100% electrification in remote and rural areas as well as to cater to the increasing energy demand. One of the commercially available option is solar PV. The limitations of solar PV technology are additional cost of battery as well as its maintenance. Therefore, there is a need to identify a 1-5 kW<sub>e</sub> capacity power generation system which is cost-effective and easy to operate and maintain in remote locations. Moreover, the resources for energy conversion such as solar or biomass should be available locally.

Low grade heat energy in the temperature range of 70 to 300 °C is not being utilized properly (Lecompte et al. 2017; Bianchi and De Pascale 2011; Mudasar et al. 2017). The utilization of suitable technologies which is capable of efficiently recovering and converting the low grade heat energy to electrical energy has been identified in open literature, as one of the major pathways towards achieving a green, sustainable and low-carbon environment (Qiu et al. 2011). Energy can be recovered from these heat sources by using various technologies such as steam Rankine cycle (Quoilin et al. 2013), Kalina cycle (Ogriseck 2009), supercritical CO<sub>2</sub> Brayton cycle (Ahn et al. 2015), organic Rankine cycle (Chen et al. 2010) etc. Steam Rankine Cycle (SRC) uses water as the working fluid. Although water satisfies most of the criteria such as good thermal stability, low viscosity, non-toxic, non-flammable etc, it is a wet fluid with negative slope of saturation vapor curve (Zhang et al. 2016). The SRC needs sufficient superheat (upto 500 to 600 °C) to avoid any damage being caused to the turbine blades. Therefore, it is not suitable to be used for low grade energy conversion and is more appropriate for large scale CPG systems.

## 1.2 Available energy conversion technologies for DPG systems

### 1.2.1 Kalina cycle

In this process, low temperature heat is transferred indirectly to a circulating fluid. The working fluid is a mixture of ammonia and water as shown in Figure 1.2. The ammonia–water mixture has a varying boiling and condensing temperature. The mixture of ammonia and water boils at a variable temperature depending on its composition. Ammonia has a lower boiling temperature compared to water. Due to this, the mixing ratio of the binary mixture changes during the evaporation process. The higher the fraction of ammonia in the mixture, the lower is its boiling temperature. With the increasing ammonia concentration, the specific enthalpy of steam decreases. Before the turbine, the ammonia-rich steam is separated from the liquid phase in a separator. Then, the steam passes through the turbine, where the expansion takes place to produce mechanical work output. Generator which is coupled to the turbine converts the mechanical work to electricity.

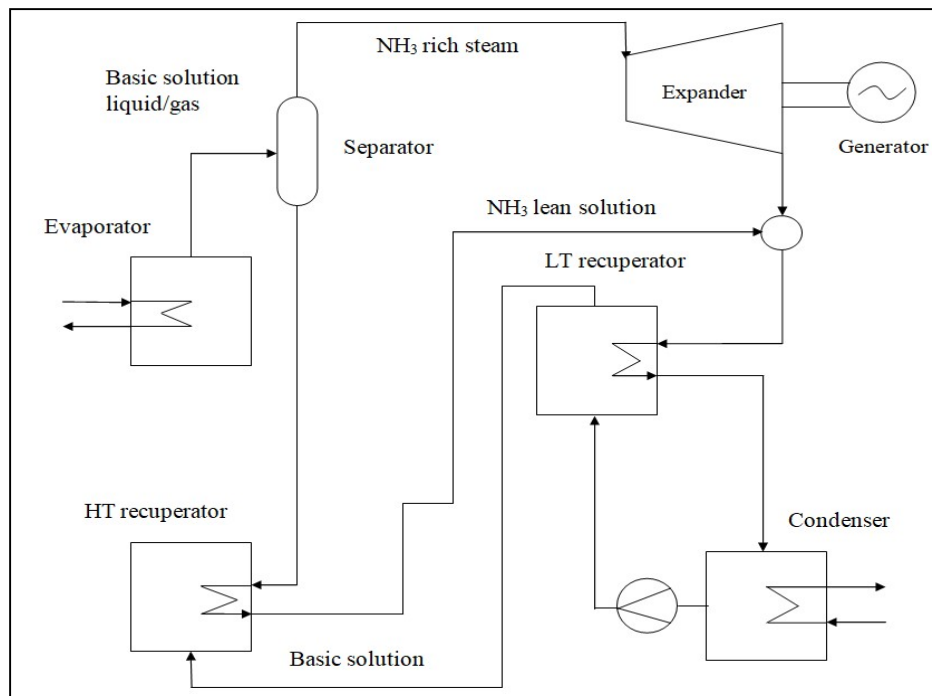


**Figure 1.2:** Schematic diagram of the Kalina cycle process (Ogriseck 2009)

### 1.2.2 Supercritical CO<sub>2</sub> Brayton cycle

Supercritical carbon dioxide is a state of carbon dioxide (CO<sub>2</sub>), where it is held at or above its critical temperature and critical pressure. CO<sub>2</sub> has a relatively low critical pressure of 7.4 MPa and a critical temperature of 31 °C. Therefore, it can be compressed directly to supercritical pressures and readily heated to a supercritical state before expansion. In a simple closed-loop Brayton cycle as illustrated in Figure 1.3, the working fluid (CO<sub>2</sub>) is heated indirectly from a heat source. Heat energy ( $Q_H$ ) is extracted from CO<sub>2</sub>, as it expands in the turbine. The CO<sub>2</sub> exiting the turbine is then cooled in a heat exchanger ( $Q_L$ ) to the desired compressor inlet temperature. After the fluid is compressed to the required pressure, the CO<sub>2</sub> is sent back to the heater to complete the cycle (Garg et al. 2013).

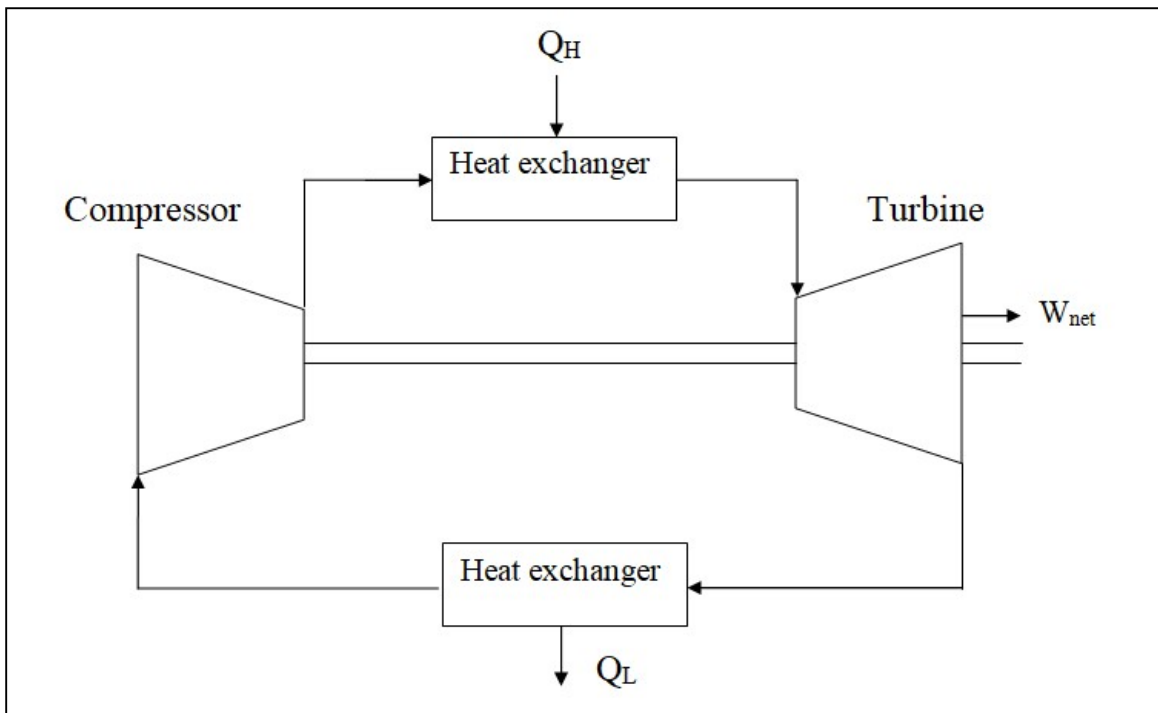


**Figure 1.3:** Schematic diagram of closed cycle brayton cycle

In a recuperated closed-loop Brayton cycle, a heat exchanger is introduced between the turbine exhaust and the compressor exhaust. This improves the cycle efficiency by reducing the amount of heat loss in the CO<sub>2</sub> cooler.

### 1.2.3 Organic Rankine cycle

The schematic setup of ORC plant is shown in Figure 1.4. The ORC power block consists of a pump which is used for pumping the working fluid to the desired pressure. This pressurized fluid is then passed on to the evaporator where heat addition takes place. The pressurized vapor passes through the expander, where the actual expansion of the working fluid takes place and the pressure drops. Finally, the vapor condenses in the condenser to complete the cycle. Small scale ORC power plants in the range  $1 \text{ kW}_e$  -  $1 \text{ MW}_e$  can be setup using low temperature heat source such as flat plate solar collectors, waste heat recovery, geothermal, biomass etc. The major advantage of using organic fluids such as hydrocarbons (Ethane, Propane, Butane, Isobutane, and Pentane etc.) or refrigerants (R22, R141b, R134a, R245fa, R152a etc.) in ORC is that, they operate at lower temperature ( $70$  to  $300 \text{ }^\circ\text{C}$ ) and pressure ( $5$ - $20$  bar) compared to water (Kuo et al. 2011; Dariusz and Jarosław 2016). Hence, heat energy from low temperature sources can be utilized to generate electricity (Baral and Kim 2014).

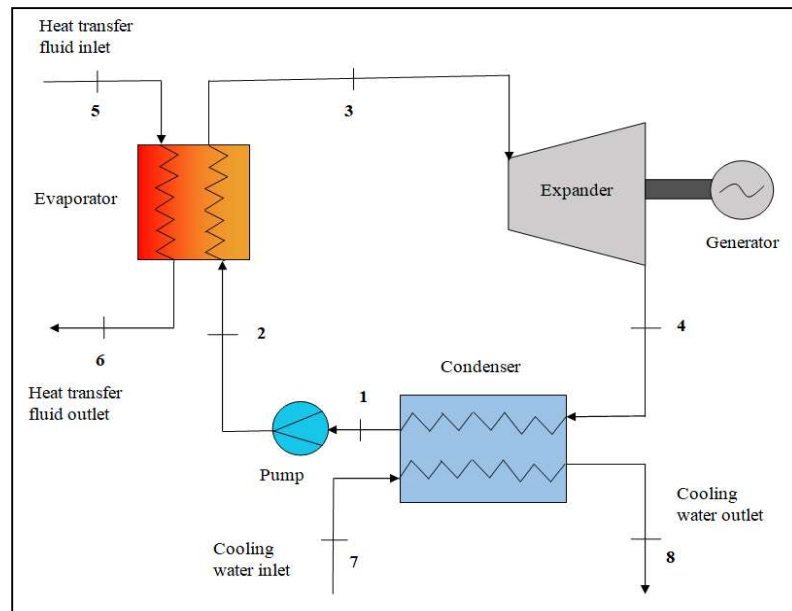


**Figure 1.4:** Schematic diagram of ORC power block

ORC has garnered the attention of the researchers in the recent past. Research studies have shown that ORC performs better than Kalina cycle because of its lower operating

pressures (Nemati et al. 2017). ORC performed better than Kalina Cycle in terms of net electricity generation for heat source temperatures ranging from 100 to 200 °C (Lin et al. 2015). Supercritical CO<sub>2</sub> Brayton cycle proved to be impractical for heat source temperatures of less than 300 °C (Bianchi and De Pascale 2011). This is because the gain in enthalpy across the turbine was negated by the compressor. Therefore, ORC technology is best suited to exploit low to medium temperature heat sources.

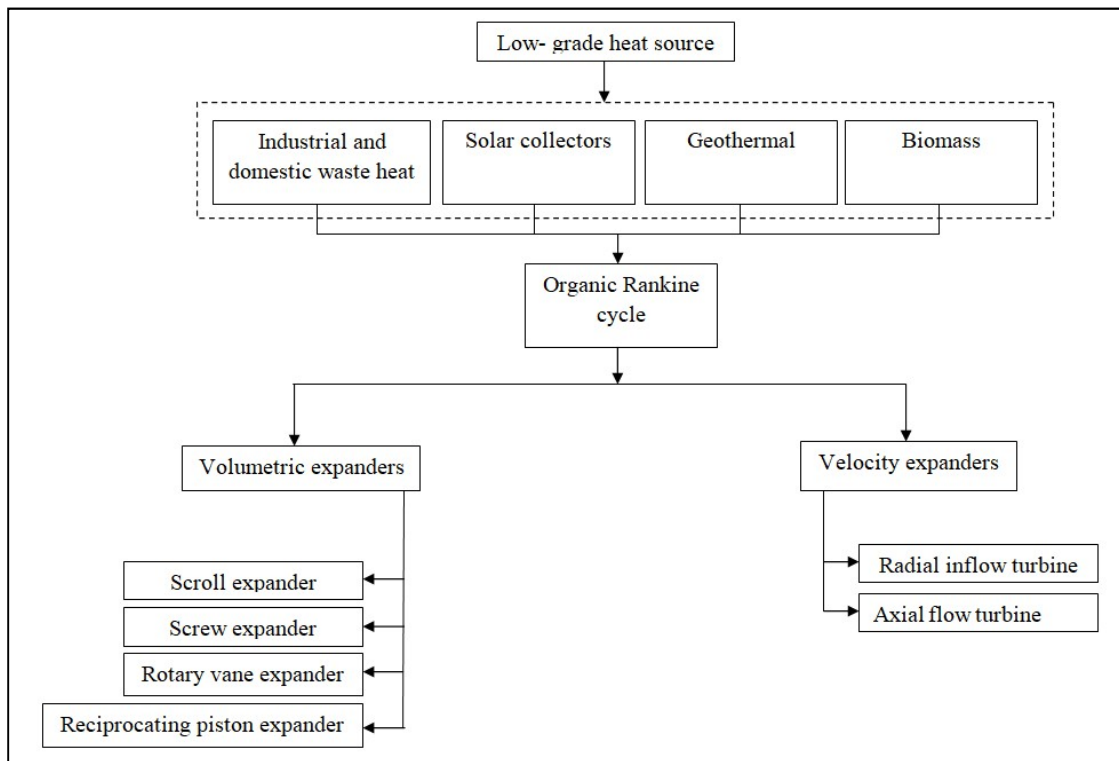


**Figure 1.5:** Various configurations and technologies available in organic Rankine cycle ORC system can be used with minor modifications, in conjunction with various heat sources such as solar, biomass, geothermal and waste heat recovery. Compared to the Kalina cycle’s complexity in design, need for superheating in steam Rankine cycles and high operating pressures in supercritical CO<sub>2</sub> brayton cycles, ORC is best suited for DPG systems because of its simple structure, low cost, compactness, reliability, and easy maintenance. Various configurations and technologies available for energy conversion

using ORC have been listed in Figure 1.5 (Qiu et al. 2012; Aboelwafa et al. 2018; Zhao et al. 2019; Altun and Kilic 2020).

ORC systems are classified under three broad categories. Firstly, they are classified on the basis of the type of heat source used such as solar energy, geothermal energy, waste heat recovery, biomass energy etc. ORC technology has been used to extract low grade energy either by use of renewable energy or by utilizing industrial waste heat. The second classification is based on the cycle configuration. This is shown in Figure 1.6. The first one is the basic ORC system consisting of the feed pump, evaporator, expander and condenser. The working fluid is pumped to the evaporator. The pressurized vapor is passed onto the expander to generate electricity. The low pressure vapor is then condensed in the condenser. The cycle with recuperator takes advantage of the residual heat after the expansion process to preheat the liquid after the pump. This leads to the reduction in the amount of heat required to vaporize the fluid in the evaporator.

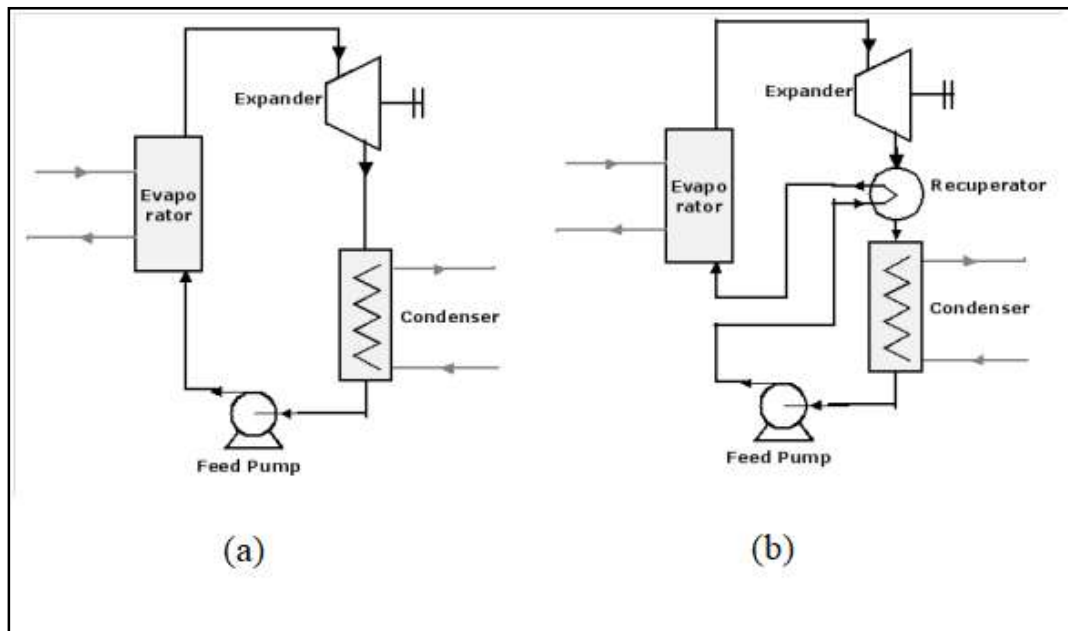


**Figure 1.6:** Schematic diagram of ORC cycle (a) Basic (b) with recuperator

The third classification is based on the temperature of the heat source. ORC systems are classified as low temperature ORC system, if the temperature of the heat source is less than 150 °C. If the temperature of the heat source is in the range of 150 -250 °C, it is called as medium temperature ORC system and if the temperature crosses 250 °C, it is referred to as a high temperature ORC system (Rahbar et al. 2017).

The important factors that are to be considered in ORC system are the selection of working fluid, the configuration of ORC system and selection of prime mover or expansion device. Each of these factors is critical for the smooth operation of the ORC system and are discussed in the subsequent sections.

### **1.3 Selection of ORC working fluid**

The most important aspect of the ORC system is the selection of the working fluid. The thermophysical properties of each fluid have a significant impact on the overall efficiency, sizing of heat exchangers, expander design and stability of the system. In addition to this, the working fluid properties has an impact on the system cost, safety and environmental aspects (Dewallef et al. 2013). Organic fluids are broadly classified based on their saturation vapor curve. There are generally three types of saturation vapor curve as shown in Figure 1.7; dry fluid with positive slope of T-s curve, wet fluid with negative slope of T-s curve and isentropic fluids with nearly vertical saturation vapor curve respectively. As the vapor expands across the expander, saturated vapor at the expander inlet will remain saturated at the expander exhaust without condensation. This is a very important characteristic of dry and isentropic fluids (Huang et al. 2013).

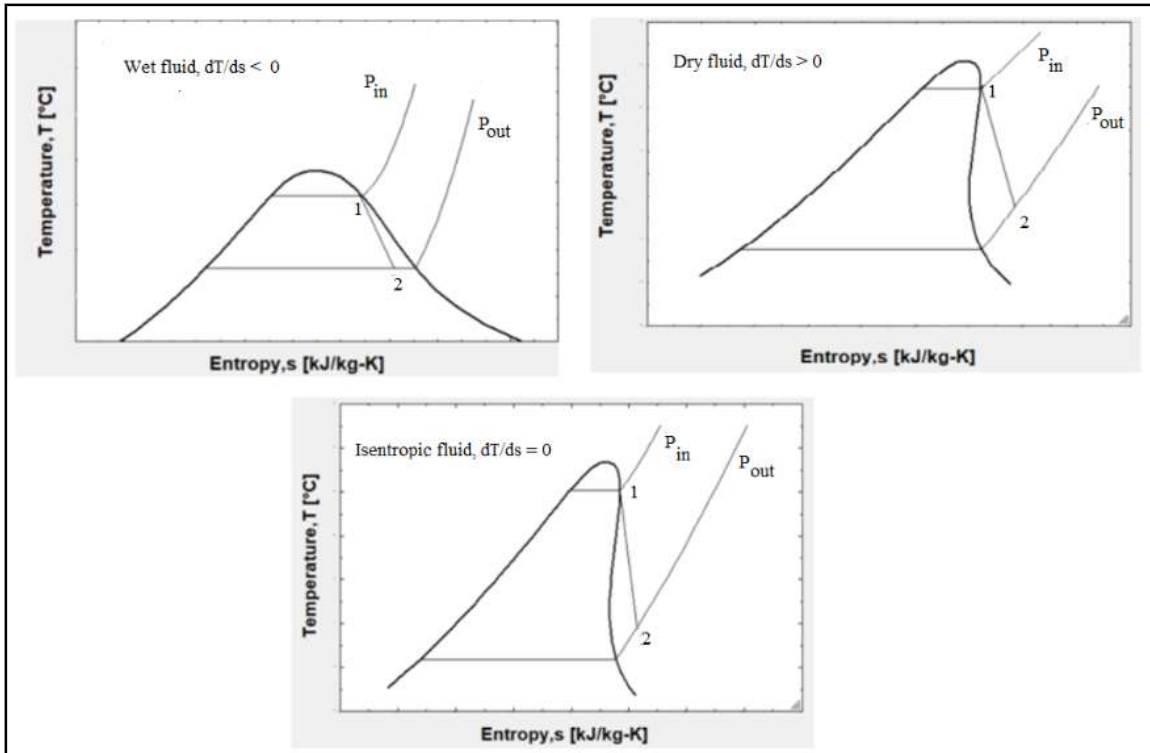


**Figure 1.7:** T-s diagram of wet, dry and isentropic fluids

There is no need for installing additional equipments such as superheater and regenerator, which makes dry and isentropic fluids ideal working fluids for ORCs (Darvish et al. 2015). In addition to this, the thermophysical properties which must be considered before selecting an organic fluid (Chen et al. 2010) are as follows:

a) **Latent heat of vaporization:** Thermal efficiency is the ratio of net work output to heat input. High latent heat of vaporization enables most of the available heat to be added during the phase change operation, hence avoiding the need to regulate the superheating and expansion of the vapor through regenerative feed heating in order to enable higher efficiency (Maizza and Maizza 2001). In terms of net work output, it was found that fluids with higher latent heat produce larger unit work output when the temperatures and other parameters are defined. However, when the heat source is either geothermal energy or waste heat, the ORC fluids with low latent heat of vaporization are preferred. Lower latent heat of vaporization of the working fluid causes the heat transfer process in the evaporator to occur mostly at variable temperature. Therefore, the temperature profile of



the ORC working fluid in the evaporator follows the temperature profile of heat transfer fluid (Bao and Zhao 2013).

**b) Density:** A low density of the ORC fluid leads to a higher volume flow rate. As a result of this, the pressure drop in the heat exchangers increases and the size of the expander also increases. This has a significant impact on the cost of the system.

**c) Critical temperature:** For a given evaporation and condensation temperatures, better thermal efficiency is obtained only from fluids with a high critical temperature. However, high critical temperatures lead to low condensation temperatures which affect the configuration of the system (Chen et al. 2010).

**d) Thermal stability:** Organic fluids generally suffer chemical deterioration and decomposition at high temperatures. Therefore, the maximum heat source temperature is limited by the chemical stability of the working fluid (Invernizzi et al. 2007).

**e) Environmental impact:** The ozone depletion potential (ODP) of a chemical compound is the relative amount of degradation to the ozone layer it can cause, with trichlorofluoromethane (R-11 or CFC-11) being fixed at an ODP of 1. The ODP of current refrigerants is either null or very close to zero, since non-zero ODP fluids are progressively being phased out under the Montreal Protocol (Schuster et al. 2009). Global warming potential (GWP) is the heat absorbed by any greenhouse gas in the atmosphere, as a multiple of the heat that would be absorbed by the same mass of carbon dioxide (CO<sub>2</sub>). GWP is 1 for CO<sub>2</sub>. GWP for organic fluids should be as low as possible (Wang et al. 2013).

**f) Safety:** Safety involves two main parameters— toxicity and flammability (Saleh et al. 2007). The ASHRAE Standard 34 classifies refrigerants based on its safety parameters and can be used for the evaluation of a particular working fluid.

**g) Viscosity and Thermal conductivity:** The fluid viscosity should be low in liquid as well as vapor phases as it enhances heat transfer coefficient and decreases the friction losses in the heat exchanger. It also leads to small pump equipment and helps in reducing the power consumption. High thermal conductivity is required to enhance the rate of heat

transfer in the heat exchangers. Large heat conductivity leads to small equipments at the heat exchanger level (Tchanche et al. 2011).

**h) Availability and cost:** Fluids which are being used in refrigeration or chemical industries are easily available and are less expensive.

The performance depends on a number of interdependent thermodynamic properties of the working fluid: critical point, specific heat, density, viscosity etc. It is not possible to determine an optimum for each specific thermodynamic property independently. The most common approach in scientific literature is simulating the cycle with a thermodynamic model using different working fluids, which is explained in the subsequent chapters. Some of the commonly used ORC working fluids which have been classified on the basis of their operating temperatures have been listed in Table 1.4 (Rahbar et al. 2017; Tchanche et al. 2011).

**Table 1.3:** List of commonly used ORC fluids categorized based on heat source temperature

<b>Low temperature (&lt;150 °C)</b>	<b>Medium temperature (150-250 °C)</b>	<b>High temperature (250-400°C)</b>
R134a	R245ca	Benzene
R245fa	n-butane	Toluene
R152a	HFE7000	MDM
R236fa	HFE7100	MD4M
R143a	n-pentane	D4
R236ea	Isopentane	Cyclohexane
Isobutane	Ethanol	
Ammonia		

## 1.4 Expansion device

The most important component in ORC is the expansion device which converts the available thermal energy into mechanical work. The choice of expansion device depends on the operating conditions, working fluid and the power output (Qiu et al. 2011).

Expansion devices are broadly classified into two types, i.e. turbines (dynamic expanders) and positive displacement expanders. In turbines, the pressure energy of the working fluid is converted to kinetic energy. This energy is then utilized to rotate the impellers of the turbine. These are further classified into axial and radial turbines. In case of positive displacement expanders, specific volume of the working fluid at the inlet of the expander is confined within a given space. Subsequently, the working fluid expands as the confined volume increases. Finally, the low pressure working fluid is passed through the discharge piping system. The main types of positive displacement expanders are scroll, screw, piston and vane. Comparison of various types of prime movers used in ORC systems are listed in Table 1.5 (Bao and Zhao 2013; Rahbar et al. 2017). Each of these is explained in detail in the subsequent sections.

**Table 1.4:** Various types of prime movers used in ORC systems

Type	Capacity range (kW <sub>e</sub> )	Rotating speed (rpm)
Scroll expander	1-10	<6000
Screw expander	15-200	<6000
Reciprocating piston expander	20-100	<6000
Rotary vane expander	1-10	<6000
Axial flow turbine	>200	<20000
Radial inflow turbine	50-500	8000-80000

### 1.4.1 Scroll expanders

A scroll expander is made up of two helical scrolls as depicted in Figure 1.8; one being the rotor and the other being the stator. The mode of operation is shown in Figure 1.9. When the rotor spins, it produces a closed volume between its contact points with the stator. Due to the increasing separation of rotor and stator, this volume increases in size through each rotation where the fluid expands, and the low pressure working fluid finally exits through the discharge port (Campana et al. 2019; Jiang et al. 2017).

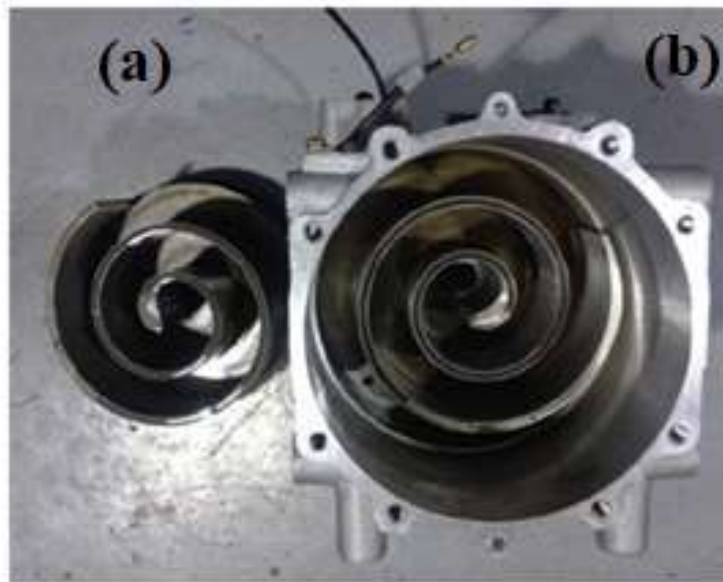


**Figure 1.8:** (a) Moving scroll (b) Fixed scroll (Wu et al. 2015)

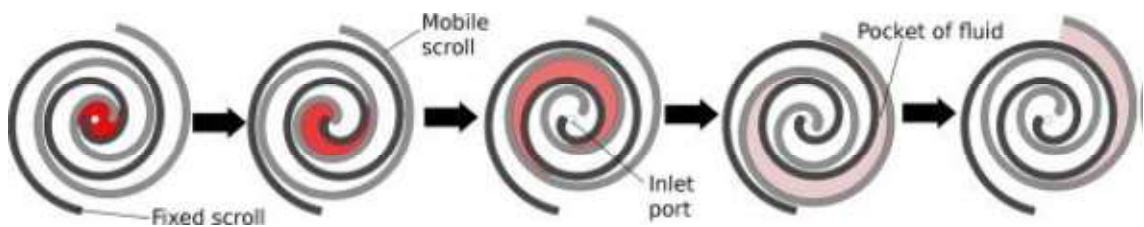


**Figure 1.9:** Diagram of mode of operation of the scroll expander (Quoilin et al. 2013)

### 1.4.2 Screw expanders

There are two types of screw expanders; single screw and twin screw. Both of them work on the same principle of trapping a volume of vapor within the expansion chamber which is formed by the geometry of the screws. As the screw rotates, the chamber enlarges itself till the vapor reaches the discharge port. In a single screw expander, this volume is created by meshing the main screw rotor with peripheral gate rotors as shown in Figure 1.10.

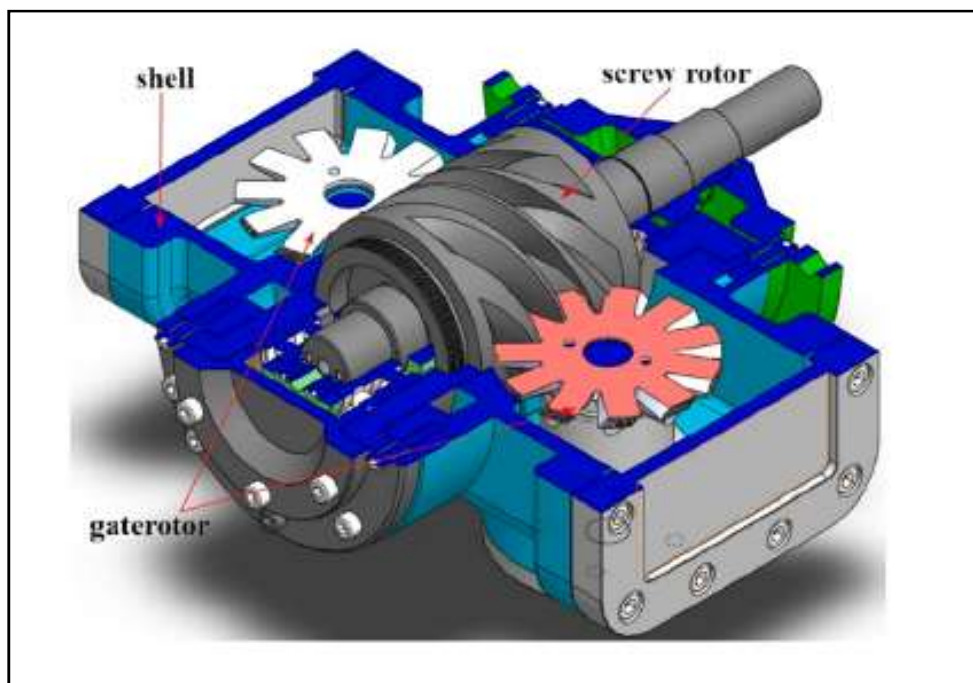


**Figure 1.10:** Diagram of a single screw expander (Shen et al. 2018)

Twin screw expander consists of a pair of helical meshing rotors; a male and a female rotor, enclosed within a casing as depicted in Figure 1.11. The high pressure working fluid reaches the space between the two rotors and begins rotation in the first step. During the expansion process, as the meshing rotors rotate, the tooth-spacing volume increases due to pressure of the working fluid. Finally, when the tooth-spacing volume is attached to the outlet, the exhaust process starts until the tooth-spacing volume reaches zero.



**Figure 1.11:** Diagram of a twin screw expander (Papes et al. 2015)

### 1.4.3 Reciprocating piston expanders

Reciprocating piston expanders (Figure 1.12) are devices which require accurate inlet and exhaust valve timing. Since it contains large number of moving parts, frictional losses tend to increase (Oudkerk et al. 2015). They have been widely used in internal combustion engines for exhaust heat recovery using ORC. One major advantage of this expander is that it can tolerate wet expansion.

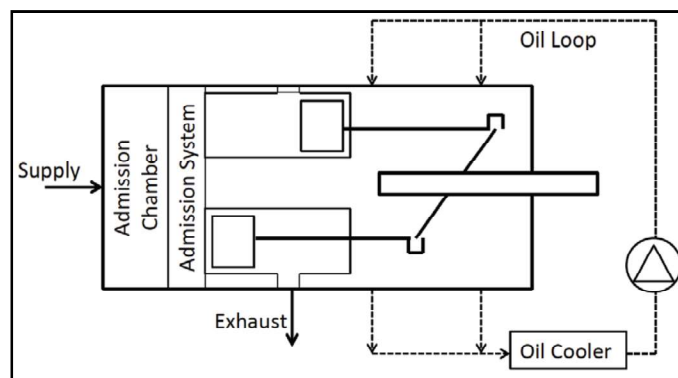


**Figure 1.12:** Schematic diagram of reciprocating type piston expander (Oudkerk et al. 2015)

#### 1.4.4 Rotary vane expander

These are air motors intended specifically for the use of compressed air to drive the rotors. The compressed air energy is transformed into mechanical energy by an air motor. Air motors are modified for reverse operation and to prevent leakage of organic fluids for ORC applications as shown in Figure 1.13. The expansion cycle is achieved when the chamber spaces between the cylinder wall and the sliding vanes slotted into the rotor increase, as the rotor turns clockwise inside the eccentric cylinder housing (Montenegro et al. 2014).

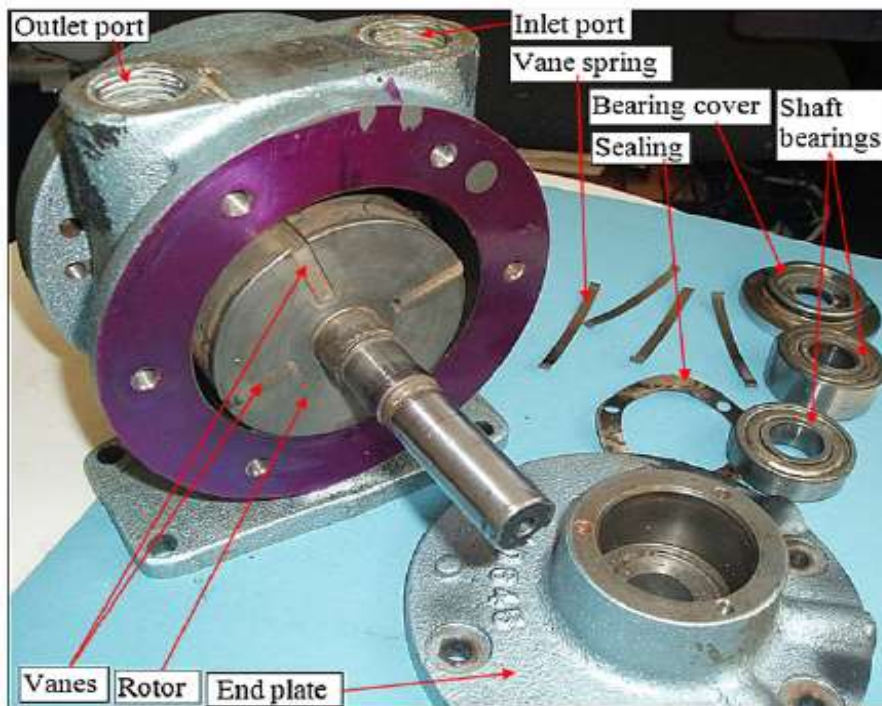


**Figure 1.13:** Vane-type air motor used as an expander (Qiu et al. 2011)

#### 1.4.5 Turbo-expanders (axial flow and radial inflow turbines)

Turbines are devices which convert kinetic energy of a flowing fluid to the mechanical energy of shaft by rotation of the blades. It is broadly classified as axial flow and radial flow depending on the path of fluid flow. In case of radial flow turbine, there is significant change in the mean radius as the fluid flows from inlet to outlet but in axial flow turbines, there is hardly any change in the mean radius as indicated in Figure 1.14.

Therefore, radial flow turbines require fewer stages compared to axial flow turbines which reduce the size and the cost. Hence, radial flow turbines are preferred for small-scale applications with low flow rates and high expansion ratios whereas axial flow turbines are used for high capacities ( $>250 \text{ kW}_e$ ) with large mass flow rates and low expansion ratios (Alshammari et al. 2018).

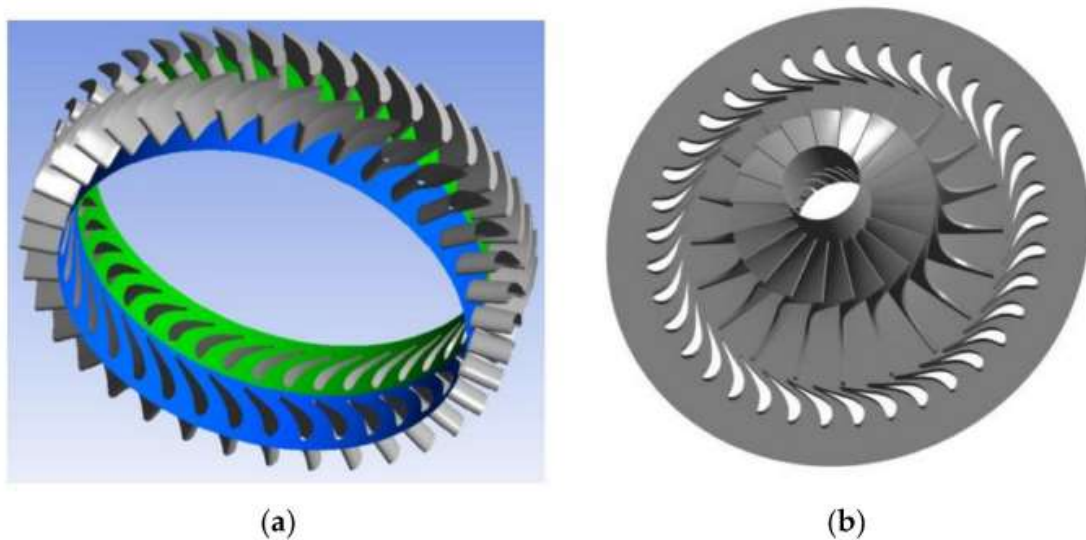


**Figure 1.14:** 3D geometry of (a) Axial turbine (b) Radial turbine (Alshammari et al. 2018)

## 1.5 Various configurations of ORC systems

### 1.5.1 Biomass combined heat and power (CHP)

Biomass can be used for both thermal and power generation simultaneously using ORC technology. Agricultural biomass is available in plenty around the world. This can also help in generating additional income for the poor farmers and can accelerate poverty alleviation in developing countries. The heat from the biomass burner is utilised from exhaust or flue gas to the heat transfer fluid. The hot fluid is then made to pass through the evaporator in the ORC power block. Heat exchange occurs in the evaporator and the ORC working fluid is vaporised (Qiu et al. 2012). Figure 1.15 shows a biomass fired ORC based cooling heating and power (CHP) system. This can be used for DPG systems with low power capacity.



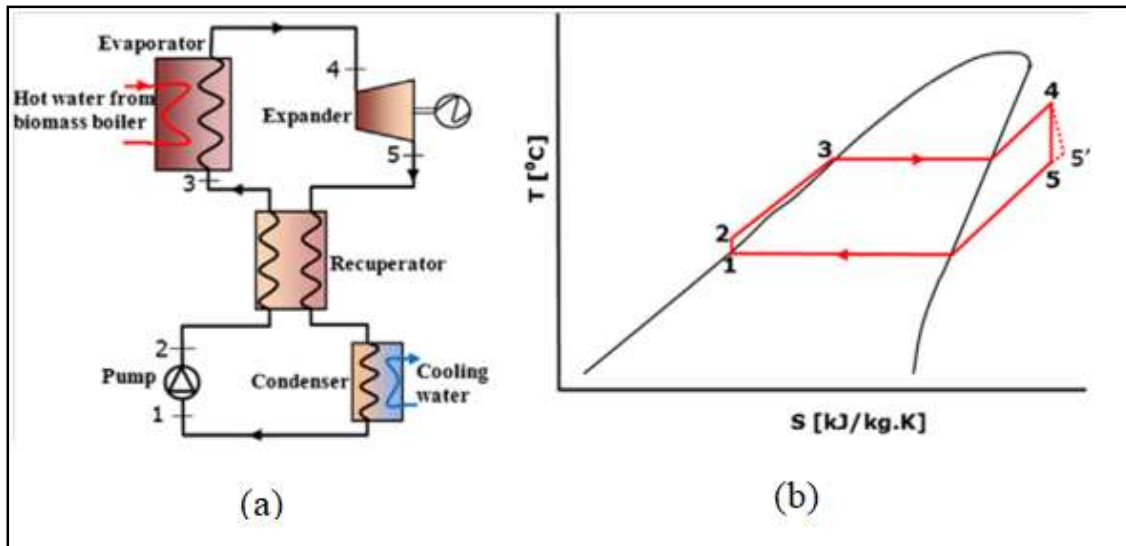


**Figure 1.15:** (a) Biomass fired ORC based cooling heating and power (CHP) system (b) T-s diagram of the CHP system (Qiu et al. 2012)

### 1.5.2 Solar power cycles

Presently, electricity is generated commercially from solar power using two methods. Solar photovoltaic (PV) directly converts solar irradiance to electricity whereas solar thermal utilizes the heat captured using solar collectors and then converts it into mechanical work. The main disadvantages of using solar PV are their low power density and battery maintenance. This means that huge amount of land is required to generate few hundreds of kW of electricity. The limitation with large scale (CPG) solar thermal systems are that they require huge amount of capital investment because energy storage is required to attenuate the fluctuations in solar energy radiation. ORC is a suitable option for low cost, small scale power generation (DPG) using low grade heat from solar energy (Aboelwafa et al. 2018). Figure 1.16 shows a solar driven ORC system.

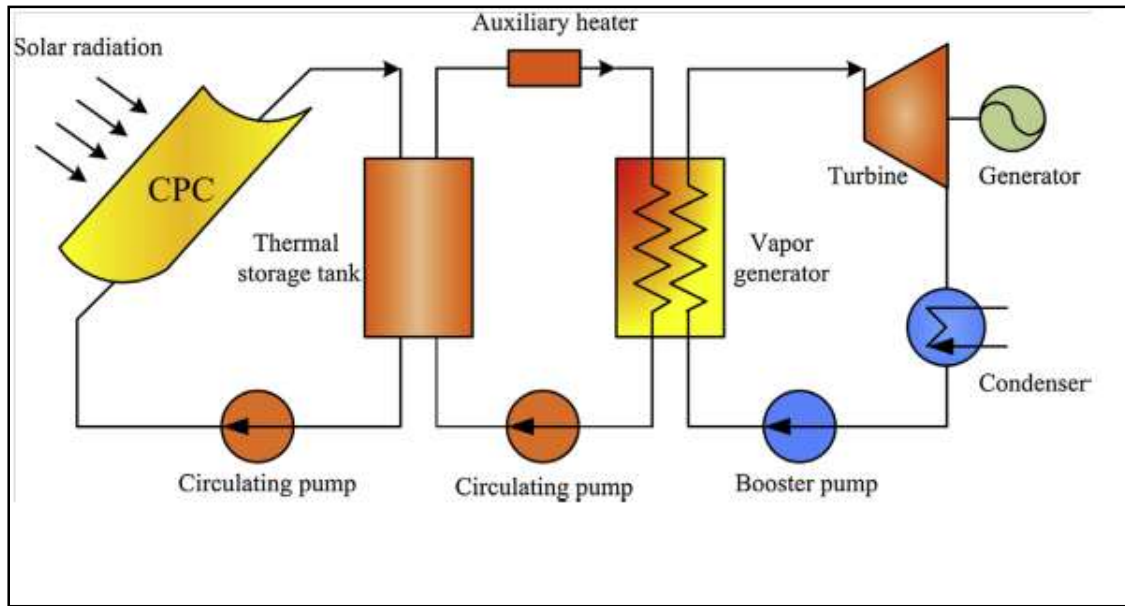


**Figure 1.16:** Schematic diagram of compound parabolic collector (CPC) driven ORC system (Wang et al. 2014)

### 1.5.3 Geothermal

Geothermal energy is estimated to be at depths of approximately 3 km from the earth's surface. This energy can be extracted by drilling production and injection well. The hot brine that is trapped below the earth's surface, is pumped from the production well and injected into the injection well while passing through the evaporator in the ORC power block. Heat exchange occurs in the evaporator and power can be produced by passing pressurized organic vapor through the expander as shown in Figure 1.17 (Quoilin et al. 2013).

### 1.5.4 Waste heat recovery

In industries, flue gases at temperature less than 200 °C are often rejected to the atmosphere and can have devastating effect on the environment. Low temperature heat cannot be utilized using traditional waste heat recovery techniques or for captive power generation. However, by integrating exhaust systems with ORC system, power can be generated for captive use and excess power can be passed onto the grid, generating extra revenue to the industries. Some of the potential industries which can adopt ORC systems

for low temperature waste heat recovery are cement, iron & steel, refineries and chemical industries (Wei et al. 2007 ; Seyedkavoosi et al. 2017).

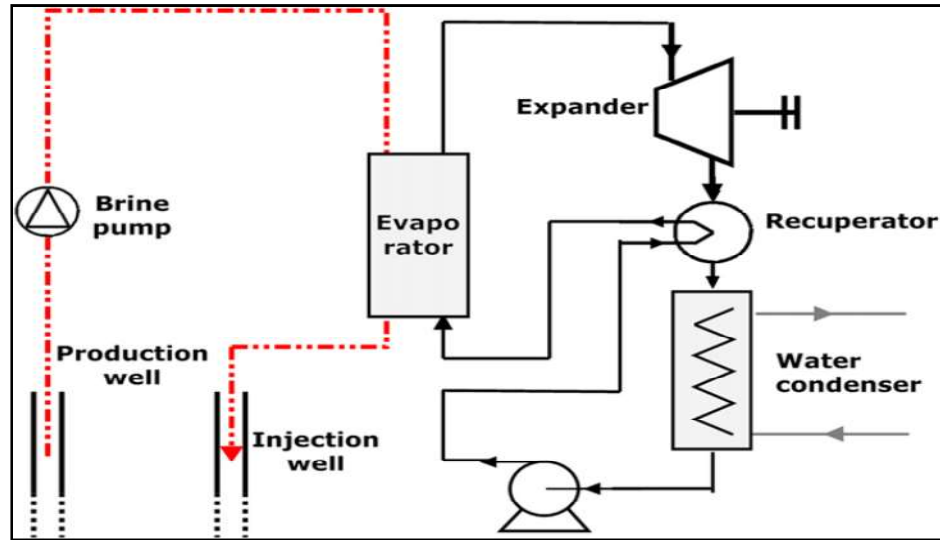


**Figure 1.17:** Schematic representation of a geothermal ORC system (Quoilin et al. 2013)

## 1.6 Organization of the thesis

The energy demand across the world is increasing rapidly as a result of massive urbanization and industrialization. This is coupled with scarcity of traditional energy sources and severe environmental issues such as global warming and climate change. In order to counter this problem, there is a sense of urgency to explore alternative sources of energy. In this regard, harnessing the renewable energies and waste heat recovery are considered as potential solutions that can effectively address these issues. ORC is proved to be reliable technology that can efficiently convert these low to medium-grade heat sources into useful power. The thesis work is proposed on parametric investigation and off-design simulation of low temperature organic Rankine cycle for residential applications (1-5 kW<sub>e</sub>).

Chapter 2: Recent studies related to energy and exergy analysis of ORC systems, thermo-economic optimization of ORC systems, modeling of Chevron plate heat exchanger evaporators in ORC systems and semi-empirical modelling of scroll expander have been

described in this chapter. The scope of work, objectives and methodology of the present work conclude the chapter.

**Chapter 3:** In this chapter, ORC power generation system is assessed with R245fa, R123, Isobutane and R134a as the working fluids. Sensitivity analysis is done to check the weightage of each thermodynamic parameter on the overall performance of the system and the system is optimized for maximum exergy efficiency, to identify the best working fluid. In addition to this, detailed exergy analysis of ORC system is carried out to evaluate the exergy losses within the ORC system.

**Chapter 4:** In this chapter, detailed parametric analysis is carried out to study the variation of evaporator area with key thermodynamic parameters such as evaporator pressure, pinch point temperature difference and expander inlet temperature using a validated Chevron plate evaporator model available in open literature.

**Chapter 5:** In this chapter, effects of expansion ratio, shaft speed and inlet temperature on the efficiency of open drive scroll expander have been examined, using a validated semi-empirical model. This study has been carried out to analyze the off-design performance of the scroll expander.

**Chapter 6:** Cost analysis and exergoeconomic optimization of 1 kW<sub>e</sub> solar driven ORC system and its comparison with the existing solar PV systems is discussed in this chapter.

**Chapter 7:** This chapter concludes the thesis with summary of main findings and presents future perspectives in the field of small scale organic Rankine cycle systems.

## CHAPTER 2

### LITERATURE REVIEW

This chapter presents a comprehensive review of ORC systems which includes selection of working fluids and thermodynamic modelling and optimization of ORC performance metrics such as thermal and exergy efficiencies, cycle net power output as well as economic factors such as levelized energy cost, specific investment cost, total product cost rate, payback period etc. In addition to this, a detailed review has been carried out on the components of ORC such as evaporator and expander. Studies related to modeling of Chevron plate heat exchangers used for ORC application are covered in this chapter. The review also takes into account semi-empirical modeling studies of scroll expanders, as the present study is focussed on low temperature and low capacity ORC systems.

#### 2.1 Exergy analysis of ORC systems

The exergy analysis methodology is a combination of first and second laws of thermodynamics and takes into account the environmental conditions. Exergy analysis is the most appropriate tool for thermodynamic analysis and process optimization of energy conversion systems.

Kas (2014) conducted exergy analysis of organic Rankine cycle for power generation from waste heat recovery in steel industry. Exergy analysis was performed using plant data for two different cases of 262.2 and 203 kW<sub>e</sub> gross power output. R245fa was used as the working fluid. The energy and exergy efficiencies of the two cases were found to be 10.2, 48.5% and 8.8, 42.2% respectively. In addition to this, variation of energy and exergy efficiencies of the system with evaporator pressure, superheating and subcooling were studied. It was found that evaporator pressure had a significant effect on both energy and exergy efficiencies of the ORC.

Safarian and Aramoun (2015) presented energy and exergy evaluation of a basic as well as three different configurations of organic Rankine cycles (ORCs). The configurations

used were, incorporating turbine bleeding, regeneration and combination of both. In case of regeneration, a feed-water heater is incorporated into the ORC. The vapor extracted from the turbine mixes with the feed-water exiting the pump. Ideally the mixture leaves the heater as a saturated liquid at the heater pressure. In turbine bleeding, internal heat exchanger is placed in between the evaporator and the pump. Hence, the fluid is preheated. The results demonstrated that the evaporator had major contribution in the exergy destruction which was improved by increase in its pressure. The results also confirmed that the integrated ORC with turbine bleeding and regeneration had the highest thermal and exergy efficiencies (22.8 and 35.5%) and lowest exergy loss (42.2 kW) compared to other configurations.

He et al. (2017) analysed a 50 kW<sub>e</sub> ORC plant driven by a low grade heat source. Hot side evaporator inlet temperature was varied from 65 to 95 °C. Thermodynamic analysis showed that the maximum net work output and thermal efficiency attained were 46.5 kW and 6.52% respectively. Maximum exergy efficiency of 36.3% was obtained. Exergy analysis showed that evaporation pressure and condensation pressure had a significant impact on the exergy efficiency and the performance of the system.

Mohammadi et al. (2018) compared various heat recovery systems for a cement plant in terms of electricity generation and exergy analysis. Two configurations were used based on the temperature of the heat source; High temperature (HT) and low temperature (LT). In the HT section, dual pressure Rankine cycle, dual pressure organic Rankine cycle (ORC) and a regenerative dual pressure ORC are compared. In the LT section, ORC is compared with a transcritical carbon dioxide cycle. System was optimized to identify the best configuration. For the HT section, regenerative ORC showed the highest exergy efficiency with net power output of 7 MW<sub>e</sub> for a cement factory with the capacity of 3400 ton per day. For the LT section, ORC showed better performance than the transcritical carbon dioxide cycle, but generated power output was lesser at 300 kW<sub>e</sub> when compared to HT section.

Liu et al. (2011) presented the results of thermodynamic model of a 2 kW<sub>e</sub> biomass fired CHP system with organic Rankine cycle (ORC). HFE7000, HFE7100 and n-pentane were used as the working fluids. The highest obtained ORC efficiency was 16.6% with n-pentane as the working fluid. Superheating and sub-cooling had a negative effect on the thermal efficiency. The electrical efficiency of the CHP system varied between 7.5 to 13.5% corresponding to electricity output of 1.5 and 2.71 kW<sub>e</sub> respectively. The main parameters affecting the overall efficiency were hot water temperature of the boiler, ORC condenser cooling water temperature and the ORC working fluid.

Bellos and Tzivanidis (2018) worked on a hybrid organic Rankine cycle (ORC) driven by parabolic trough collectors and waste heat. The temperature of the heat source varied from 150 to 300 °C. In this study, Toluene, cyclohexane, MDM and n-pentane were used as the working fluids. The system was designed in such a way that maximum electricity could be produced using waste heat. The steady state thermodynamic model was developed using Engineering Equation Solver (EES). Results showed that maximum electricity production was achieved with Toluene. For the given set of operating conditions, electricity output ranged between 479 to 845 kW<sub>e</sub> and the system efficiency varied from 11.6 to 19.7%. It was also inferred that, higher the waste heat source temperature, greater was the fraction of the waste heat input in the ORC for all working fluids.

Karellas and Braimakis (2016) carried out energy and exergy analysis of micro-scale trigeneration system capable of combined heating, power generation and refrigeration. The system was a combination of organic Rankine cycle (ORC) and vapor compression cycle (VCC). The heat input to the ORC was through the parabolic trough collectors and biomass boiler. In summer, the system operated in trigeneration mode where, a part of the power generated was utilized to run the VCC and the surplus power was used to generate electricity. Hot water demand was met by the continuous heat removal in the condenser. During winter, the VCC was disconnected and the system operated as a cogeneration unit. R245fa was used as the working fluid. At evaporation temperature of 90 °C, 50 kW<sub>th</sub> heat input and 5 kW<sub>th</sub> cooling load, the system delivered electricity output of 1.42 kW<sub>e</sub>

and heating output of 53.5 kW<sub>th</sub>. The exergy efficiency for full load operation was found to be at 7%.

Mohammadi et al. (2017) analyzed a hybrid system composed of a gas turbine, ORC cycle and an absorption refrigeration cycle. Thermodynamic analysis was carried out to investigate the effect of different parameters on the system performance and output cooling, heating and power. The results showed that the plant can produce 30 kW<sub>e</sub> power, 8 kW cooling and almost 7.2 ton hot water with an efficiency of 67.6%. Parametric studies showed that pressure ratio and gas turbine inlet temperature had a significant impact on the performance of the system.

Senturk Acar and Arslan (2019) performed energy and exergy analysis of integrated solar energy and geothermal energy-powered ORC plant. The net power output, energy, and exergy efficiencies of the geothermal-powered ORC and solar-integrated, geothermal-powered ORC were determined. The solar energy was integrated into the power plant using a thermal energy storage unit. R600a, Therminol VP-1, and molten salt were used as a working fluid in organic Rankine cycle, solar field, and thermal energy storage, respectively. The electrical and exergetic efficiencies of the solar energy-aided, geothermal-powered ORC were calculated as 14.54 and 67.84%, respectively. For the same conditions, the electrical and exergetic efficiency of the geothermal-powered ORC was calculated as 14.56 and 70.91%, respectively. As a result of this study, energy and exergy efficiencies of the geothermal-powered ORC decreased with the integration of solar energy. But the net power output of the system increased.

Al-Sulaiman et al. (2012) presented energy and exergy analyses of a biomass trigeneration system using ORC. Four cases were considered for analysis: electrical-power, cooling-cogeneration, heating-cogeneration and trigeneration cases. The results revealed that the best performance of trigeneration system considered can be obtained with the lowest ORC evaporator pinch temperature of 20 K, and the lowest ORC minimum temperature of 345 K. The study revealed that there is a significant improvement when trigeneration is used, as compared to only electrical power



production. The fuel utilization efficiency increased from 12% for electrical power to 88% for trigeneration. Moreover, the maximum exergy efficiency of the ORC increased from 13 to 28%, when trigeneration was used. Maximum exergy destruction occurred in the biomass burner which contributed to 55% of the total destructed exergy.

El-Emam and Dincer (2013) performed energy and exergy analysis of a novel-type geothermal regenerative ORC. The capacity of the plant was 5 MW<sub>e</sub>. An optimization study was also performed based on the heat exchangers total surface area parameter. Parametric studies were performed to investigate the effect of operating parameters, and their effects on the system energetic and exergetic efficiencies. In addition to this, economic parameters were investigated. The energy and exergy efficiency values were found to be 16.37 and 48.8%, respectively, for optimum operating conditions at a reasonable temperature range of the geothermal water from 78.49 to 116.2 °C.

Selbas and Yilmaz (2016) conducted energy, exergy analyses and sustainability analysis of solar driven ORC. R410a was used as the working fluid. Using the actual solar energy radiation data of Isparta, performance of the cycle was assessed. Furthermore, variations of energy and exergy efficiencies of the ORC system with evaporator and condenser pressures were studied. Results showed that the energy, exergy efficiencies and sustainability index of the system were calculated as 10.6%, 69.2% and 2.8 respectively. It was observed that the evaporation pressure had significant effect on both energy and exergy efficiencies.

Ashouri et al. (2017) performed exergy and energy analysis of a regenerative ORC based on flat plate solar collectors. Key parameters such as exergetic efficiency, thermal efficiency, exergy destruction rate, fuel depletion ratio and irreversibility ratio were investigated. Exergy efficiency and exergy destruction ratio were calculated for the overall system. Four different working fluids were considered including R245fa, R134a, pentane and toluene for evaluation of the system. Results showed that the solar collector, thermal storage tank and the vapor generator were the main sources of exergy destruction. Pentane showed the best performance followed by R245fa, toluene and

R134a. The corresponding daily exergy efficiencies of the 4 working fluids were 24.08, 22.53, 22.09 and 21.76%.

Li et al. (2012) presented energetic and exergetic investigation of an ORC at different heat source temperatures of 70, 80, 90 and 100 °C. R123 was used as the working fluid. The exergy loss associated with the heat exchangers amounted to 74% of the total system exergy loss. The study proposed two-stage heat exchangers to reduce the heat transfer irreversibility in the evaporator and a regenerator to reduce the exergy loss in the condenser.

Kahraman et al. (2018) carried out energy and exergy analysis of ORC system under different heat source and expander inlet temperature conditions using R113, R123 and Isopentane as the working fluids. Key parameters such as heat input to the system, expander work output, thermal efficiency, total exergy destruction and exergy efficiency were determined. At expander inlet temperature of 80 °C and heat source temperature of 110 °C, Isopentane reached maximum thermal efficiency of 8.8% while R113 achieved thermal efficiency of 12.4% for the same design conditions. Results also showed that, in all cases, Isopentane needed more heat input per unit mass compared to other fluids. While the maximum value of 531.7 kJ/kg heat input was required for Isopentane, R113 and R123 fluid required a maximum of 220.2 and 246.8 kJ/kg respectively. In terms of work output, a maximum of 21.63 and 26.98 kJ/kg expander work output were obtained for R113 and R123, while 45.35 kJ/kg expander work output was obtained using Isopentane. In exergy analysis, it was found that the best exergy efficiency performance was obtained using R113 fluid with 56.3%.

## **2.2 Optimization of ORC systems**

Numerous studies are available in scientific literature contributing to the optimization of ORC parameters and performance indices for various low grade heat sources such as solar energy, biomass energy and waste heat recovery. These parameters include both thermodynamic criteria such as thermal and exergy efficiencies, cycle net power output

as well as economic factors such as levelized energy cost, specific investment cost, total product cost rate, payback period etc.

Seyedkavoosi et al. (2017) performed exergetic optimization of organic Rankine cycle (ORC) for waste heat recovery from an internal combustion engine. The working fluids used were R123, R134a and water. System optimization was carried out to maximize net power output and exergy efficiency. The design variables used were operating pressures, pump and expander isentropic efficiencies and exhaust gas temperature. The results showed that R123 was the best working fluid which delivered a power output of 468 kW<sub>e</sub> and exergy efficiency of 21%.

Darvish et al. (2015) performed exergo-economic optimization of a regenerative organic Rankine cycle utilizing a low temperature heat source. Exergy efficiency and cost rate of electricity were chosen as objective functions. Nine working fluids were tested. The degree of superheat and the pressure ratio were chosen as independent variables. R134a and Isobutane delivered the highest energy and exergy efficiencies. At source temperature of 120 °C, the system exergy efficiencies for R134a and Isobutane were 19.6 and 20.3% respectively. The largest exergy destructions occurred in the boiler and the expander. With R134a as the working fluid, the electricity cost rates for the system varied from 0.08 to 0.12 USD/kWh (6 to 9 Rs/kWh), depending on the fuel input cost.

Boyaghchi and Heidarnejad (2015) carried out thermo-economic assessment of solar driven micro combined cooling heating and power cycle integrated with ORC. Thermal storage tank was installed to ensure uninterrupted operation of the system. The system was analyzed and optimized from thermodynamics and economic point of view. The results showed that, for summer mode, the thermal efficiency, exergy efficiency and product cost rate were found to be 23.66%, 9.51% and 5114.5 USD/year, while for winter mode, it was 48.45%, 13.76% and 5688.1 USD/year, respectively. Turbine inlet temperature, turbine inlet pressure, turbine back pressure, evaporator temperature and heater outlet temperature were chosen as the decision variables to investigate the performance of the overall system. The thermal efficiency, exergy efficiency and total

product cost rate were selected as three objective functions and Genetic Algorithm (GA) was employed for optimization of the system. The optimal values for thermal efficiency, exergy efficiency and total product cost rate were found to be 28, 27 and 17% in summer and 4, 13 and 4% in winter respectively.

Imran et al. (2014) performed thermo-economic optimization of basic and regenerative ORC for waste heat recovery application. Thermal efficiency and specific investment cost of basic ORC, single stage regenerative and double stage regenerative ORC was optimized by using Non-dominated Sorting Genetic Algorithm-II (NSGA-II). Maximum thermal efficiency and minimum specific investment cost were selected as objective functions and relative increase in thermal efficiency and cost was analyzed, keeping basic ORC as the reference. Evaporation pressure, superheat, pinch point temperature difference in evaporator and condenser were chosen as the decision variables. R123, R11, R245fa, R141b and R134a are the working fluids which were considered for the analysis. Results showed that R245fa was the best working fluid and basic ORC configuration had low specific investment cost and thermal efficiency compared to regenerative ORC. The average increase in thermal efficiency from basic ORC to single stage regenerative ORC was 1.01% with an additional cost of 187 USD/kW while from basic ORC to double stage regenerative ORC was 1.45% with an average increase in cost of 297 USD/kW.

Thermodynamic modeling of an integrated system consisting of a micro gas turbine, a single pressure heat recovery steam generator (HRSG), an ORC and an multi-effect desalination (MED) was conducted by Ameri and Jorjani (2016). Multi-objective optimization was performed to determine optimized design parameters. Desalination production and the power generation price were chosen as two objective functions. The inlet steam pressure to MED, pinch point temperature difference, evaporator pressure, condenser pressure and refrigerant mass flow rate were selected as design parameters. In addition, the optimization was performed for the different working fluids namely R123, R134a and R245fa. The exergy analysis results showed that the combustion chamber and the HRSG had the highest exergy destruction rate compared to other components. The results also showed that the exergy efficiency increased as the power generation price

decreased and when the compressor pressure ratio increased. Exergy efficiency of the cycle improved by 3%. R134a showed the best exergy efficiency compared to R123 and R245fa.

Barse and Mann (2016) compared constrained ORC system design to non-constrained system design using 12 working fluids. The ORC model was developed using Aspen Hysys tool and validated with data obtained from the literature. The constrained design compared the performance of ORC fluids for a fixed heat exchanger and expander configuration. A non-constrained design was studied by altering the design specifications for the heat exchangers and turbine to match the working fluid. The exergy analysis was used to study exergy destruction across the ORC components. Cost analysis was performed by comparing the levelized cost of electricity (LCOE) for each working fluid in both designs. Non-constrained ORC system design lowered the LCOE for higher critical temperature working fluids such as R601, R601a, R123, R245ca, R245fa, R600, and R236ea. R245ca, R601, and R236ea showed 11, 10, and 9% decrease in LCOE respectively. However, there was no change in efficiency for lower critical temperature ORC fluids such as R236fa and R134a.

Ge et al. (2015) proposed a simplified optimal design method to optimize main thermodynamic parameters for a regenerative ORC driven by flue gas waste heat, using interior penalty function optimization algorithm. Flue gas inlet temperature, evaporation temperature, pinch point temperature & regenerator effectiveness were used as the design variables and net power output was selected as the objective function. R245fa was used as the working fluid. Results showed that the regenerator always increased the flue gas temperature at the exit of the vapor generator, but it reduced the net output of the system. Therefore, when the flue gas inlet temperature is low, the regenerator should not be equipped. However, when the flue gas inlet temperature is high, the regenerator is required to avoid low-temperature dew point corrosion and to maximize the power output.

Baldi et al. (2015) performed optimization of a combined diesel and ORC system for marine application, using GA technique. R236ea, R245fa, MM, MDM, benzene, toluene and cyclopentane were used as the working fluids. Ship operational profile and engine control variables were included in the optimization procedure. Engine brake specific fuel consumption was selected as the objective function. Evaporator pressure, pinch point temperature difference & engine load factor were selected as the design variables. The study found cyclopentane and benzene to be the most suitable fluids. The results indicated that, the application of an optimisation procedure which takes the operational profile into account increased the savings of the installation of an ORC from 7.3 to 11.4% of the original yearly fuel consumption. The results also showed that, including the engine control strategy in the optimisation procedure led to significantly larger fuel savings than the optimisation of the waste heat recovery system alone.

Nazari et al. (2016) proposed a novel steam-organic Rankine cycle to recover the waste heat of a gas turbine. The system consisted of a subcritical steam Rankine cycle that is coupled with a transcritical ORC. Three different organic fluids such as R124, R152a, and R134a were selected to monitor the thermodynamic and exergo-economic performance of the system. Results showed that maximum exergy efficiency and minimum total product cost rate of the system were 57.62% and 396.7 USD/h for the combined cycle with R124 and R152a, respectively. In addition to this, parametric investigation was carried out to investigate the effect of key parameters such as steam turbine inlet pressure, ORC expander inlet pressure, ORC preheater pinch temperature and ORC condensation temperature on exergetic efficiency and total product cost rate of the system. GA was used to conduct a multi-objective optimization of the system with two objective functions including exergy efficiency and total product cost rate. The results of optimization revealed that combined cycle with R152a showed the best performance among the analyzed fluids.

Quoilin et al. (2011) presented the results of thermodynamic and economic optimization of ORC for waste heat recovery application. R245fa, R123, n-butane, n-pentane, R1234yf and Solkatherm were used as the working fluids. Results indicated that, the operating

point for maximum power does not correspond to that of the minimum specific investment cost. The economical optimum and thermodynamic optimum were different for each working fluid. The economical optimum was obtained for n-butane with a specific cost of 2136 €/kW<sub>e</sub>, a net output power of 4.2 kW<sub>e</sub>, and an overall efficiency of 4.47%, while the thermodynamic optimum was obtained for the same fluid with an overall efficiency of 5.22%.

Xi et al. (2013) performed a parametric optimization of regenerative ORC for low grade waste heat recovery using GA. The performances of three different ORC systems including the basic ORC (BORC) system, the single-stage regenerative ORC (SRORC) system and the double-stage regenerative ORC (DRORC) system using six different working fluids were examined. The optimized thermodynamic parameters were turbine inlet pressure, turbine inlet temperature and the fractions of the flow rate of regenerative ORC systems. The maximum exergy efficiencies of the BORC, the SRORC and the DRORC system were 50.61, 55.01 and 56.87%, respectively. The best cycle performance was achieved in DRORC system with an exergy efficiency of 56.87% using R11 as the working fluid.

Wang et al. (2019) studied a novel biomass fired, double pressure ORC based cogeneration (CHP) system. In this study, mathematical model was proposed to evaluate thermodynamic and economic performance of the system. Parametric analysis was performed to investigate the effect of key operating parameters such as inlet pressures of the high pressure (HP) expander and the low pressure (LP) expander, the extracting ratio, and the superheating temperature at the HP expander inlet, on the system performance. Results showed R141b as working fluid performed better than R123. All operating parameters had significant effect on the ORC performance and the overall capital cost rate. An optimization algorithm was developed to determine the best operating condition of system, based on the equilibrium point method. Optimization results showed that the proposed system with R141b delivered net electric power output of 1.66 kW with ORC thermal efficiency of 11.28%, CHP thermal efficiency of 77.7% and capital cost rate of 0.363 USD/h.

Le et al. (2014) carried out thermodynamic and economic optimizations of a subcritical ORC using two pure organic compounds; n-pentane and R245fa, and their mixtures with various concentrations. Two optimization studies were carried out to find the optimal conditions of the system and to determine the best working fluid. Exergy efficiency and LCOE (Levelized Cost of Electricity) were selected as the objective functions. Hot water at temperature of 150 °C and pressure of 5 bar were used to simulate the heat source medium. Cooling water at temperature of 20 °C was considered to be the heat sink medium. The mass flow rate of heat source was fixed at 50 kg/s for the optimization process. Optimization results showed that, the n-pentane-based ORC showed the highest maximum exergy efficiency (53.2%) and the lowest minimized LCOE (0.0863 USD/kWh). In LCOE minimization optimization, n-pentane-based ORC delivered the most profitable cycle: the lowest specific total capital investment (3184 USD/kW), the shortest payback period (10.78 years) and the smallest minimized LCOE (0.0863 USD/kWh). The study also concluded that R245fa based ORC system was least profitable at maximum exergy efficiency.

## **2.3 Review of components in ORC system**

The heat exchange process in the ORC evaporator has been a subject of interest for many researchers. Analysis of heat exchangers using computational fluid dynamics (CFD) is very expensive and time consuming. Moreover, such models cannot be used to study the off design performance of the ORC systems, as it cannot be integrated with the ORC system models. The other alternative is using predetermined heat transfer correlations to estimate the heat exchanger surface area. Some recent studies on heat exchangers in ORC based on heat transfer correlations have been reported in section 2.3.1.

### **2.3.1 Evaporator**

Walraven et al. (2014) compared shell and tube heat exchangers with plate heat exchangers for low temperature ORC applications. Models for heat exchangers used in single-phase flow, evaporation and condensation which are available in open literature were implemented and was incorporated in ORC model. The study concluded that ORCs



with all plate heat exchangers perform better than ORCs with all shell-and-tube heat exchangers.

Imran et al. (2015) presented a hydraulic and thermal design model of a chevron type plate evaporator and conducted an optimization study of its geometrical parameters for a low temperature geothermal ORC system. Geometrical parameters such as length, width and plate spacing were selected as decision variables. The minimum cost of evaporator and minimum pressure drop were chosen as objective functions under constraint of constant heat transfer. Optimization results were presented in the form of Pareto Front solution which is trade-off between pressure drop and cost of evaporator. The minimum cost of evaporator was 1570 USD corresponding to a pressure drop of 125 kPa while the maximum cost was 6988 USD corresponding to a pressure drop of 5.2 kPa. The sensitivity analysis showed that the plate length had a promising effect on pressure drop and cost of evaporator.

Rohmah et al. (2015) analyzed the effect of plate spacing in plate heat exchanger (PHE) which was used as a condenser in low temperature ORC plant. The results showed that the increase in plate spacing had effects on the channel cross sectional area, channel velocity, equivalent diameter, and Reynolds number at both, hot and cold sides of the PHE. These parameters affected the total heat transfer area and total pressure drop which influenced the PHE condenser performance. The design was carried out by calculating condenser capacity in single and two phase zones, estimating overall heat transfer coefficient, and calculating heat transfer area and plate film coefficient. The study concluded that the increase in plate spacing results in increase in total heat transfer area and decrease in total pressure drop within the heat exchanger.

Wang et al. (2013) analyzed an ORC system driven by a low grade heat source. Using the thermodynamic mathematical models of ORC, they examined the effects of key thermodynamic design parameters, including turbine inlet pressure, turbine inlet temperature, pinch temperature difference and approach temperature difference in (heat recovery vapor generator) HRVG, on the net power output and surface areas of both the

HRVG and the condenser using R123, R245fa and isobutane. Considering the economic factor for the system optimization design, a ratio of net power output to total heat transfer area was selected as the performance evaluation criterion. Genetic algorithm was employed to optimize the system performance. The results showed that turbine inlet pressure, turbine inlet temperature, pinch point temperature difference and approach temperature difference had significant effects on the net power output and surface areas of both the HRVG and the condenser. From parametric optimization it was inferred that the ORC system with Isobutane showed the best system performance than that with R123 or R245fa.

Imran et al. (2017) presented thermal and hydraulic optimization of water to water Chevron type plate heat exchanger. The optimization was carried out using the multi objective GA in Matlab optimization environment. The two objective functions were pressure drop of hot side and heat transfer. Sensitivity analysis was performed to analyse the effect of geometrical parameters of heat exchanger on thermal and hydraulic performance. The sensitivity results showed that the heat transfer and pressure drop were greatly affected by the vertical port centre distance, plate spacing and number of thermal plates.

Feng et al. (2015) carried out sensitivity analysis of organic Rankine cycle for low temperature waste heat recovery. Parametric sensitiveness was evaluated for five different parameters of the system. The exergy efficiency and the heat exchanger area per unit net power output were selected as the objective functions for multi-objective optimization. R123 was used as the working fluid. The heat source temperature was maintained at 423 K. The Pareto frontier solution was obtained for maximizing exergy efficiency and minimizing heat exchanger area. The results indicated that increasing the evaporator outlet temperature led to the improvement in thermal efficiency and exergy efficiency. The optimum exergy efficiency and heat exchanger area of the regenerative ORC were 59.93% and  $3.07 \text{ m}^2/\text{kW}$ , which were 8.10% higher and 15.89% lower than that of the basic ORC, respectively.

### 2.3.2 Expander

The most critical component in ORC is the expansion device which converts the available thermal energy into mechanical work. Selection of expanders in ORC systems requires in-depth assessment of different parameters such as power output, expansion ratio, complexity in design, cost and isentropic efficiency. Mathematical models are used for performance characterization of the expanders and to optimize their geometries and operating parameters. Some researchers developed mechanistic models which predict the behaviour of the machine based on their geometry and configuration (Garg et al. 2016; Ma et al. 2017; Oralli et al. 2011). But the geometric models has to be combined with other sub-models such as valve model, internal leakage model, motion equation, heat transfer equation etc. to complete the expander modelling. Hence, it becomes more complicated and cannot be integrated into cycle models. Therefore, empirical and semi-empirical models are preferred. Since, the present study is focussed on low temperature and low capacity ORC systems; the review is restricted to semi-empirical modeling of scroll expanders only.

Dumont et al. (2017) compared various modelling methods for the off-design simulation of ORC systems. Constant-efficiency method, polynomial-based method and semi-empirical method were compared. Measurements obtained on two experimental ORC facilities (3 and 10 kW<sub>e</sub>) were used as reference for the model calibration and evaluation. The study was first applied at a component level and then extended to the characterization of the entire organic Rankine cycle power systems. The results showed that semi-empirical models were the most reliable for simulating the off-design working conditions of ORC systems.

Yang et al. (2018) proposed a semi-empirical model for the study of expansion process within the scroll expander using R1223zd (E) as the working fluid. The model is validated with experimental data based on genetic algorithm. Input parameters were assigned to mass flow rate, expander rotational speed, supply temperature and exhaust pressure. Supply pressure, exhaust temperature and net power were computed as output

results. The maximum deviation between the measured and predicted results was found to be 3.35%, 2.24 K and 6.09% respectively. Polynomial curve fitting showed that the expander isentropic efficiency could be predicted over a wide range with  $R^2 = 97.997\%$ .

Lemort et al. (2009) presented the results of an experimental study carried out on a prototype of an open-drive oil-free scroll expander integrated into an ORC using R123 as the working fluid. By extracting the measurements of expander performance, the parameters of a scroll expander semi-empirical model were then identified. The model was able to compute variables such as the mass flow rate, the delivered shaft power and the discharge temperature. The maximum deviation between the predictions by the model and the measurements were 2% for the mass flow rate, 5% for the shaft power and 3 K for the discharge temperature. The validated model of the expander was finally used to quantify the different losses. This analysis pointed out that the internal leakages, the supply pressure drop and the mechanical losses were the main losses affecting the performance of the expander.

Lemort et al. (2011) presented the results of an experimental study carried out on a prototype of a hermetic scroll expander, integrated into an ORC test rig, whose working fluid is R245fa. The expander was originally a compressor designed for heat pump applications and was characterized by a nominal power input of 2.5 kW<sub>e</sub>. Performance of the expander was evaluated in terms of isentropic effectiveness and filling factor as functions of the main operating conditions. The study also investigated the impact of oil mass fraction on the expander performance. Using the experimental data, parameters of a semi-empirical simulation model of the expander were identified. This model was used to analyze the measured performance of the expander. Finally, a polynomial empirical model of the expander was proposed for fast and robust simulations of organic Rankine cycle systems.

Giuffrida (2014) proposed a generalized semi-empirical model to simulate the performance of the expander for ORC fluids other than R123. This model took correction of heat transfer coefficients into account, according to fluid density, viscosity, specific heat and thermal conductivity. This model was also used to calculate the efficiency of the

simple organic Rankine cycle with the power output fixed at 1, 1.5 and 2 kW<sub>e</sub> and the differences were noted for other working fluids. Results suggested that R141b is better than R123 in terms of cycle efficiency. However, considering the environmental regulations for phasing out HCFC's, the new R1233zd (E) was found to be a potentially interesting fluid for studying a low-temperature ORC system.

The review shows that significant amount of work has been done on thermodynamic analysis and optimization of various configurations of ORC systems. However, studies related to standalone ORC systems for small scale applications (1-5 kW<sub>e</sub>) are limited in open literature. Chevron plate heat exchangers are preferred over shell and tube heat exchangers for small scale ORC systems. It is observed from the review that sizing of the chevron plate heat exchanger evaporator for micro ORC systems using thermo-hydraulic models are less explored. Although the open literature gives lot of information on semi-empirical modeling of scroll expanders and its performance characterization, more needs to be explored to understand the behavior of the scroll expander under varying operating conditions such as shaft speed, expansion ratio and expander inlet temperature.

## **2.4 Research objectives**

- To carry out sensitivity analysis and thermodynamic optimization of organic Rankine cycle (ORC) for selection of working fluid and to analyze the off-design behavior of the ORC system.
- To study the magnitude and distribution of exergy losses within the ORC system and also to investigate the losses with respect to key thermodynamic parameters such as expander inlet pressure, superheat, condensation temperature and pinch point temperature difference.
- To investigate the effect of key thermodynamic and geometric parameters on the plate heat exchanger evaporator surface area using a three zone evaporator steady state model.

- Parametric investigation of scroll expander using a validated semi-empirical model to study the effect of expansion ratio, shaft speed and inlet temperature on its performance.
- Cost analysis and exergo-economic optimization of solar driven ORC system.

## **2.5 Motive and scope of the present work**

It is evident from the open literature that, research works on standalone micro ORC systems are limited. Most of the scientific studies on ORC systems have mainly focused on ORC as bottoming cycle or is used in trigeneration or co-generation applications. In ORC systems, the temperature drop across the expanders is less. Net work output per unit mass of the working fluid is small in ORC plants. In order to achieve higher power output (greater than 10 kW<sub>e</sub>), mass flow rate of working fluids has to increase. This will increase the size and cost of the ORC system. Therefore, it is reasonable to adopt small capacity ORC systems (1-5 kW<sub>e</sub>). This feature makes them attractive in the scenario of DPG systems, where low-temperature thermal energy can be exploited. In particular, the development of mini ORC technologies, suitable for residential applications (1-5 kW<sub>e</sub>), has received more attention over the last few years (Galloni et al. 2015; Lemort et al. 2011; Muhammad et al. 2015; Ziviani et al. 2018) but satisfactory efficiencies has been one of the major drawback. Selection of ORC working fluid is equally important to enhance the performance output for a given ORC system and the system has to be optimized for a particular working fluid. ORC systems has been largely used for waste heat recovery systems in industrial applications and as bottoming cycle in combination with other applications such as internal combustion engines, desalination, geothermal etc. In addition to this, the other advantages of using ORC systems are compact design, easy installation and environmentally friendly. Studies related to analysis of Chevron type plate heat exchangers used in ORC systems are limited in open literature. Heat transfer correlations will help in sizing of heat exchangers for ORC systems without using computational techniques such as CFD, which is tedious and expensive. Although, positive displacement expanders are suitable for small capacity plants, they are characterized by poor expansion efficiency (<75%). Therefore, this area

needs focus, to improve the overall energy conversion efficiency. It was revealed from the scientific literature that, studies on performance characterization of scroll expanders using semi-empirical modeling techniques are limited. Studies on economic analysis of ORC systems are also limited in open literature.

## **2.6 Methodology**

Research methodology has been detailed in the form of flowchart in Figure 2.1. In this study, sensitivity analysis is carried out to investigate the effect of some important thermodynamic parameters such as expander inlet pressure, expander inlet temperature, condensation temperature and pinch point temperature difference, on the performance of the ORC system. Energy and exergy analysis has been conducted to identify the location and magnitude of the losses within the ORC system and to optimize the system for maximum exergy efficiency. Effort has been made to study the effect of thermodynamic and geometric parameters on the size and cost of the chevron type plate evaporator, using a three-zone evaporator model. Parametric investigation of the scroll expander is carried out using semi-empirical scroll expander model to study the effect of expansion ratio, shaft speed and inlet temperature on the performance of the expander. Finally, cost analysis and exergoeconomic optimization of 1 kW<sub>e</sub> driven solar ORC system is performed and a comparison is made with the existing solar PV systems in India.

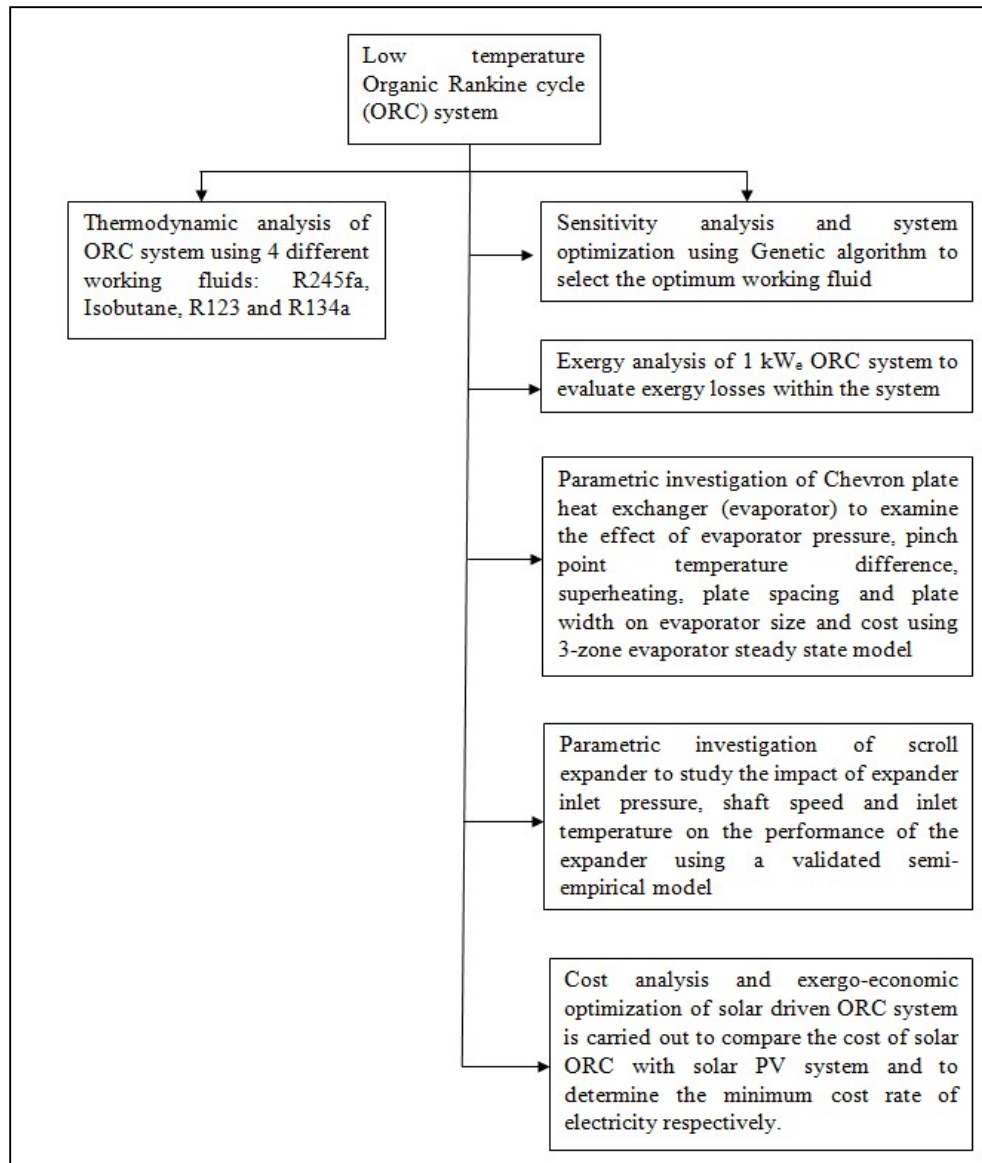


**Figure 2.1:** Research methodology of the present study



## CHAPTER 3

### ENERGY AND EXERGY ANALYSIS OF MICRO ORGANIC RANKINE CYCLE SYSTEM

The exergy analysis methodology is a combination of first and second laws of thermodynamics which takes into account the environmental conditions. It is the most appropriate tool for thermodynamic analysis and process optimization (Al-Sulaiman et al. 2012; Ashouri et al. 2017; Cihan and Kavasogullari 2017; Pei et al. 2010; Seyedkavoosi et al. 2017). Exergy is a measure of the maximum capacity of a system to perform useful work as it proceeds to a specified final state in equilibrium with its surroundings. Every substance not in equilibrium with its environment has some quantity of exergy, while a system that is in equilibrium with its environment has zero exergy since it has no ability to produce work with respect to its environment. Exergy destruction is the measure of irreversibility that is the source of performance loss. Exergy analysis assessing the magnitude of exergy destruction identifies the location, the magnitude and the source of thermodynamic inefficiencies in a thermal system. Therefore, energy analysis based on first law of thermodynamics does not give a clear picture of the irreversibilities occurring within the system. In contrast, the second law efficiency or exergy efficiency gives a realistic view of different components of ORC system for evaluation of system performance and exergy losses.

The selection of the working fluid plays a key role in ORC design in order to achieve efficient and safe operation. Ideally the working fluids should have a high enthalpy drop across the expander to achieve higher power output, higher latent heat for compactness of the ORC module, favourable thermophysical properties, such that the ORC fluids does not suffer from chemical deterioration and decomposition at higher temperatures, higher thermal conductivity, low viscosity, lower operating pressures, non-toxic, non-corrosive that is compatible with equipment material and must be non-flammable. After evaluation of variety of substances comprehensively from previous works based on thermodynamic properties, cost, stability etc. the major working fluids investigated in this study of a small-scale basic ORC system are R245fa, R123, Isobutane

and R134a (Wang et al. 2013). The thermo physical properties and other aspects related to the chosen working fluids are listed in Table 3.1.

**Table 3.1:** Properties of the selected ORC working fluids (Wang et al. 2013)

<b>Working fluid</b>	<b>Molecular mass (kg/k mol)</b>	<b>Critical temperature (°C)</b>	<b>Critical pressure (bar)</b>	<b>Boiling point (°C)</b>	<b>ODP</b>	<b>GWP</b>
R245fa	134.05	154.01	36.4	15.14	0	950
R123	152.93	183.68	36.68	27.82	0.02	77
Isobutane	58.12	134.7	36.3	-11.73	0	20
R134a	102.03	101.06	40.6	-26.07	0	1430

In this study, a small-scale ORC power generation system is assessed. The working fluids used are R245fa, R123, Isobutane and R134a. The organic Rankine cycle is modeled based on the laws of mass and energy conservations. This helps in studying the off-design performance of the ORC system. A parametric investigation has been carried out to study the impact of key thermodynamic parameters such as expander inlet pressure, expander inlet temperature, condensation temperature and pinch point temperature difference (PPTD), on the performance of the system. Sensitivity analysis is done to check the weightage of each parameter on the overall performance of the system. Genetic algorithm optimization technique is adopted to find the optimal parameters for each working fluid, at which maximum exergy efficiency is achieved. In the second part of this work, detailed exergy analysis of small scale ORC system is carried out to evaluate the exergy losses in ORC components and to analyze the performance of the system from the exergy analysis viewpoint. Parametric investigation is performed to study the effect of evaporator pressure, condenser pressure, pinch point temperature difference, superheating and dead state temperature on energy & exergy efficiencies and irreversibilities within the system.

### 3.1 System description

In this study, ORC power generation system which is driven by low grade heat energy is assessed. The working fluids analyzed are R245fa, R123, Isobutane and R134a. The working principle of ORC is analogous to the conventional steam Rankine cycle. The ORC subsystem consists of a pump, an evaporator, an expander and a condenser as shown in Figure 3.1. ORC comprises of the following processes.

2-3: Isobaric absorption of heat to produce high pressure vapor in the evaporator.

3-4s: Isentropic expansion of the pressurized vapor through the expander

3-4: Actual expansion of the pressurized vapor through the expander

4-1: Isobaric rejection of heat in the condenser

1-2: Actual compression of the working fluid in the pump.

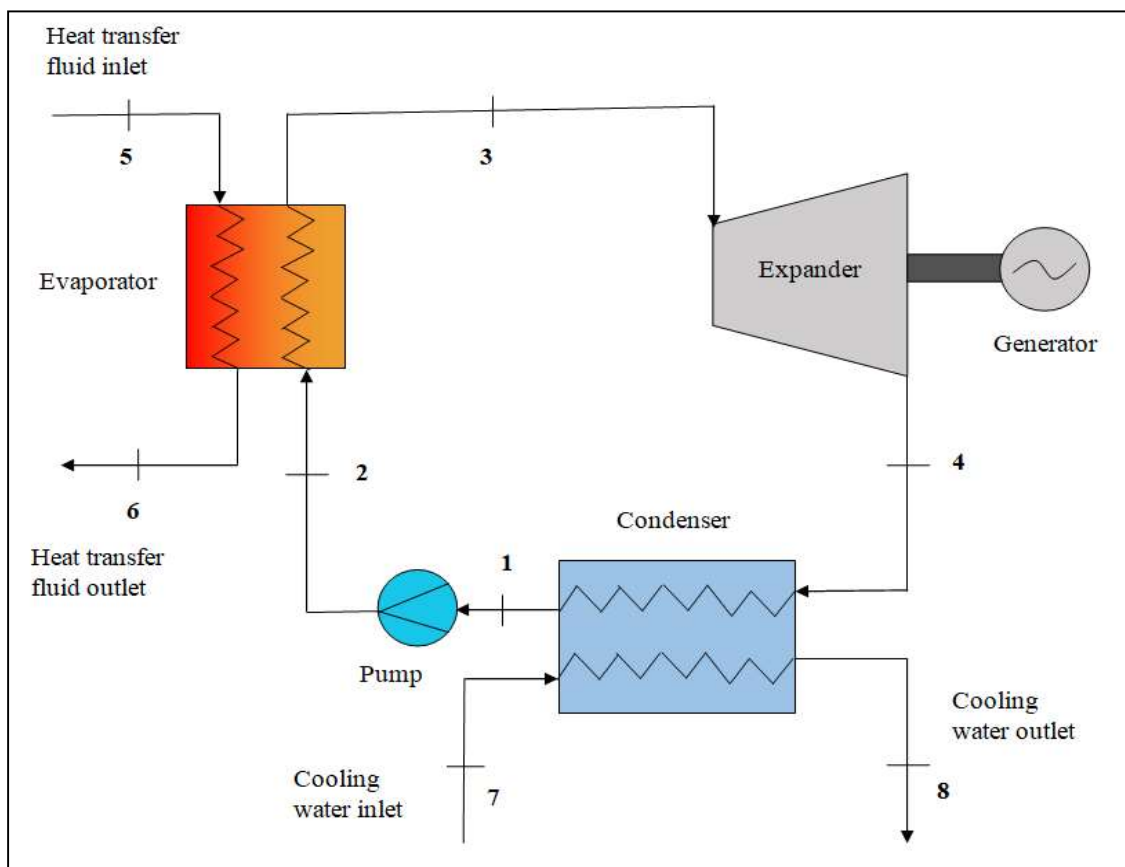


**Figure 3.1:** Schematic demonstration of a low temperature ORC system

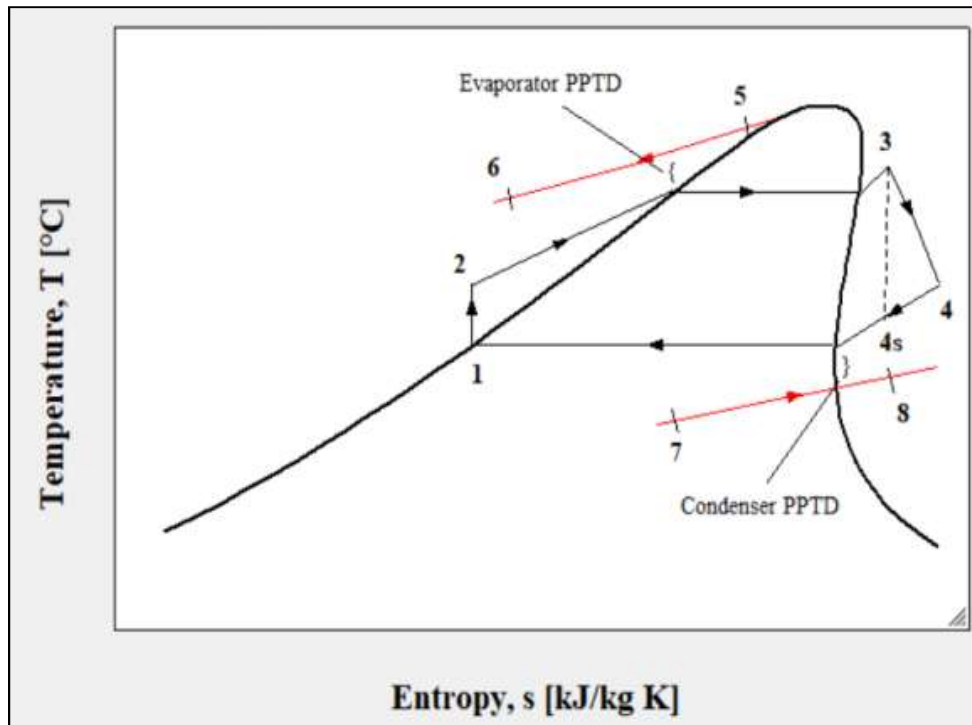


**Figure 3.2:** Temperature-entropy (T-s) diagram of R245fa

All the processes are shown in T-s diagram of R245fa which is depicted in Figure 3.2. Working fluid is delivered by the pump into the evaporator where heat exchange occurs from external heat source to the working fluid. The pressurized vapor passes through the turbine, where it expands and rotates the shaft. Power is produced by the electric generator which is coupled to the turbine. Lastly, the ORC fluid enters the condenser where the heat rejection occurs. The working fluid then returns to the pump to complete the cycle.

### 3.2 Thermodynamic model of ORC system

The organic Rankine cycle is modeled based on the laws of mass and energy conservations. General expressions of mass and energy balances of any steady state control volume, by neglecting the potential and kinetic energy changes is expressed as:

$$\sum \dot{m}_{in} = \sum \dot{m}_{out} \quad (3.1)$$

$$\dot{Q} + \dot{W} = \sum \dot{m}_{out} h_{out} - \sum \dot{m}_{in} h_{in} \quad (3.2)$$

where, subscripts ‘in’ and ‘out’ represent the inlet and exit states, ‘Q’ and ‘W’ are the net heat and work inputs (Kas 2014).

Certain assumptions were made to simplify the analysis. These are as follows:

- a) The calculated points are obtained when the system has reached steady state.
- b) The working fluid is in saturated liquid state at the condenser outlet.
- c) The dead state temperature and pressure are 25 °C and 1 bar (atmospheric) respectively.
- b) Isentropic efficiency of pump and expander are constant at 70%.
- c) Pressure drops in heat exchangers and connecting pipes are neglected.
- d) The fouling effects of the heat exchanger are negligible.

**Table 3.2:** Design conditions of ORC system

SI No	Name	Value	Unit
1	Specific heat of the heat transfer fluid	4.19	kJ/kg °C
2	Isentropic efficiency of pump	70	%
3	Isentropic efficiency of expander	70	%
4	Mass flow rate of the heat transfer fluid	0.3	kg/s
5	Temperature at dead state	25	°C
6	Pressure at dead state	1.0	bar

The input conditions for the thermodynamic analysis are tabulated in Table 3.2. The details of the mathematical model are expressed as follows:

Pump work is calculated as,

$$\dot{W}_{pp} = M_1 \times v_1 \times \frac{(P_2 - P_1)}{\eta_{pp}} \quad (3.3)$$

The heat addition in the evaporator,

$$\dot{Q} = M_1 \times (h_3 - h_2) \quad (3.4)$$

Isentropic efficiency of the expander is calculated as the ratio of actual work done by the expander to that of the isentropic work done by the expander.

$$\eta_t = \frac{(h_3 - h_4)}{(h_3 - h_{4s})} \quad (3.5)$$

Actual work done by the expander,

$$\dot{W}_t = M_1 \times (h_3 - h_4) \quad (3.6)$$

For a given isentropic efficiency of the expander, the actual work done by the expander can be calculated as,

$$\dot{W}_t = M_1 \times (h_3 - h_{4s}) \times \eta_t \quad (3.7)$$

The thermal efficiency is calculated as,

$$\eta_{th} = \frac{\dot{W}_t - \dot{W}_{pp}}{\dot{Q}} \quad (3.8)$$

The exergy efficiency is given by,

$$\eta_{exg} = \frac{\dot{W}_t - \dot{W}_{pp}}{\dot{E}_{in}} \quad (3.9)$$

$$\eta_{exg} = \frac{\dot{W}_t - \dot{W}_{pp}}{M_2 \times [(h_5 - h_6) - T_o (s_5 - s_6)]} \quad (3.10)$$

### **3.3 Parametric analysis**

Parametric investigation is carried out by varying single parameter while keeping all other parameters constant. Four key thermodynamic parameters such as expander inlet temperature, expander inlet pressure, condensation temperature and pinch point temperature difference are analysed and its impact on net work output, mass flow rate, thermal and exergy efficiencies are studied in detail.

#### **3.3.1 Expander inlet temperature**

This analysis is based on the assumption that various ORC fluids at the inlet of expander are in superheated condition (degree of superheat is maintained at 5 °C) and the inlet pressure of expander was kept constant for each working fluid. (R245fa at 3.43 bar, R123 at 2.13 bar; Isobutane at 6.84 bar; R134a at 13.19 bar). The condensation temperature was set to 35 °C, heat source temperature and pinch point temperature difference was fixed at 100 and 5 °C respectively.

The variations of net work output, mass flow rate of ORC working fluid, enthalpy drop across the expander, thermal and exergy efficiency with expander inlet temperature has been illustrated in Figure 3.3 to Figure 3.7. It can be seen that the increase of expander inlet temperature yields an increase in enthalpy drop across the expander increases and decrease in mass flow rate of the ORC working fluid. Since the evaporation temperature and the pinch point temperature difference (PPTD) remains constant, a higher enthalpy difference is attained as a result of increasing expander inlet temperature. Hence, the mass flow rate of the ORC working fluid decreases according to energy balance. The increase in enthalpy difference across the expander is lesser than the decrease in mass flow rate of the working fluid. Thus, the net work output reduces. The thermal efficiency increases accordingly and exergy efficiency shows a slight reduction.

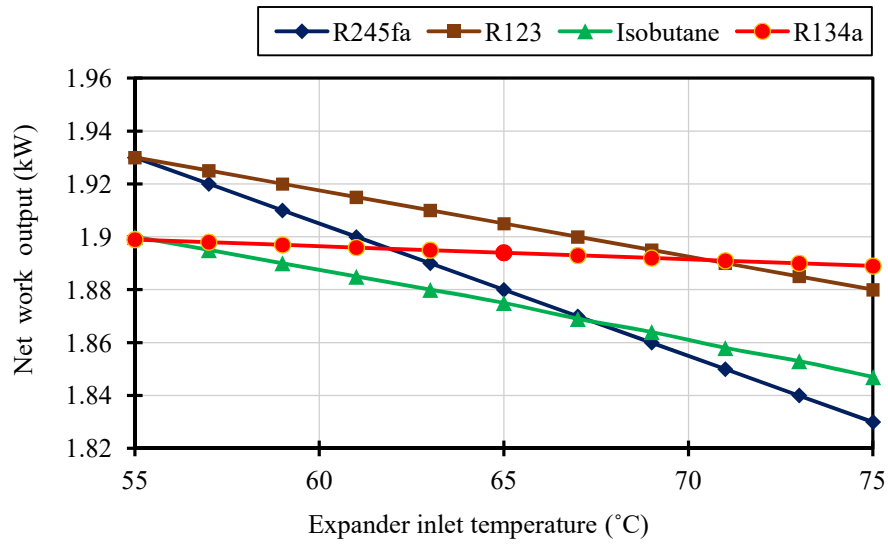


**Figure 3.3:** Effect of expander inlet temperature on net work output

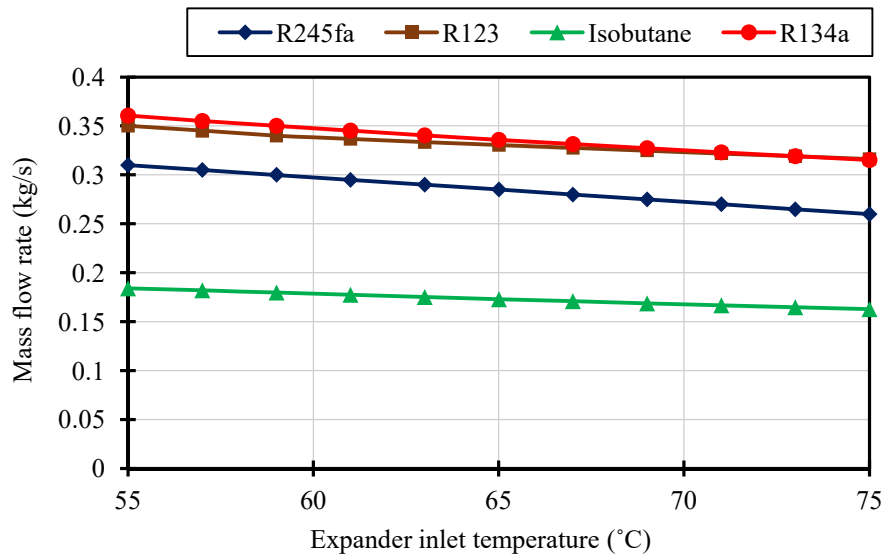


**Figure 3.4:** Effect of expander inlet temperature on working fluid mass flow rate



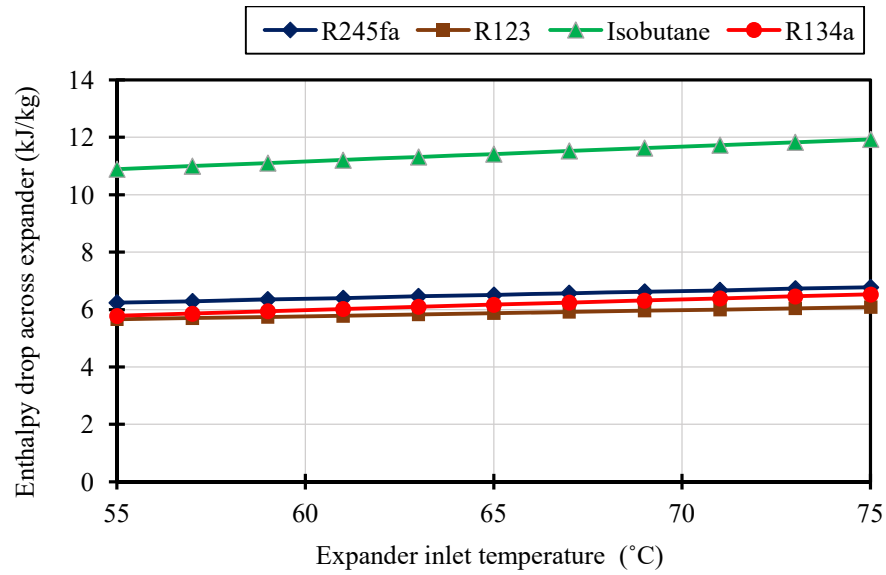


**Figure 3.5:** Effect of expander inlet temperature on enthalpy difference across the expander

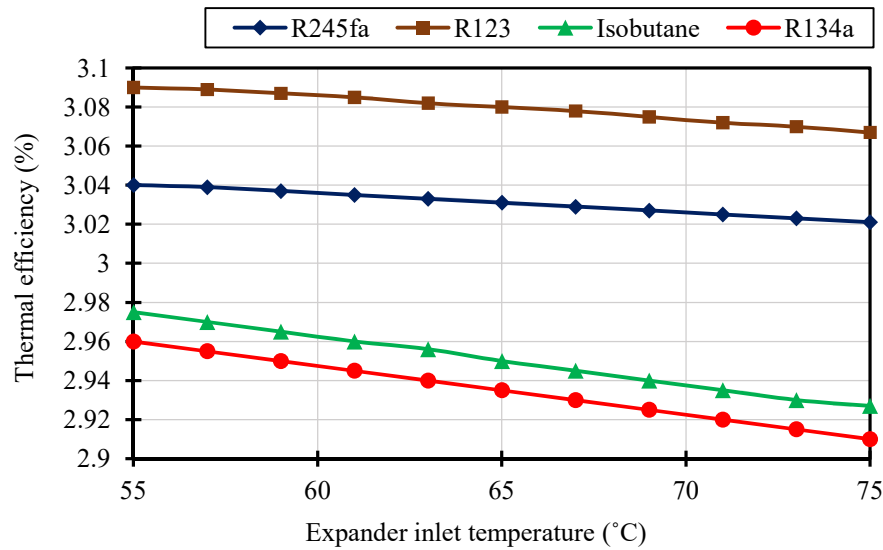


**Figure 3.6:** Effect of expander inlet temperature on thermal efficiency

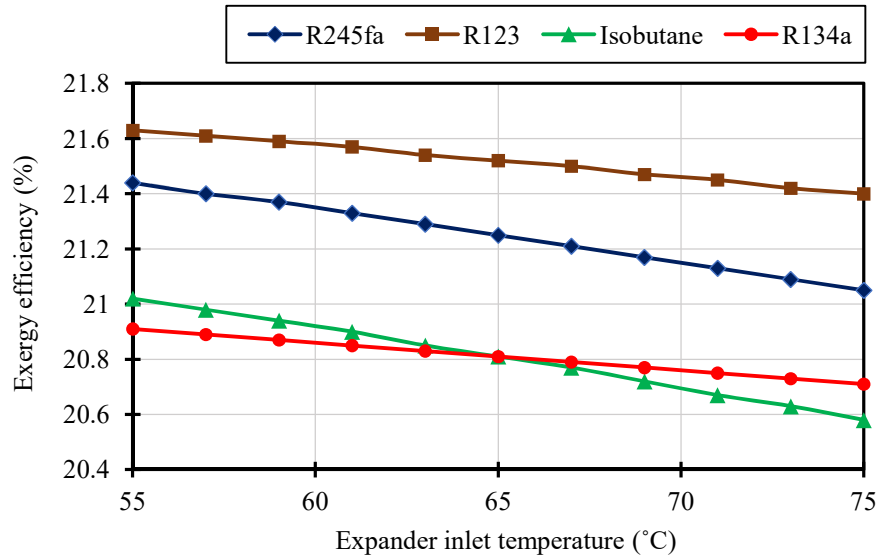


**Figure 3.7:** Effect of expander inlet temperature on exergy efficiency

### 3.3.2 Expander inlet pressure

Expander inlet temperature was set to 70 °C, condensation temperature was maintained at 35 °C and pinch point temperature difference was set to 5 °C. Depending on the design constraints, different range of operating pressure was used for different working fluids (R245fa: 3 bar to 8 bar, R123: 2.5 bar to 3.5 bar, Isobutane: 6 bar to 11 bar & R134a: 12 bar to 20 bar). It is observed from Figure 3.8 to Figure 3.12 that, with the increase in expander inlet pressure, the net work output increases at first and then decreases, Moreover, the thermal efficiency and overall exergy efficiency keeps increasing with increase in expander inlet pressure. The increase in expander inlet pressure results in an increase in enthalpy difference across the expander and a reduction in mass flow rate. Thus, increase in net work output is because of the increase in enthalpy difference across the expander. When the inlet pressure is raised further, the reduction in mass flow rate becomes more dominant and hence, the net work output reduces. The maximum net work output is observed at 5.5 bar for R245fa, at 3.2 bar for R123, at 10 bar for Isobutane and at 19 bar for R134a. Due to higher enthalpy difference in expander at higher inlet

pressure, the thermal efficiency and exergy efficiency also shows an increasing trend with increase in expander inlet pressure.

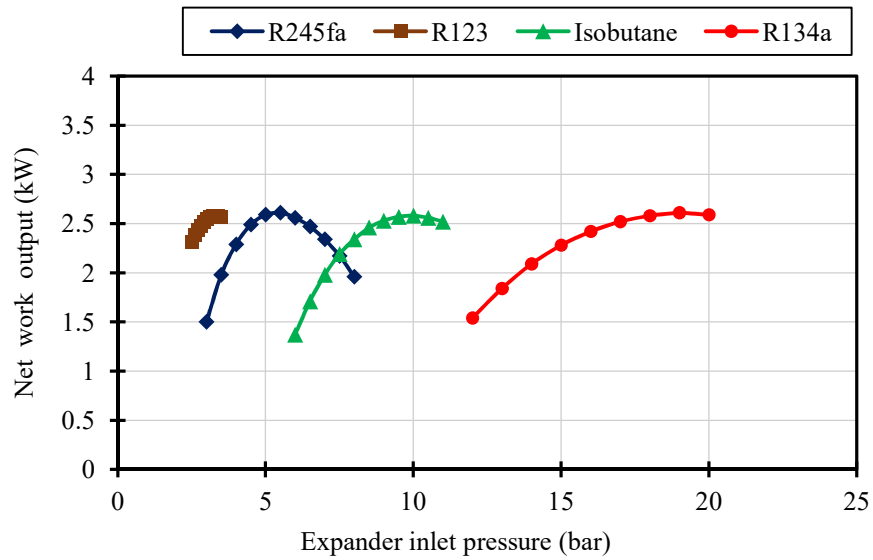


**Figure 3.8:** Effect of expander inlet pressure on net work output

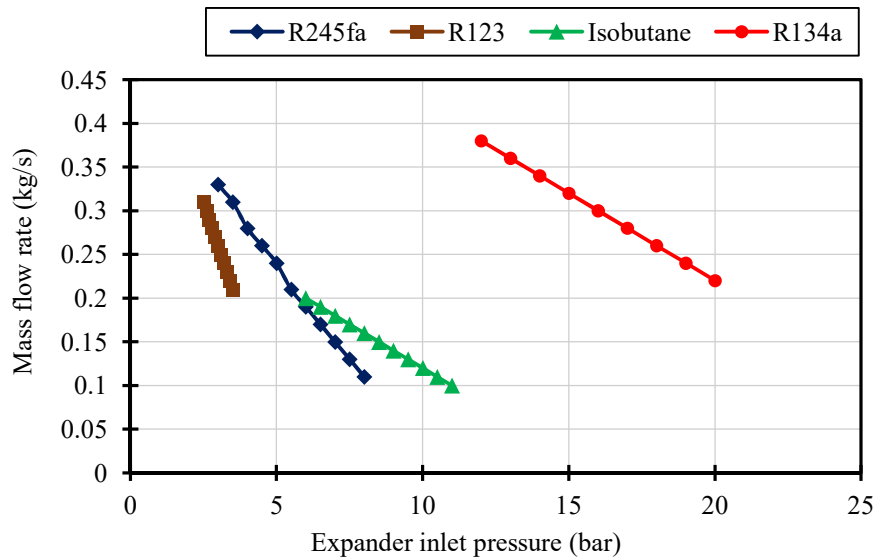


**Figure 3.9:** Effect of expander inlet pressure on working fluid mass flow rate

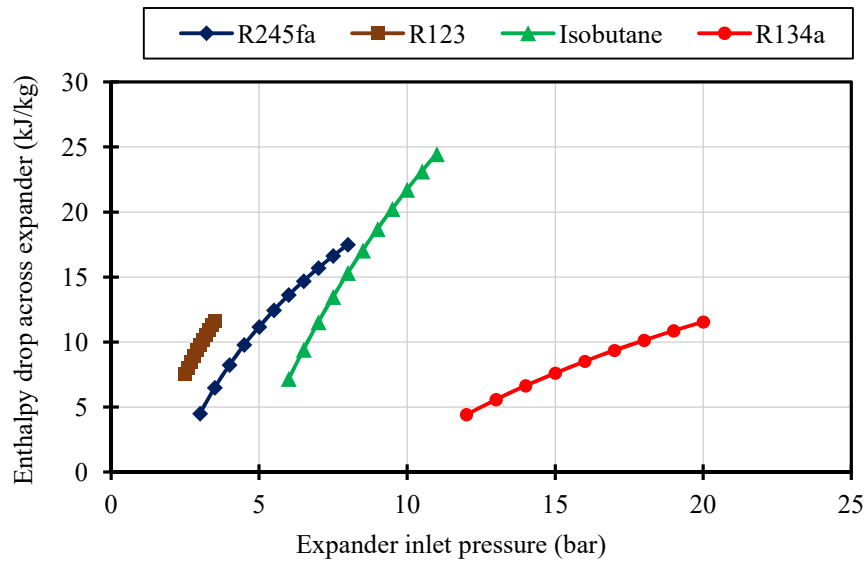


**Figure 3.10:** Effect of expander inlet pressure on enthalpy difference across the expander

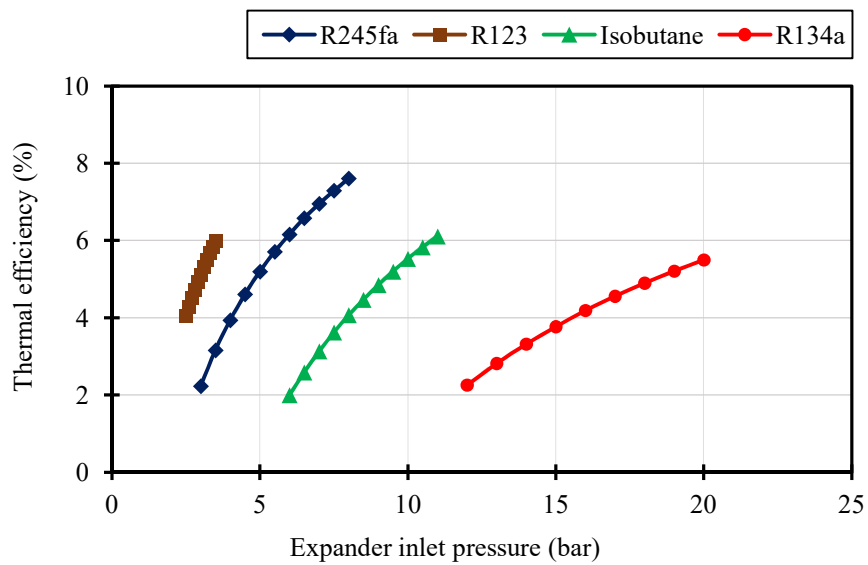


**Figure 3.11:** Effect of expander inlet pressure on thermal efficiency

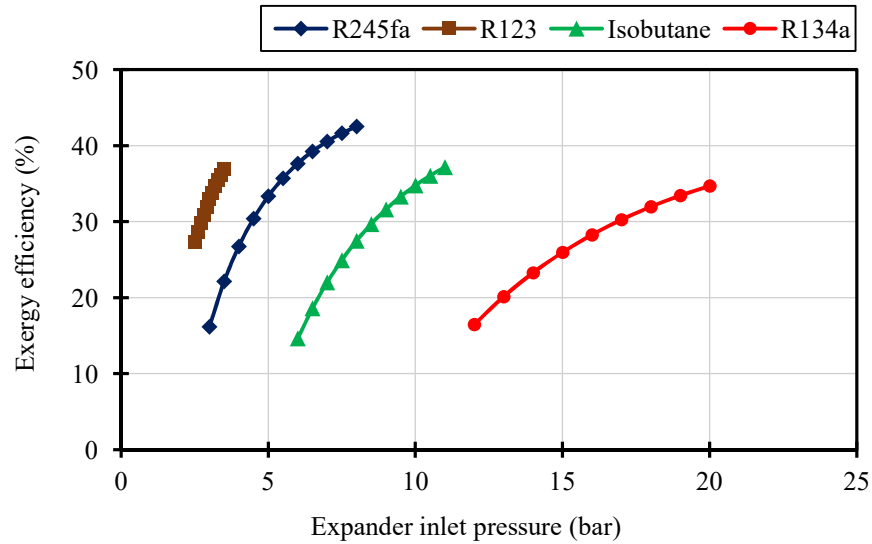


**Figure 3.12:** Effect of expander inlet pressure on exergy efficiency

### 3.3.3 Effect of Pinch point temperature difference

Pinch point temperature difference (PPTD) is an important aspect in heat exchanger design. Lesser the PPTD, evaporator size increases. The PPTD is defined as the temperature difference between hot water exit temperature from evaporation zone and saturation temperature corresponding to evaporation pressure. Figure 3.13 to Figure 3.17 highlights the effect of PPTD on the performance of the system. Evaporation pressure was kept constant for each working fluid (R245fa at 6 bar; R123 at 4 bar, Isobutane at 8 bar and R134a at 20 bar). Heat source temperature and the condensation temperature were set to 100 and 35 °C respectively. The PPTD was varied from 6 to 20 °C and its effect on all thermodynamic parameters was analyzed. The analysis showed that with the increase in PPTD, the net work output and exergy efficiency decreases, while the enthalpy difference across the expander and the thermal efficiency remains constant. When PPTD increases, the mass flow rate decreases resulting in the reduction in net work output. It shows less heat is being utilized in the evaporator region as the PPTD is increased. However, PPTD has no influence on enthalpy drop across the expander and thermal efficiency.

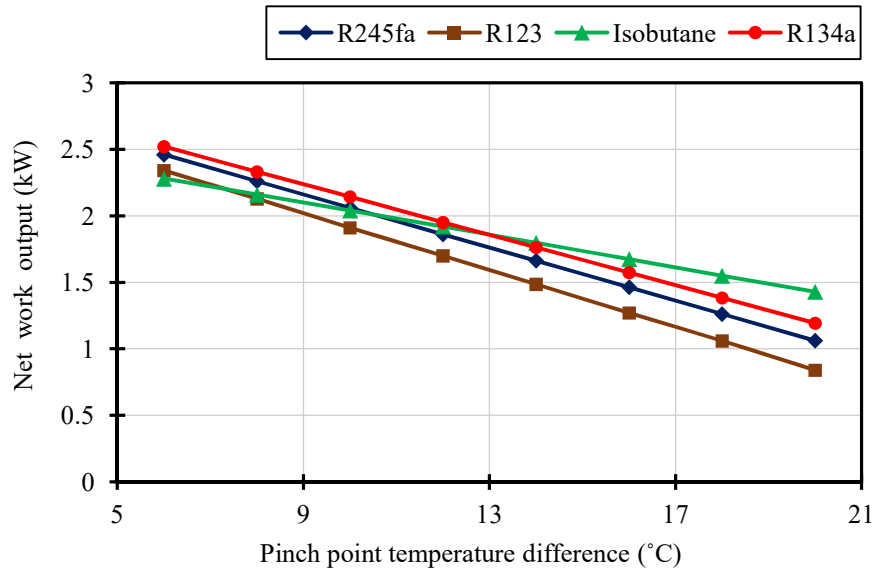


**Figure 3.13:** Effect of pinch point temperature difference on net work output

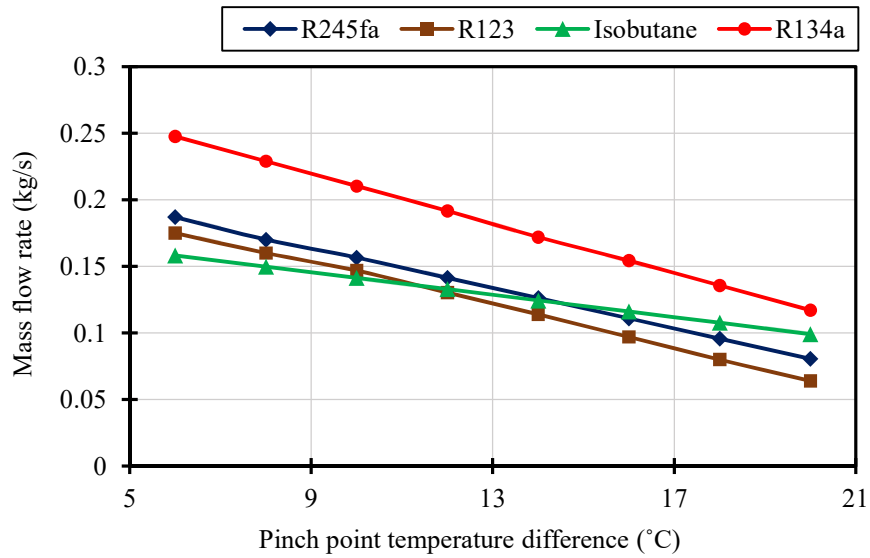


**Figure 3.14:** Effect of pinch point temperature difference on working fluid mass flow rate

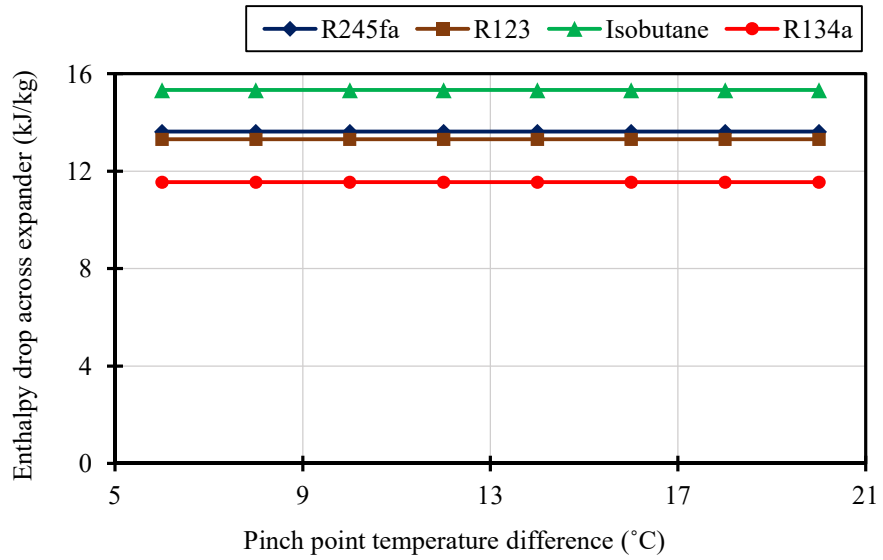


**Figure 3.15:** Effect of pinch point temperature difference on enthalpy difference across the expander

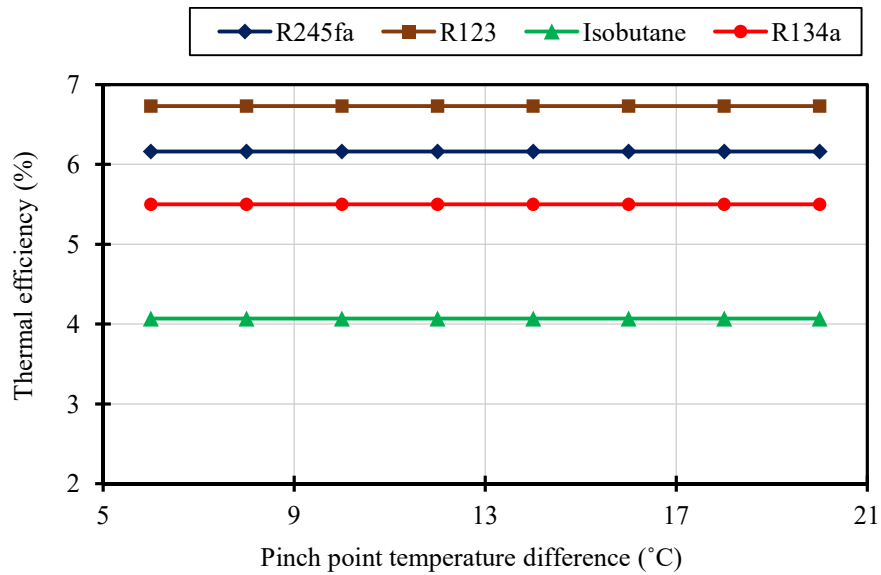


**Figure 3.16:** Effect of pinch point temperature difference on thermal efficiency

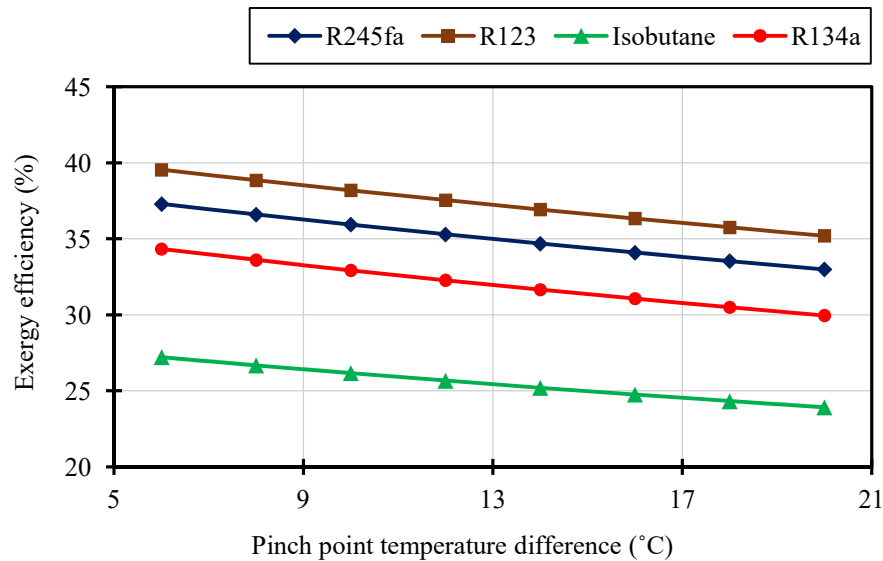


**Figure 3.17:** Effect of pinch point temperature difference on exergy efficiency

### 3.3.4 Effect of condensation temperature

The condensation temperature is an important criterion to be considered while examining the system performance. Evaporation pressure was set constant for each working fluid (R245fa at 6 bar; R123 at 4 bar, Isobutane at 8 bar and R134a at 20 bar). Heat source temperature and PPTD in condenser was set to 100 and 5 °C respectively. The condensation temperature was set to vary from 30 to 40 °C. The state of the fluid at entry of the expander is superheated (with a degree of superheat of 5°C). Figure 3.18 to Figure 3.22 depicts the variation of system performance with condenser temperature. The net work output, thermal efficiency and exergy efficiency decreases with increase in condensation temperature. Higher thermal efficiency is obtained by decreasing the condensation temperature, as more work can be extracted from the expander for a given expander inlet temperature. With the increase in condensation temperature, it is observed that the enthalpy difference across the expander reduces and the mass flow rate of the working fluid remains the same. As a result, the net power output also shows a decreasing trend with the increase in condensation temperature, because less energy is available for extraction. As a result, enthalpy difference across the expander, thermal efficiency and exergy efficiency reduces.



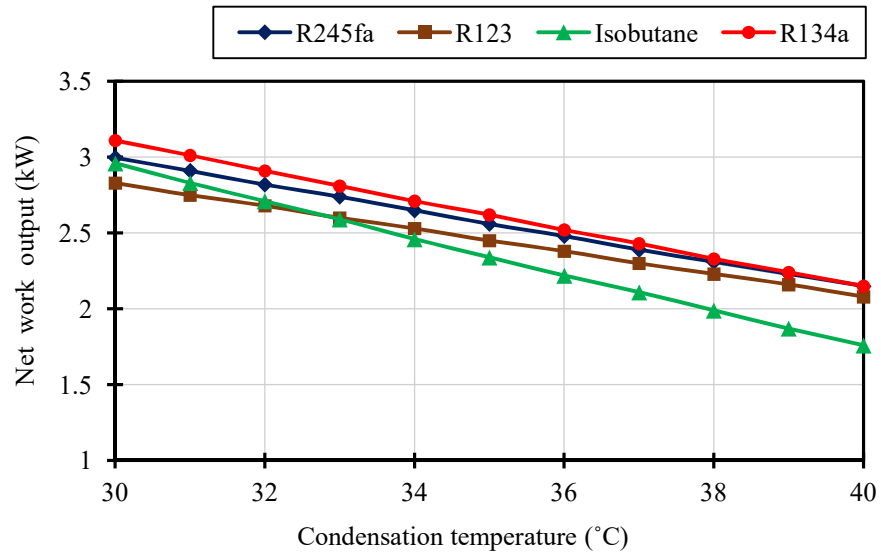


**Figure 3.18:** Effect of condensation temperature on net work output

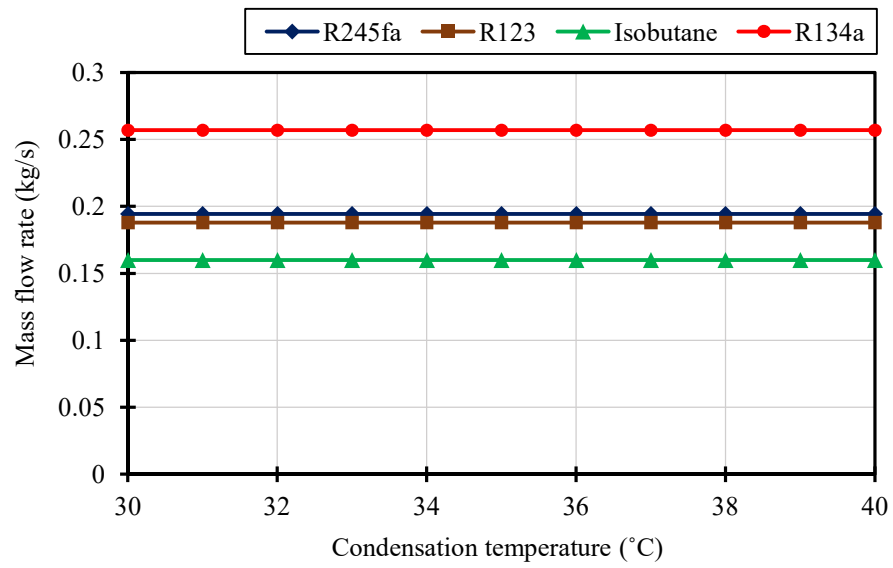


**Figure 3.19:** Effect of condensation temperature on working fluid mass flow rate

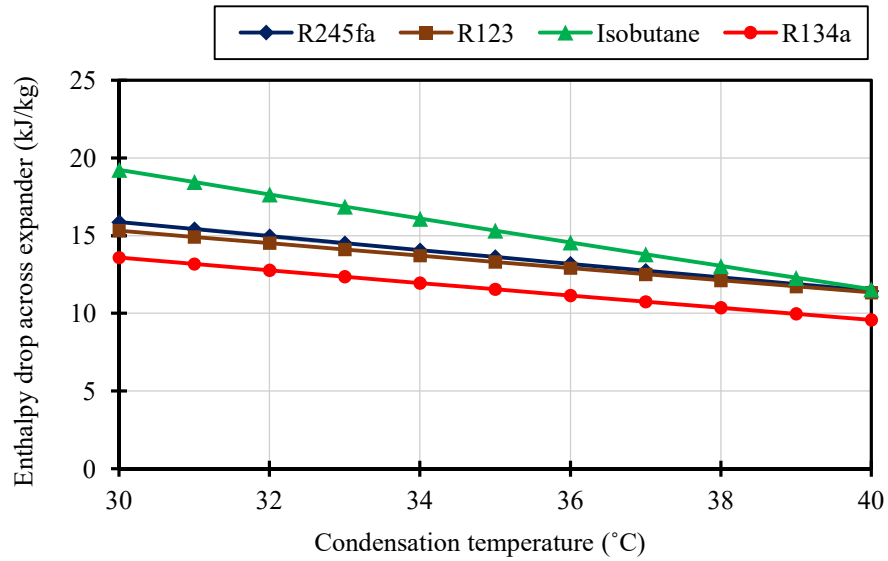


**Figure 3.20:** Effect of condensation temperature on enthalpy difference across the expander

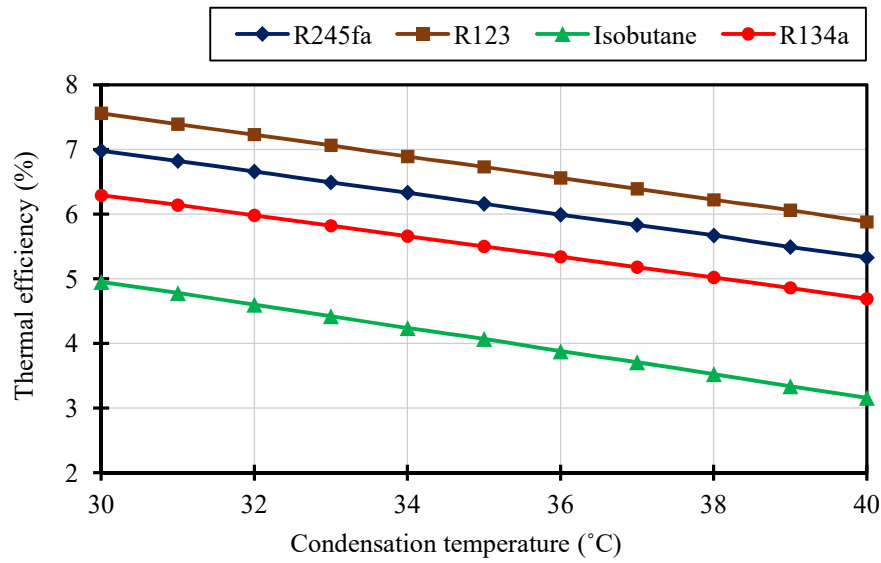


**Figure 3.21:** Effect of condensation temperature on thermal efficiency

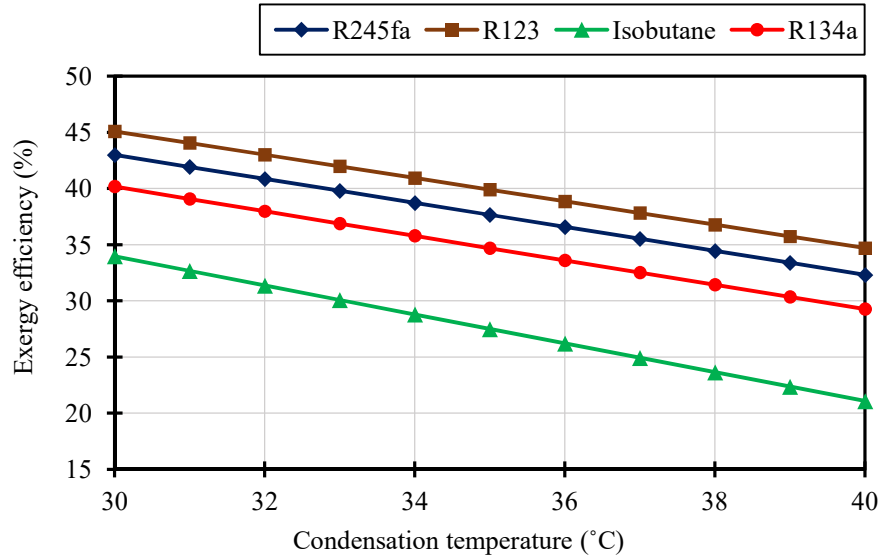


**Figure 3.22:** Effect of condensation temperature on exergy efficiency

### 3.4 Sensitivities of system parameters

Sensitivity analysis is a process to determine the derivatives of system performance parameters with respect to operational parameters. Degree of sensitiveness of each parameter is calculated as the ratio of two infinitesimal quantities. For e.g. the ratio of difference in thermal efficiency to the corresponding difference in expander inlet pressure is calculated to know the sensitivity of thermal efficiency with respect to expander inlet pressure. Similarly, the tabulation is done for all parameters and all working fluids. The average derivatives for R245fa, R123, Isobutane and R134a are presented in Table 3.3, 3.4, 3.5 & 3.6 respectively.

From the analysis, it is evident that the expander inlet pressure has the highest degree of sensitiveness. Considering the net power output, the highest average derivatives of 0.35, 0.3, 0.25 and 0.13 is obtained for R245fa, R123, Isobutane and R134a respectively. In the case of R245fa, this is about 70 times greater than that of expander inlet temperature, 3 to 4 times greater than that of condensation temperature and pinch point temperature difference. Hence, it is preferable to increase expander inlet pressure to

improve net work output, followed by decreasing condensation temperature and pinch point temperature difference.

When R245fa is used, expander inlet temperature, whose average derivative is 0.0000095, hardly makes any impact on thermal efficiency. In case of exergy efficiency, the average derivative for the expander inlet temperature is 0.00017. However, average derivatives with respect to expander inlet pressure (0.011 for thermal efficiency, 0.056 for exergy efficiency) show that expander inlet pressure seems to make a significant impact on the thermal and exergy efficiencies. The average derivative of 0.35 for net work output shows that there is a tremendous improvement in the expander work output when the expander inlet pressure is increased. Variation in PPTD has zero change on the thermal efficiency. Furthermore, very little impact is made by PPTD on the exergy efficiency (0.0031) also. Hence, expander inlet pressure should be increased to enhance the system performance. Condensation temperature should also be reduced to achieve maximum performance. Other working fluids also exhibited similar trend.

**Table 3.3:** Sensitivity analysis of net power output, thermal efficiency and exergy efficiency for R245fa

Parameters	$W_{net}$	$\eta_{th}$	$\eta_{ex}$
Expander inlet temperature	0.005	0.0000095	0.00017
Expander inlet pressure	0.35	0.011	0.056
Condensation temperature	0.085	0.0016	0.010
PPTD	0.1	0	0.0031

**Table 3.4:** Sensitivity analysis of net power output, thermal efficiency and exergy efficiency for R123

<b>Parameters</b>	<b><math>W_{net}</math></b>	<b><math>\eta_{th}</math></b>	<b><math>\eta_{ex}</math></b>
Expander inlet temperature	0.0025	0.000012	0.00012
Expander inlet pressure	0.30	0.019	0.095
Condensation temperature	0.075	0.0017	0.010
PPTD	0.1	0	0.0031

**Table 3.5:** Sensitivity analysis of net power output, thermal efficiency and exergy efficiency for Isobutane

<b>Parameters</b>	<b><math>W_{net}</math></b>	<b><math>\eta_{th}</math></b>	<b><math>\eta_{ex}</math></b>
Expander inlet temperature	0.0027	0.000024	0.0022
Expander inlet pressure	0.25	0.0082	0.045
Condensation temperature	0.12	0.0018	0.013
PPTD	0.06	0	0.0023

**Table 3.6:** Sensitivity analysis of net power output, thermal efficiency and exergy efficiency for R134a

<b>Parameters</b>	<b><math>W_{net}</math></b>	<b><math>\eta_{th}</math></b>	<b><math>\eta_{ex}</math></b>
Expander inlet temperature	0.0005	0.000025	0.0001
Expander inlet pressure	0.13	0.0041	0.023
Condensation temperature	0.096	0.0016	0.011
PPTD	0.094	0	0.0031

### **3.5 Genetic Algorithm optimization for selection of working fluid**

Genetic algorithm (GA) was first developed by Prof. John Holland at University of Michigan in 1975. GA is based on the mechanics of natural selection and natural genetics. The algorithm moves towards the optimal solution by applying Darwinian principle of 'survival of the fittest'. The algorithm simulates the process of evolution where successive generations will be better compared to the previous generations. GA is preferred over other traditional optimization techniques because of its robustness and faster convergence. GA works with the coding of the parameter set. In GA optimization, the algorithm searches for a population of points compared to single point in traditional optimization methods. This prevents the convergence of the algorithm to sub-optimal solutions.

In GA method, a population of  $2n$  to  $4n$  solutions is assumed where 'n' is the number of variables. These are called individuals. Each individual is represented by a string of binary variables, which corresponds to chromosomes in genetics. The numerical value of the objective function corresponds to the concept of fitness in genetics. After trial solutions are selected, a new set of strings or generation is produced by using stochastic principles, selecting the fittest parents to produce children from trial solutions or individuals. Fitness function is the criteria for selecting the individuals. The initial population is generated randomly. New population is created by applying crossover and mutation operators to the selected individuals (parents). In crossover operation, a portion of string of each of the two parents is exchanged which generates new solutions. Mutation is the random alteration of binary digits in a string. The procedure is shown in the form of a flowchart in Figure 3.23.

The thermodynamic model shown in section 3.2 is used for GA. However, the equations are modified to create five degrees of freedom (or independent variables) and to frame a constrained maximization problem. Exergy efficiency is chosen as the objective function. Expander inlet pressure, expander inlet temperature, condensation temperature, evaporator hot fluid inlet temperature, and pinch point temperature difference were

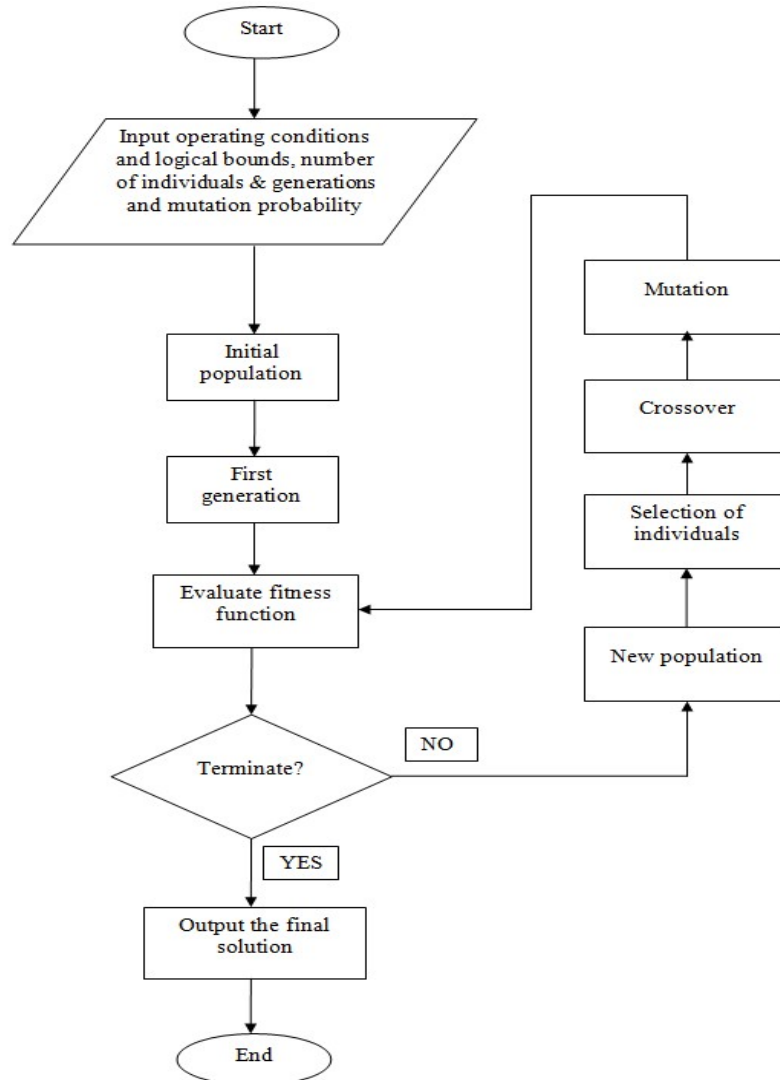


**Figure 3.23:** Schematic diagram indicating the genetic algorithm process

selected as the independent variables. The upper and lower bounds for each variable were defined for all working fluids. The objective function for the basic ORC cycle is given by,

Maximize  $\eta_{\text{exg}}$ ,

Subjected to constraints,

$2.5 \text{ bar} \leq P \leq 8 \text{ bar}$  for R245fa;  $2.5 \text{ bar} \leq P \leq 5 \text{ bar}$  for R123;  $4 \text{ bar} \leq P \leq 12 \text{ bar}$  for Isobutane;  $10 \text{ bar} \leq P \leq 20 \text{ bar}$  for R134a

$$30 \leq T_{\text{cond}} \leq 40$$

$$90 \leq T_i \leq 120$$

$$55 \leq T_{\text{sup}} \leq 75$$

$$5 \leq \text{PPTD} \leq 20$$

The input operating conditions and constraints for optimization for each working fluid are mentioned in Table 3.7. GA optimization is carried out using EES. After the constraints and the objective function are defined, the GA tool evaluates the objective function. The iterations continue till it finds the optimal solution.

**Table 3.7:** Input data for GA optimization

<b>Fluids</b>	<b>R245fa</b>	<b>R123</b>	<b>Isobutane</b>	<b>R134a</b>
Population size	64			
Stop generation	128			
Mutation probability	0.25			
Range of turbine inlet temperature (°C)	55-75			
Range of expander inlet pressure (bar)	2.5 – 8	2.5 – 5	4-12	10–20
Range of condensation temperature (°C)			30–40	
Range of evaporator hot side inlet temperature (°C)			90-120	
Range of pinch point temperature difference (°C)			5-20	



**Table 3.8:** Optimization results of ORC system for all working fluids

<b>Working Fluid</b>	<b>T<sub>sup</sub></b> <b>(°C)</b>	<b>P</b> <b>(bar)</b>	<b>T<sub>cond</sub></b> <b>(°C)</b>	<b>T<sub>i</sub></b> <b>(°C)</b>	<b>PPTD</b> <b>(°C)</b>	<b>W<sub>net</sub></b> <b>(kW<sub>e</sub>)</b>	<b>η<sub>th</sub></b> <b>(%)</b>	<b>η<sub>exg</sub></b> <b>(%)</b>
R245fa	74.85	6.07	30.03	90.4	5.009	1.82	7.04	44.98
R123	74.37	3.66	30.00	90.17	5.18	1.83	7.1	45.53
Isobutane	74.58	10.36	30.01	90.01	5.12	1.89	6.56	42.89
R134a	74.98	19.94	30.00	90.02	5.00	1.98	6.32	41.91

The upper limit of the expander inlet temperature is fixed at 75 °C to enable stable operation of the system. Table 3.8 lists the results of optimization using 4 ORC fluids, i.e. R245fa, R123, Isobutane and R134a. From the optimization results, it can be seen that, expander inlet temperature is close to the upper limit value (75 °C) which was set before the start of GA. Optimized inlet pressure values for each working fluid is the saturation pressure corresponding to expander inlet temperature of 75 °C. R123 has the highest thermal efficiency (7.1%) and exergy efficiency (45.53%) at lowest expander inlet pressure (3.66 bar) compared to other ORC fluids. This characteristic aids in safe operation of the system and shows better utilization of the heat source compared to other working fluids. The optimal heat source temperature is 90 °C approximately for all working fluids. From the optimization results, it can be inferred that R245fa and R123 is better suited for low temperature ORC applications compared to R134a and Isobutane because of its efficient system performance at lower operating pressures and temperatures.

### 3.6 Exergy analysis of ORC system

It is observed from the energy analysis that, R245fa is efficient at low operating pressures. The thermophysical properties of R245fa are listed in Table 3.9. R245fa is non-corrosive, non-flammable, inexpensive and has zero ODP (Cioccolanti et al. 2018). R245fa has a lower specific volume when compared to R123. Therefore, R245fa is selected as the working fluid for further analysis. In this study, exergy analysis is carried

out to identify the location and to assess the magnitude of exergy destruction in each component of ORC power block. In addition to this, parametric investigation is done to study the effect of evaporator pressure, condenser pressure, pinch point temperature difference, superheating and dead state temperature on energy & exergy efficiency and exergy destruction.

**Table 3.9:** Thermophysical properties of R245fa

SI No	Property	Value	Unit
1	Molecular mass	134.05	kg/K mol
2	Critical temperature	154.05	°C
3	Critical pressure	4.25	MPa
4	Boiling point	14.90	°C
5	Ozone depletion potential	0	-
6	Global warming potential	950	/100 year

The thermodynamic model used for exergy analysis is the extension of the model shown in section 3.2. The governing equations used in this analysis are as follows:

The rate of irreversibility in each component of organic Rankine cycle is evaluated by applying exergy balance across the device at steady state. Specific flow exergy is given by

$$e = (h - h_o) - T_o (s - s_o) \quad (3.11)$$

Exergy rate is calculated as,

$$E = m \times e \quad (3.12)$$

where 'm' is the mass flow rate.

Irreversibilities in evaporator, condenser, working fluid pump and expander is calculated by applying exergy balance across each component.

Evaporator:

$$I_{\text{evp}} = (E_5 - E_6) - (E_3 - E_2) \quad (3.13)$$

Condenser:

$$I_{\text{cond}} = (E_7 - E_8) - (E_1 - E_4) \quad (3.14)$$

Working fluid pump:

$$I_{\text{pump}} = (E_1 + \dot{W}_{\text{pp}}) - E_2 \quad (3.15)$$

Expander:

$$I_{\text{exp}} = E_3 - (E_4 + \dot{W}_t) \quad (3.16)$$

Total irreversibility is calculated as the sum of irreversibilities in the subcomponents i.e. evaporator, condenser, pump and expander and the exergy transferred to the condenser cooling water. This is given by,

$$I_{\text{total}} = I_{\text{evp}} + I_{\text{cond}} + I_{\text{pump}} + I_{\text{exp}} + I_{\text{rej}} \quad (3.17)$$

Total rate of exergy destruction can also be defined as the difference between input exergy and net work output of the cycle.

$$I_{\text{total}} = \dot{E}_{\text{in}} - \dot{W}_{\text{net}} \quad (3.18)$$

The exergy efficiency of a component is defined as the ratio of used exergy of the component to the available exergy of the same component. The exergy efficiencies of evaporator and condenser is defined in Equation (3.19) & Equation (3.21), respectively, as the ratio of exergy recovered by the cold stream to the exergy supplied by the hot

stream. Exergy efficiency of the expander as shown in Equation (3.20) shows how much of useful work has been extracted by the expander from the exergy stream. Similarly, exergy efficiency of the pump is defined in Equation (3.22).

$$\eta_{\text{exg\_evp}} = \frac{E_3 - E_2}{E_5 - E_6} \quad (3.19)$$

$$\eta_{\text{exg\_exp}} = \frac{\dot{W}_t}{E_3 - E_4} \quad (3.20)$$

$$\eta_{\text{exg\_cond}} = \frac{E_8 - E_7}{E_4 - E_1} \quad (3.21)$$

$$\eta_{\text{exg\_pump}} = \frac{(E_2 - E_1)}{\dot{W}_{\text{pp}}} \quad (3.22)$$

**Table 3.10:** Input parameters for energy and exergy analysis (Galloni et al. 2015)

Sl No	Name	Value	Unit
1	Isentropic efficiency of pump	80	%
2	Isentropic efficiency of expander	80	%
3	Hot water mass flow rate	0.288	kg/s
4	Cold water mass flow rate	0.248	kg/s
5	Hot water inlet temperature in Evaporator	95	°C
6	Cold water inlet temperature in condenser	27	°C
7	Pinch point temperature difference in evaporator and condenser	5	°C
8	R245fa pressure at evaporator outlet	10	bar
9	R245fa pressure at condenser inlet	2.02	bar
10	Temperature at dead state	25	°C
11	Pressure at dead state	1.0	bar

The input parameters are listed in Table 3.10. These parameters are selected based on the experimental study conducted by Galloni et al (2015). They designed and developed a prototype of a 1 kW<sub>e</sub> ORC power plant using R245fa as the working fluid. The ORC system delivered a net electric work output of 1.2 kW and a thermal efficiency of 10.2% as presented in Table 3.11.

**Table 3.11:** Energy analysis

SI No	Parameter	Value	Unit
1	Net work output	1.2	kW <sub>e</sub>
2	Thermal efficiency	10.2	%

Figure 3.24 shows the exergy losses in major components of ORC system, which is represented as the percentage of total rate of exergy destruction. The objective of this analysis is to identify the location and the magnitude of the inefficiencies within the ORC power block. The total exergy input to the ORC is 2.28 kW. Net power output of 1.2 kW<sub>e</sub> constitutes to 52.63% of the exergy input. Evaporator accounted for the maximum exergy loss which is around 0.446 kW or 19.6% of the inlet exergy. This is followed by exergy loss in the expander which accounts for 12.5% of the exergy input (0.285 kW). Exergy rejection to condenser cooling water is about 0.254 kW or 11.14% of the exergy input. 8% of the exergy input or 0.087 kW exergy loss occurs in the condenser. Exergy destruction in working fluid pump is negligible. 41.3% of the total exergy loss occurred in the evaporator followed by expander (26%), exergy rejection to cooling water (24%), Condenser (8%) and pump (0.7%). Table 3.12 indicates the exergy performance data for the cycle. Properties of R245fa and the heat transfer fluid (water) at all thermodynamic state points have also been tabulated in Table 3.13. The exergy efficiencies for the evaporator, expander, condenser and pump were 80.43%, 81.35%, 74.29% and 80.60%. The cycle exergy efficiency was found to be 52.77%.

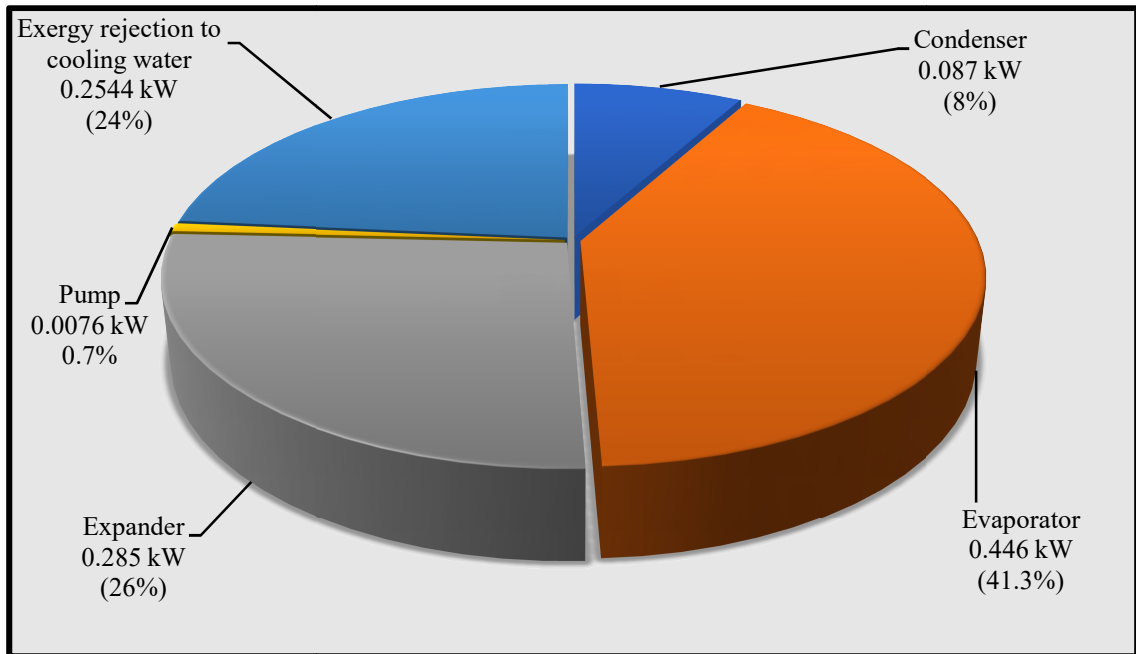


**Figure 3.24:** Exergy loss distribution in ORC components

**Table 3.12:** Results obtained from exergy analysis of ORC system

Component	Exergy destruction (kW)	Exergy efficiency (%)
Evaporator	0.446	80.43
Expander	0.285	81.35
Condenser	0.087	74.29
Pump	0.0076	80.6
Exergy rejection at condenser	0.2544	-
Cycle	1.08	52.77

**Table 3.13:** Properties of water and R245fa at each thermodynamic state

State No	Fluid	Mass flow rate (kg/s)	Temperature (°C)	Pressure (bar)	Enthalpy (kJ/kg)	Entropy (kJ/kg K)	Exergy rate, E (kW)
0	Water	-	25	1	104.92	0.37	-
0'	R245fa	-	25	1	424.65	1.72	-
1	R245fa	0.052	33.74	2.02	244.11	1.15	0.35
2	R245fa	0.052	33.74	10	244.86	1.15	0.38
3	R245fa	0.052	94.61	10	474.15	1.802	2.21
4	R245fa	0.052	33.74	2.02	450.02	1.82	0.69
5	Hot water	0.288	100	1.2	423.29	1.32	10.07
6	Hot water	0.288	91.25	1.2	382.21	1.21	7.79
7	Cooling water	0.248	27	1.1	113.23	0.395	0.013
8	Cooling water	0.248	37.23	1.1	156.04	0.535	0.26

### 3.7 Effect of key thermodynamic parameters on cycle exergy efficiency and rate of exergy destruction

Key thermodynamic parameters such as evaporator pressure, degree of superheat, condensation temperature, dead state temperature and pinch point temperature difference are investigated. Its effect on exergy destruction rates of ORC components, thermal & exergy efficiencies are analysed.

### 3.7.1 Effect of evaporation pressure

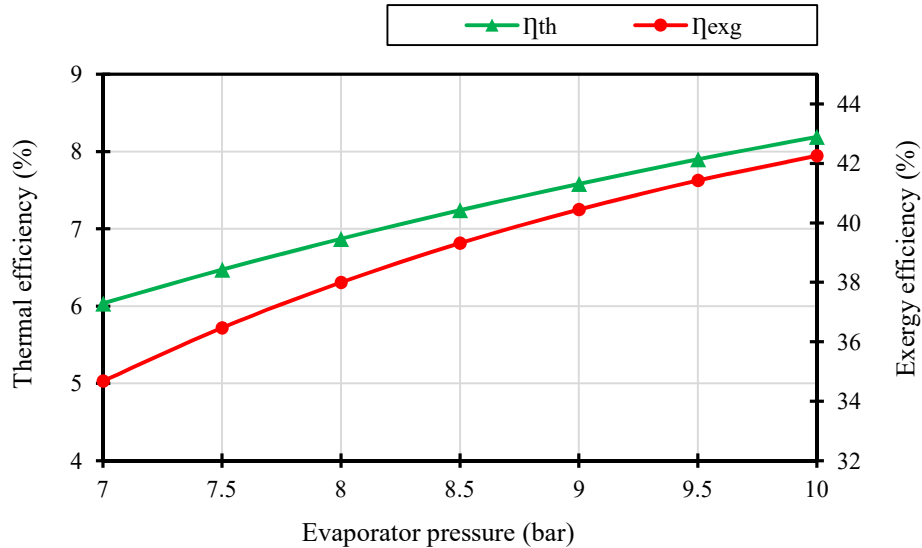


**Figure 3.25:** Effect of evaporation pressure on thermal and exergy efficiency

Condensation pressure was set to 3 bar and the evaporation pressure of R245fa was varied from 7 bar to 10 bar. The other input parameters which are used for this study are the same as listed in table 3.2. The thermal efficiency of the cycle increases by 35.71% and the cycle exergy efficiency by 21.86%. The increase in thermal efficiency is due to higher enthalpy drop across the expander which results in better net work output. This is also accompanied by increase in pump work. However, pump power consumption is much lower than the expander work output which leads to an increase in the thermal efficiency. The exergy efficiency of the cycle is the ratio of net work output to exergy input. With the increase in evaporation pressure, the net work output increases and the exergy input decreases. Therefore, the ratio of net work output to exergy input increases as depicted in Figure 3.25.

Total irreversibility decreases from 2.06 to 0.99 kW as indicated in Figure 3.26, when evaporation pressure is increased from 7 to 10 bar. Irreversibilities of expander, pump and evaporator decreases with increase in evaporation pressure. For a fixed temperature



of the heat source, at higher evaporation pressure, more heat is being utilized from the source. This reduces the exergy loss in the evaporator.

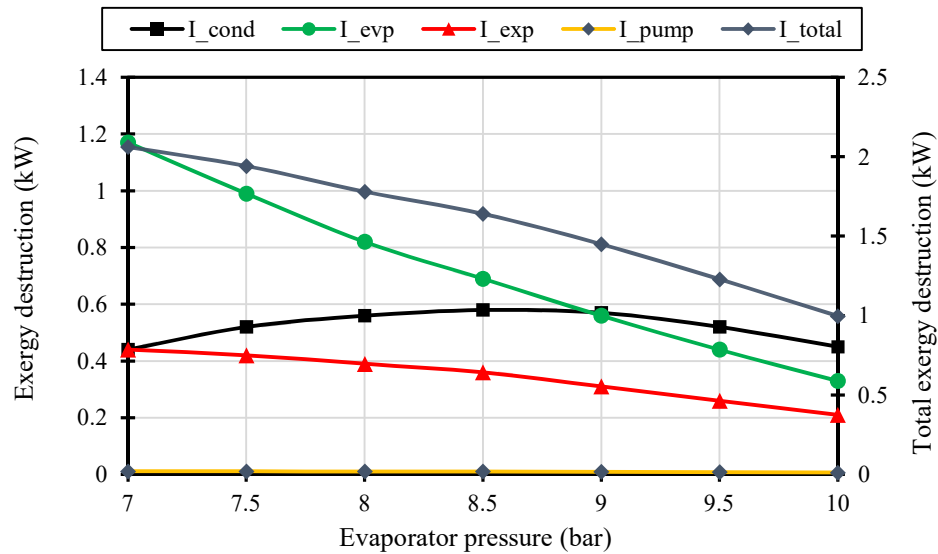


**Figure 3.26:** Effect of evaporation pressure on component irreversibilities

Higher net work output results in drop in exergy loss in the expander. Exergy loss in condenser increases upto evaporator pressure of 8.5 bar and then decreases. This is primarily due to decreasing mass flow rate of the working fluid. The enthalpy of the condenser cooling water is dependent on the mass flow rate of the ORC fluid due to energy balance. Therefore, such a variation is observed in the case of condenser. However, total exergy destruction reduces as evaporation pressure increases.

### 3.7.2 Effect of superheating

Condensation pressure was set to 3 bar, Evaporation pressure was fixed at 8 bar and the degree of superheat was varied from 4 to 20 °C. The other input parameters used, are the same as listed in Table 3.2. Figure 3.27 indicates the effect of superheating on thermal and exergy efficiencies, at constant evaporation pressures and Figure 3.28 shows the effect of superheat on component irreversibilities.

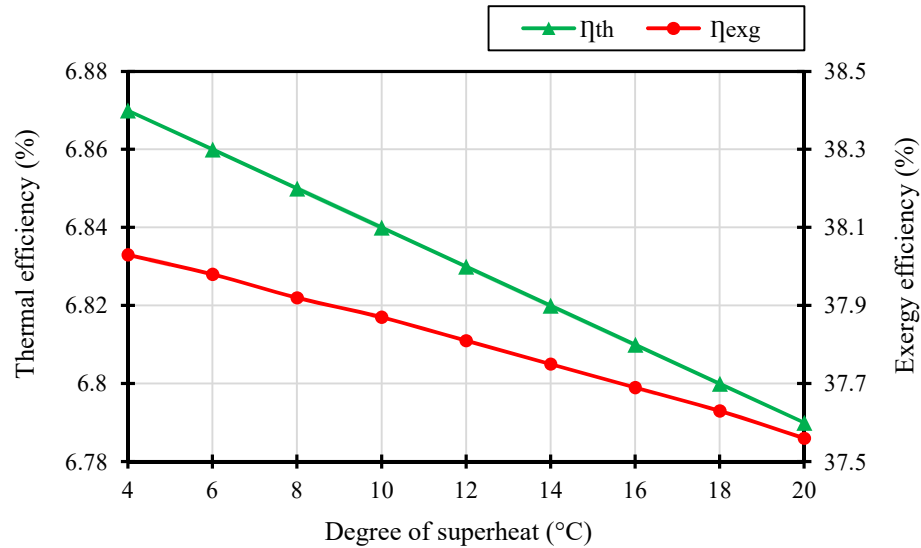


**Figure 3.27:** Effect of degree of superheat on thermal and exergy efficiency

Irreversibility rate in evaporator and expander reduces with increase in superheat value, whereas exergy loss increases slightly in case of condenser. Thermal and exergy efficiencies show a slight reduction with increase in degree of superheat. Mass flow rate of R245fa decreases with increase in degree of superheat due to higher energy input. Enthalpy drop across the expander increases. However, the rate of reduction in mass flow rate of R245fa is greater. Hence, a small reduction in both energy and exergy efficiencies is observed. The magnitude of change in efficiencies and exergy destruction rates are very low. Thermal efficiency & exergy efficiency decreases by 1.18 & 1.25% respectively. The rate of total exergy destruction increases by 0.51%.

### 3.7.3 Effect of condenser pressure

Figure 3.29 shows the variation of the thermal efficiency and exergy efficiency with condenser pressure. Evaporation pressure was maintained constant at 10 bar. Condenser pressure was varied from 2 to 3 bar. Thermal efficiency decreases from 10.24 to 8.19% and exergy efficiency reduces from 53.02 to 42.26%. Increase in condenser pressure results in less work being extracted from the expander. Lower net work output leads to drop in thermal and exergy efficiency.

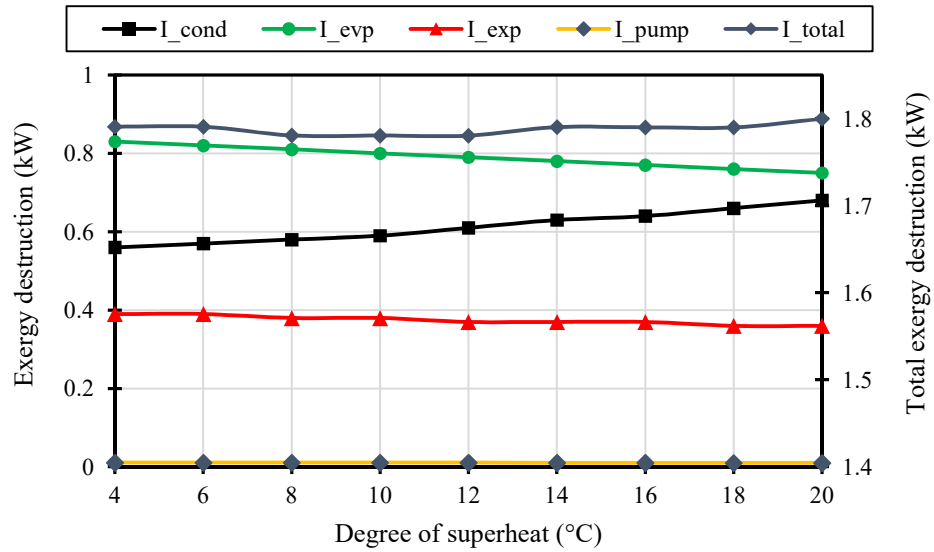


**Figure 3.28:** Effect of degree of superheat on component irreversibilities

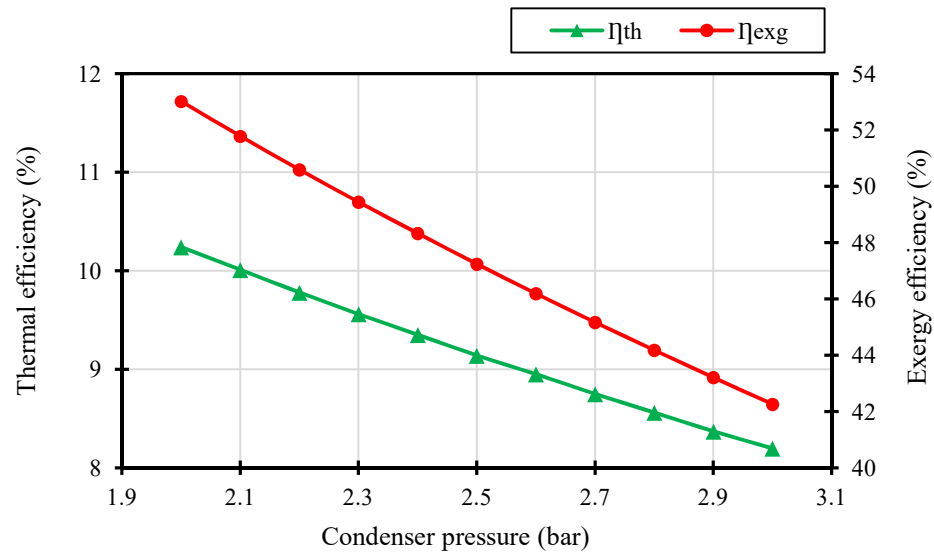


**Figure 3.29:** Effect of condenser pressure on thermal and exergy efficiency

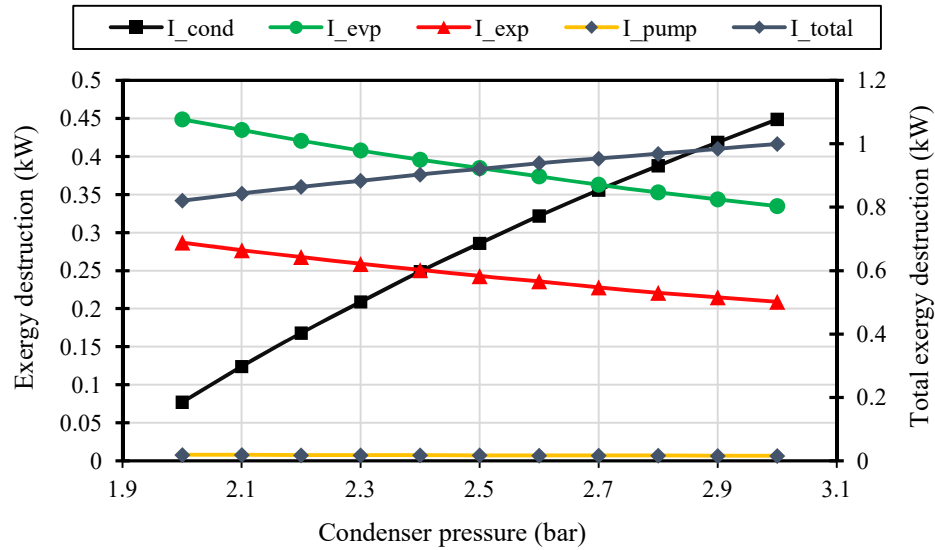
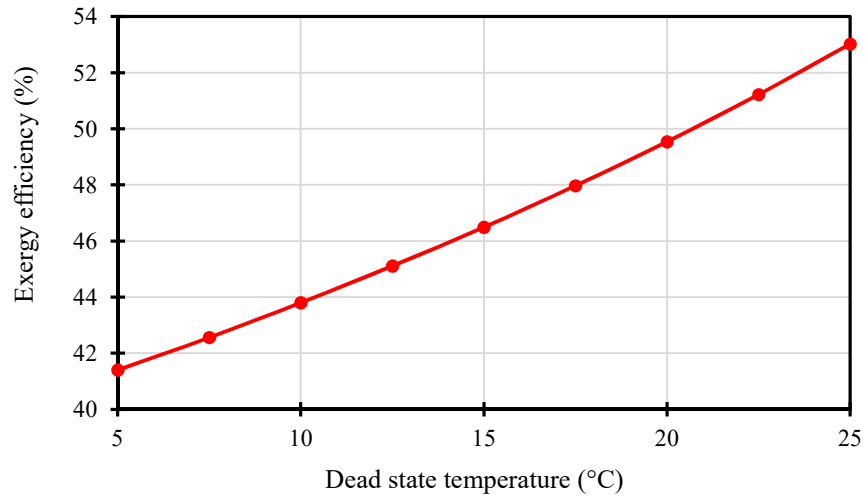


**Figure 3.30:** Effect of condenser pressure on component irreversibilities

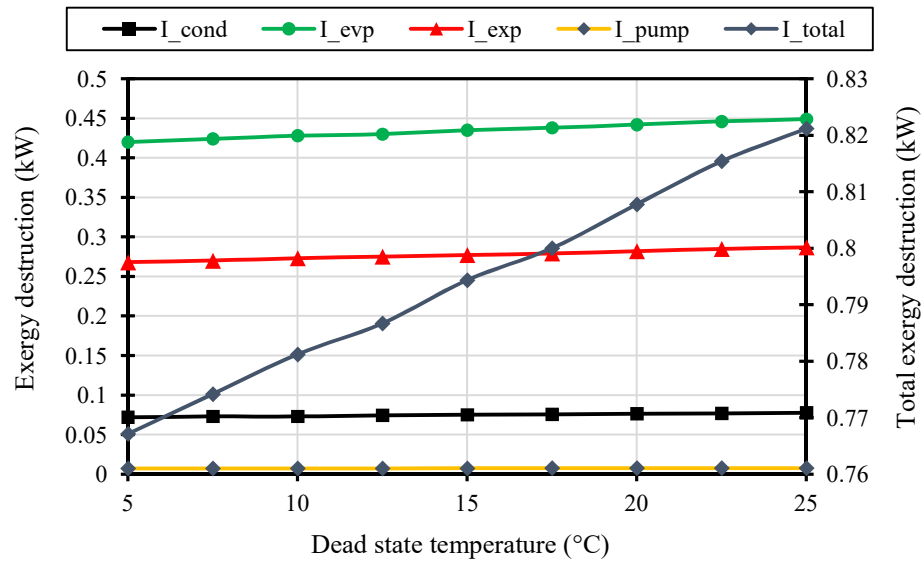
It is seen from Figure 3.30 that exergy loss in evaporator, expander and pump decreases while that of condenser increases with increase in condenser pressure. The increase in enthalpy at state points 1, 2 and 4 causes the decrease in exergy destruction at evaporator and expander. From Equation (3.14), it can be inferred that, the exergy loss in condenser increases due to increase in difference in exergy rates at state 1 and 4. Exergy destruction increases from 0.077 to 0.449 kW in condenser. Total irreversibility increases from 0.82 to 0.99 kW when condenser pressure is increased from 2 to 3 bar, because the exergy loss in condenser is greater than the combined rate of exergy loss in evaporator, expander and pump.

### 3.7.4 Effect of dead state temperature

Condenser pressure was maintained at 3 bar and evaporation pressure was fixed at 10 bar. Exergy efficiency increases with increase in dead state temperature. As dead state temperature increases from 5 to 25 °C, exergy efficiency increases from 41.4 to 53.02% as depicted in Figure 3.31.



**Figure 3.31:** Effect of dead state temperature on exergy efficiency



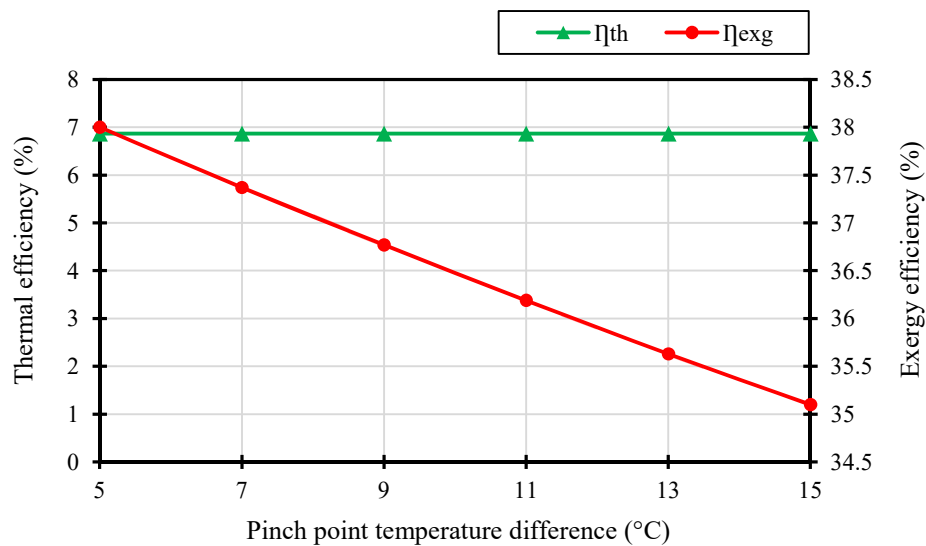
**Figure 3.32:** Effect of dead state temperature on component irreversibilities

Figure 3.32 shows the variation of component irreversibilities with dead state temperature. It is seen that the exergy losses in all components increases with increase in dead state temperature. But, exergy efficiency of the cycle increases. This is because,

total irreversibility of the system also takes into account the exergy transferred to condenser cooling water ( $E_{rej}$ ). Despite increase in total exergy destruction of the components with higher dead state temperatures, decrease in  $E_{rej}$  leads to higher exergy efficiency of the cycle.

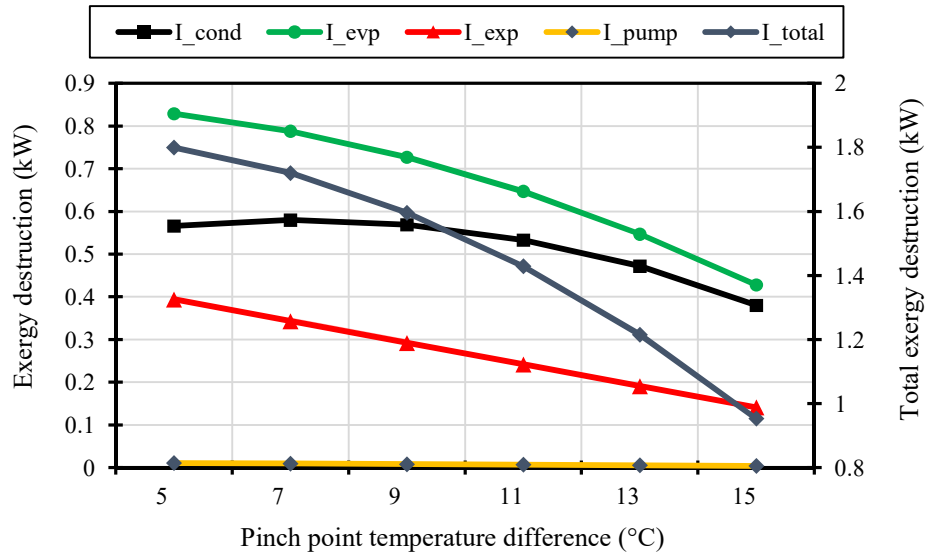
### 3.7.5 Effect of evaporator pinch point temperature difference (PPTD)

Figure 3.33 illustrates the variation of thermal and exergy efficiency of the cycle with evaporator pinch point temperature difference. Condenser pressure was maintained constant at 3 bar, Evaporation pressure was set to 8 bar and PPTD was varied from 5 to 15 °C. The analysis shows that with the increase in PPTD, the work output and exergy efficiency of the cycle decreases, while the enthalpy drop across the expander and the thermal efficiency remains constant.



**Figure 3.33:** Effect of PPTD on thermal and exergy efficiency

When PPTD increases, less heat is being extracted by R245fa in the evaporator region. To maintain constant evaporation pressure, the mass flow rate decreases by energy balance. This results in the reduction in net work output. However, PPTD has no influence on enthalpy drop across the expander and hence its thermal efficiency. Exergy efficiency of the cycle decreases primarily because of the reduction in net work output.



**Figure 3.34:** Effect of PPTD on component Irreversibilities

Although, exergy input decreases, the decrease in work output is much greater. Therefore, the ratio of net work output to exergy input decreased. Exergy efficiency decreases by 7.63% when PPTD increases by 10 °C. Variation of irreversibilities in ORC components with PPTD is shown in Figure 3.34. Rate of exergy loss in evaporator, expander and pump showed a decline, whereas in condenser, exergy destruction rate increased upto PPTD of 7 °C and then decreased. This is because; the effect of decrease in mass flow rate of the ORC fluid is predominant beyond PPTD of 7 °C. The total rate of exergy loss decreases by 47.05%.

### 3.8 Chapter closure

A thermodynamic model for ORC system was developed based on laws of mass and energy conservation. Using this model, ORC thermal and exergy efficiencies were evaluated for four different working fluids; R245fa, R123, Isobutane and R134a. Sensitivity analysis was performed using key thermodynamic parameters including expander inlet temperature, expander inlet pressure, condensation temperature and pinch point temperature difference to study its effect on net work output, thermal and exergy efficiencies. In addition to this, exergy analysis was carried out to investigate the

distribution of exergy losses within the ORC system and to study the impact of evaporator pressure, condensation pressure, dead state temperature, pinch point temperature difference and degree of superheat on the exergy losses and the system performance. Optimization of the ORC system was carried out using genetic algorithm (GA) for selection of working fluid based on maximum exergy efficiency.



## CHAPTER 4

### PARAMETRIC STUDY OF PLATE HEAT EXCHANGER EVAPORATOR FOR ORGANIC RANKINE CYCLE SYSTEMS

Evaporator is one of the critical components of the ORC system where the exchange of thermal energy occurs between the heat transfer fluid and the ORC working fluid. During the design of ORC systems, focus must be given to the design of the heat exchangers, since their cost represents an important share of the total investment of the plant. The types of heat exchangers that are normally preferred for organic Rankine cycles are shell-and-tube heat exchangers and plate heat exchangers.

Shell and tube heat exchangers consists of a bundle of tubes mounted in a cylindrical shell. One fluid flows through the tubes whereas the other fluid flows across them, through the shell. These heat exchangers are generally preferred at high operating temperatures and pressures (250-1000 °C and 100 MPa). The high-pressure fluid normally flows through the tubes, while the low-pressure fluid flows through the shell. Therefore, the working fluid will evaporate in the tubes while the heat transfer fluid will flow through the shell. A plate exchanger consists of a series of parallel plates that are placed one above the other so as to allow the formation of a series of channels for fluids to flow between them. The space between two adjacent plates forms the channel in which the fluid flows. Inlet and outlet holes at the corners of the plates allow hot and cold fluids through alternating channels in the exchanger so that a plate is always in contact on one side with the hot fluid and the other with the cold. Generally, these plates are corrugated in order to increase the turbulence, the thermal exchange surface and to provide mechanical rigidity to the exchanger. Corrugation is achieved by cold forging of sheet metals. Plate heat exchangers are preferred at lower operating temperatures and pressures (<150 °C and 1-3 MPa).

The advantages of plate heat exchangers over shell and tube heat exchangers are as follows (Shah 1981):

- a) They can easily be dismantled into their individual components for cleaning, inspection, and maintenance.
- b) High turbulence and mixing due to plate corrugation patterns reduce fouling to about 10 to 25% of that of a shell-and-tube heat exchanger and enhance heat transfer.
- c) Very high heat transfer coefficients are achieved due to swirl or vortex flow generation and small hydraulic diameter flow passages.
- d) Because of high heat transfer coefficients, reduced fouling and counter flow arrangements, the surface area required for a plate exchanger is one-half to one-third that of a shell-and tube exchanger for a given heat duty, thus reducing the cost, overall volume, and space requirement for the heat exchanger.

#### 4.1 Plate heat exchanger design

The plate heat exchanger is divided into three zones *i.e.* preheating zone, 2 phase zone and superheating zone as shown in Figure 4.1. Under the considered operating conditions, each section is designed separately using Logarithmic Mean Temperature Difference (LMTD) method.

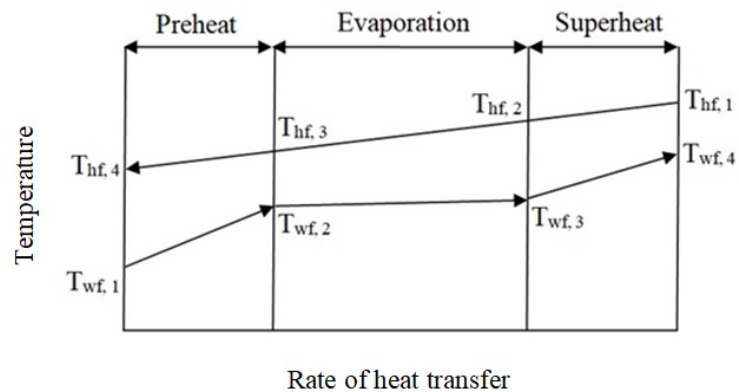


**Figure 4.1:** Three zone plate heat exchanger evaporator model

The main dimensions of the plate heat exchanger are shown in Figure 4.2. This evaporator model estimated the cost of a plate heat exchanger based on the total surface area of the evaporator, using heat transfer correlations presented by Han et al. (2003). In addition to

this, effect of key thermodynamic and geometric parameters on the evaporator area was analyzed using the same model. The following assumptions were made to simplify the analysis.

- a) The system is in steady state.
- b) R245fa is in saturated condition at the condenser outlet.
- c) Isentropic efficiency of pump and expander are constant at 70%.
- d) The fouling effects of the heat exchanger are negligible.

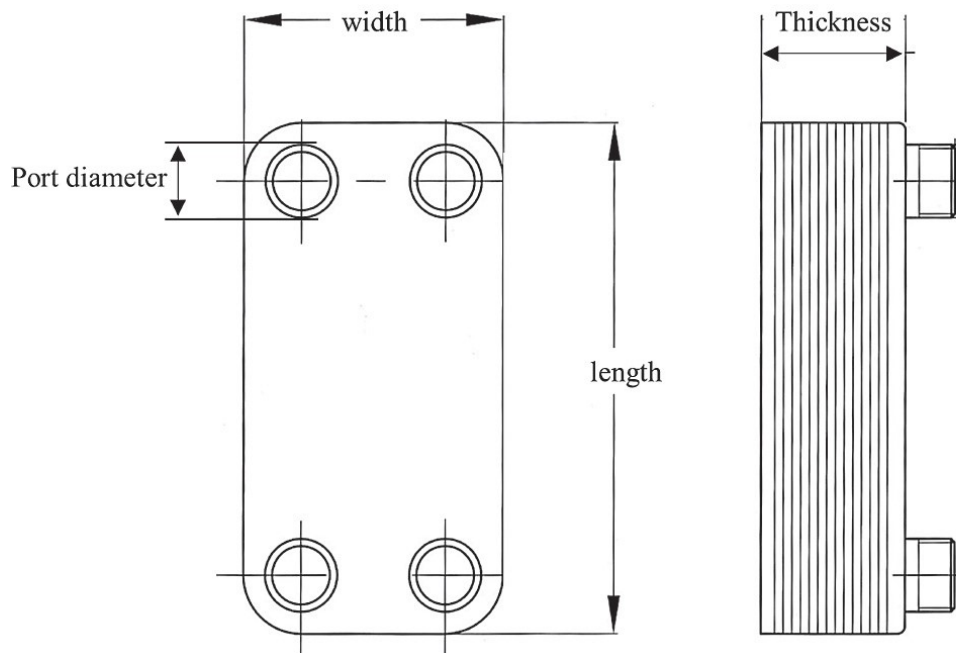


**Figure 4.2:** Main dimensions of the plate heat exchanger (Konstantinos and Sotirios, 2017)

The thermodynamic model of basic ORC system was integrated with the evaporator sub model. The thermodynamic model was executed on the same lines as in section 3.2 (Appendix A1). Net work output of the system was calculated using this model. R245fa was used as the working fluid. The program was written in function format using Engineering Equation Solver (EES) (Appendix A2). The design process is iterative and the iterations were carried out until pressure drop on the cold side of the heat exchanger converged. The evaporator was redesigned for each iteration and its cost was evaluated based on the surface area of the heat exchanger. The inputs to the model are listed in

Table 4.1. The governing equations used in the model are explained in section 4.2.

**Table 4.1:** Inputs to the model

Sl No	Symbol	Parameter	Value	Unit
1	$D_h$	Hydraulic diameter	0.0035	m
2	$\beta$	Chevron angle	45	degree
3	$P_{co}$	Corrugation pitch	0.007	m
4	$k_{pl}$	Thermal conductivity of the plate	13.5	W/m °C
5	$n$	Number of segments in evaporation zone	20	-
6	$t_{pl}$	Thickness of the plate	0.0005	m
7	$\eta_{pp}$	Isentropic efficiency of pump	70	%
8	$\eta_t$	Isentropic efficiency of expander	70	%
9	$M_2$	Mass flow rate	0.7	kg/s

## 4.2 Evaporator sub-model

In case of single phase heat transfer, the heat transfer coefficient is determined using Hsieh and Lin correlation (Hsieh and Lin 2002). This correlation was proposed based on experimental data obtained for R-410a and it showed that the proposed empirical correlation could be used to determine non-boiling heat transfer coefficient for all working fluids. In two-phase heat transfer, the correlation is proposed by Han et al. (2003). This was developed based on experimental results with R-22 and R-410a. The comparison between experimental results and correlations for Nusselt number and friction factor showed that, regardless of the type and configuration of Brazed plate heat exchanger and refrigerants, the experimental data were within  $\pm 25\%$  for the proposed Nusselt number correlation and  $\pm 15\%$  for proposed friction factor correlation.

### 4.2.1 Single phase

The heat transfer in the single phase section is calculated as,

$$Q_{sp} = U_{sp} \times A_{sp} \times \text{LMTD}_{sp} \quad (4.1)$$

Log mean temperature difference for single phase heat transfer is given by,

$$\text{LMTD}_{sp} = \frac{\Delta T_{\max} - \Delta T_{\min}}{\ln\left(\frac{\Delta T_{\max}}{\Delta T_{\min}}\right)} \quad (4.2)$$

The overall heat transfer coefficient of single phase is given by (Imran et al. 2014).

$$\frac{1}{U_{sp}} = \frac{1}{\alpha_{ws}} + \frac{t_{pl}}{k_{pl}} + \frac{1}{\alpha_{r,sp}} \quad (4.3)$$

The convective heat transfer coefficient for R245fa in plate heat exchanger is calculated as (Imran et al. 2015),

$$\alpha_{r,sp} = 0.2092 \times \left(\frac{k_f}{D_h}\right) \times \text{Re}^{0.78} \times \text{Pr}^{0.33} \times \left(\frac{\mu_m}{\mu_{\text{wall}}}\right)^{0.14} \quad (4.4)$$

#### 4.2.2 Two phase

In this region, the correlations used in single phase, based on constant fluid properties cannot be used. The fluid properties tend to vary as the quality of the fluid changes. Therefore, a modified LMTD method is employed.

The evaporation region is discretised into 'n' smaller sections so that there are incremental changes in fluid properties at each section. Therefore, constant fluid properties are assumed in each section. In this analysis, the value of 'n' was restricted to 20 as the processing time of the model increased when the value of 'n' was increased and negligible change in evaporator area was observed.

The heat transfer rate for  $i^{\text{th}}$  section is evaluated as

$$Q_i = U_i \times A_i \times \text{LMTD}_i \quad (4.5)$$

Log mean temperature difference is calculated as,

$$\text{LMTD}_i = \frac{\Delta T_{\max,i} - \Delta T_{\min,i}}{\ln\left(\frac{\Delta T_{\max,i}}{\Delta T_{\min,i}}\right)} \quad (4.6)$$

The two-phase overall heat transfer coefficient is given by (Imran et al. 2014),

$$\frac{1}{U_{\text{tp},i}} = \frac{1}{\alpha_{\text{ws},i}} + \frac{t_{\text{pl}}}{k_{\text{pl}}} + \frac{1}{\alpha_{\text{r,sp},i}} \quad (4.7)$$

The Nusselt number correlation for R245fa evaporation in plate heat exchanger is calculated as (Han et al. 2003),

$$\text{Nu}_{\text{tp}} = \text{Ge}_1 \times \text{Re}_{\text{eq}}^{\text{Ge}_2} \times \text{Bo}_{\text{eq}}^{0.3} \times \text{Pr}^{0.4} \quad (4.8)$$

where,

$$\text{Ge}_1 = 2.81 \times \left(\frac{P_{\text{co}}}{D_h}\right)^{-0.041} \times \left(\frac{\pi}{2} - \beta\right)^{-2.83} \quad (4.9)$$

$$\text{Ge}_2 = 0.746 \times \left(\frac{P_{\text{co}}}{D_h}\right)^{-0.082} \times \left(\frac{\pi}{2} - \beta\right)^{0.61} \quad (4.10)$$

The equivalent Reynolds number and boiling number are given by,

$$\text{Re}_{\text{eq}} = \frac{\text{Ge}_{\text{eq}} \times D_h}{\mu_f} \quad (4.11)$$

$$\text{Bo}_{\text{eq}} = \frac{q''}{\text{Ge}_{\text{eq}} \times h_{\text{fg}}} \quad (4.12)$$

where,  $q''$  is the heat flux at the wall, ' $h_{fg}$ ' is the enthalpy of vaporization, ' $D_h$ ' is the hydraulic diameter of the flow channel and ' $\mu_f$ ' is the dynamic viscosity of the fluid at the wall. ' $Ge_{eq}$ ' is an equivalent mass flux which is calculated as,

$$Ge_{eq} = G \times \left[ (1-x) + x \left( \frac{\rho_f}{\rho_g} \right)^{0.5} \right] \quad (4.13)$$

where, the subscript 'f' represents the saturated liquid and the subscript 'g' represents the saturated vapour phase and 'G' denotes the mass velocity.

$$D_h = \frac{(4 \times A)}{P} = \frac{(4 \times w \times b)}{2 \times (w + b)} \quad (4.14)$$

where, 'w' is the plate width and 'b' is the plate spacing (Jiangfeng et al., 2013).

Frictional pressure drop on either side of the heat exchanger is calculated as (Imran et al. 2014),

$$\Delta P = \frac{4 \times f \times L \times G^2}{2 \times \rho \times D_h} \quad (4.15)$$

Single phase frictional pressure drop factor is given by (Imran et al. 2015),

$$f = \frac{0.572}{Re^{0.217}} \quad (4.16)$$

Two phase frictional factor is expressed as (Han et al. 2003),

$$f = Ge_3 \times Re_{eq}^{Ge_4} \quad (4.17)$$

$$Ge_3 = 64710 \times \left( \frac{P_{co}}{D_h} \right)^{-5.27} \times \left( \frac{\pi}{2} - \beta \right)^{-3.03} \quad (4.18)$$

$$Ge_4 = -1.314 \times \left( \frac{P_{co}}{D_h} \right)^{-0.62} \times \left( \frac{\pi}{2} - \beta \right)^{-0.47} \quad (4.19)$$

Cost of the evaporator is linearly related to evaporator heat transfer area which is evaluated as (Imran et al. 2015),

$$\text{Cost(USD)} = 310 + (160 \times A) \quad (4.20)$$

where, 'A' is the heat transfer area in m<sup>2</sup>.

### 4.3 Effect of thermodynamic parameters on evaporator area and cost

#### 4.3.1 Evaporator pressure

**Table 4.2:** Effect of evaporator pressure

Sl No	Symbol	Parameter	Value	Unit
1	$T_{hf,in}$	Temperature of heat source	100	°C
2	$T_{wf,in}$	Condensation temperature	40	°C
3	PPTD	Pinch point temperature difference	5	°C
4	$DT_{sup}$	Degree of superheat	5	°C

The operational parameters are listed in Table 4.2. The heat source temperature and the condensation temperature were set to 100 and 40 °C respectively. Evaporator pinch point



temperature and degree of superheat were kept constant at 5 °C. Figure 4.3 shows the effect of expander inlet pressure on the net work output when R245fa is used as the working fluid. It can be observed that the work output increases initially and then declines. Hence, for a given working fluid, there exists an optimum expander inlet pressure at which, work output is maximum. Mass flow rate of the working fluid decreases with increase in expander inlet pressure. The initial increase in the work output is due to the higher enthalpy difference across the expander. But, when the pressure is increased beyond 6 bar, the effect of reduced mass flow rate outweighs the increase in enthalpy difference across the expander. This results in the reduction of net work output at higher expander inlet pressures. Figure 4.4 shows the effect of evaporator pressure on evaporator area and cost. The surface area decreases with increase in evaporator pressure. Evaporation temperature increases as a result of increasing evaporator pressure. As the pinch point temperature difference (PPTD) remains constant, the exit temperature of the heat transfer fluid increases correspondingly. As a consequence of this, heat transfer rate decreases in the evaporator. Hence, reduction in surface area of the evaporator is observed with increase in evaporator pressure. Since, evaporator area decreases with increase in evaporator pressure, the cost also decreases. As the evaporator pressure increases from 4 to 10 bar, there is a reduction of 75.87% in evaporator surface area and decrease of 63.59% in its cost. However, in practical applications, the evaporator surface area cannot be varied. Therefore, this theoretical study only helps the designer to identify the operating condition of ORC where evaporator area (and hence, the cost) is minimum. The maximum net work output of 5 kW was obtained at 6 bar whereas, minimum evaporator area of 2.42 m<sup>2</sup> was achieved at evaporator pressure of 10 bar.

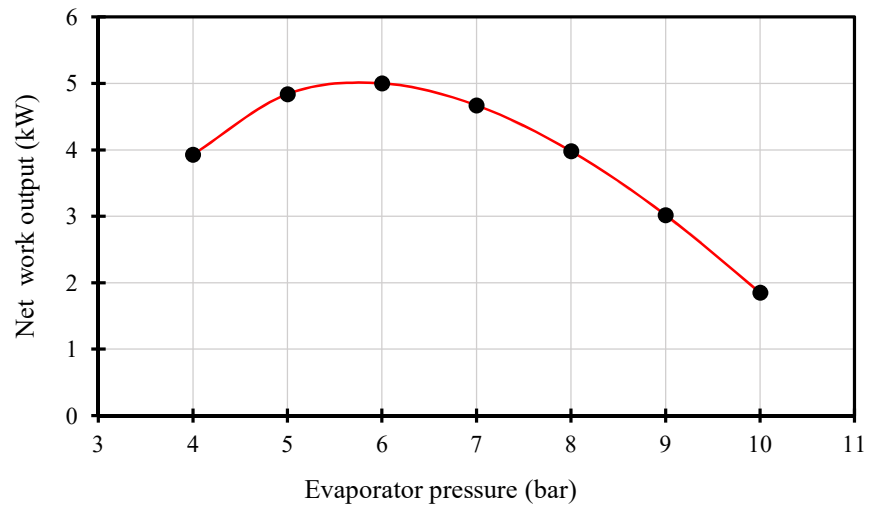


**Figure 4.3:** Effect of evaporator pressure on net work output

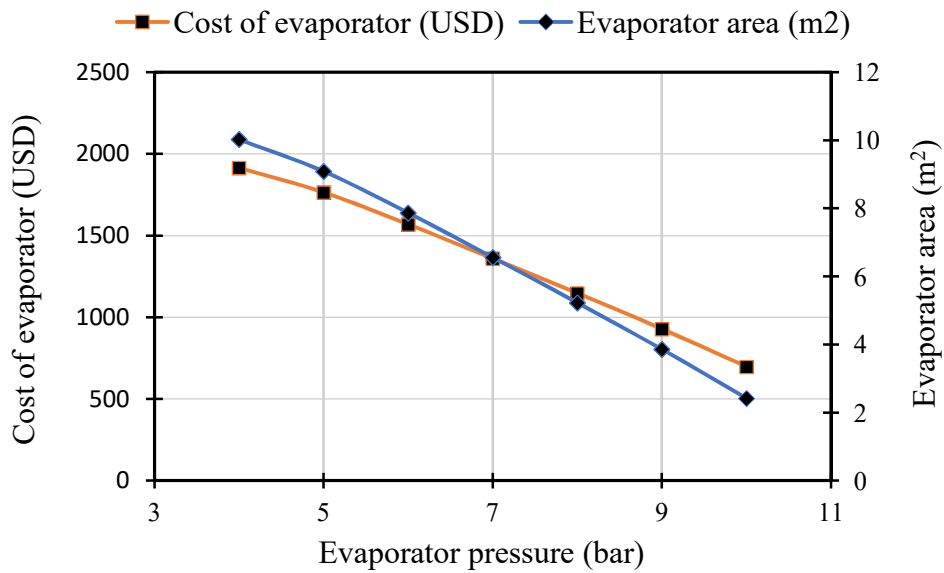


**Figure 4.4:** Effect of evaporator pressure on evaporator area and cost

### 4.3.2 Pinch point temperature difference

**Table 4.3:** Effect of pinch point temperature difference

SI No	Symbol	Parameter	Value	Unit
1	$T_{hf,in}$	Temperature of heat source	100	°C
2	$T_{wf,in}$	Condensation temperature	40	°C
3	P	Evaporation pressure	8	bar
4	$DT_{sup}$	Degree of superheat	5	°C

The operational parameters are tabulated in Table 4.3. The heat source temperature and the condensation temperature were set to 100 and 40 °C respectively. Evaporator pressure was fixed at 8 bar. Degree of superheat was maintained constant at 5 °C. The pinch point temperature difference was varied from 2 to 14 °C. When pinch point temperature is increased while maintaining all other parameters constant, hot fluid exit temperature,  $T_{hf,3}$ , increases. However, since, expander inlet and exit conditions remain constant, by energy balance, mass flow rate of the working fluid decreases. Net work output of the system decreases because of the reduction in the mass flow rate as seen in Figure 4.5. Figure 4.6 shows the effect of PPTD on evaporator area and its cost. In addition to the reduction in mass flow rate, log mean temperature difference also increases. As a result of this, heat exchanger area decreases with increase in PPTD. The cost of the evaporator decreases because of the reduction in surface area of the evaporator. Heat exchanger area decreases by 89.65% and evaporator cost is reduced by 74.86% when PPTD is increased from 2 to 14 °C.

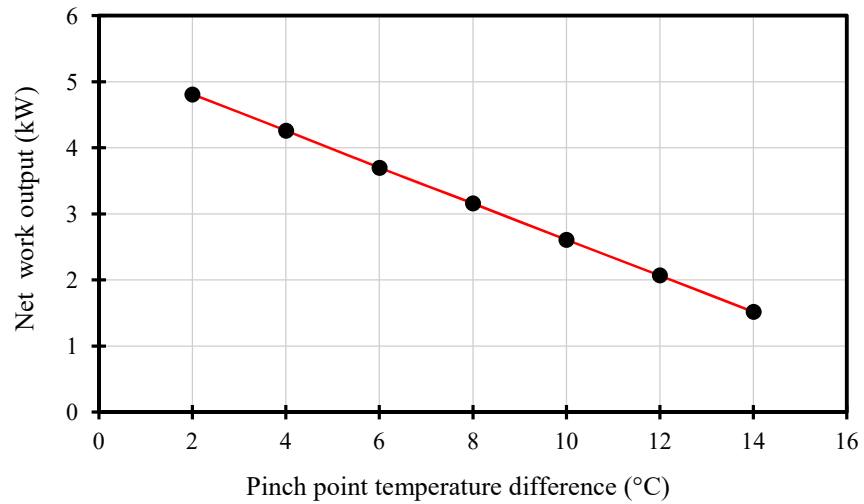


**Figure 4.5:** Effect of pinch point temperature difference on net work output

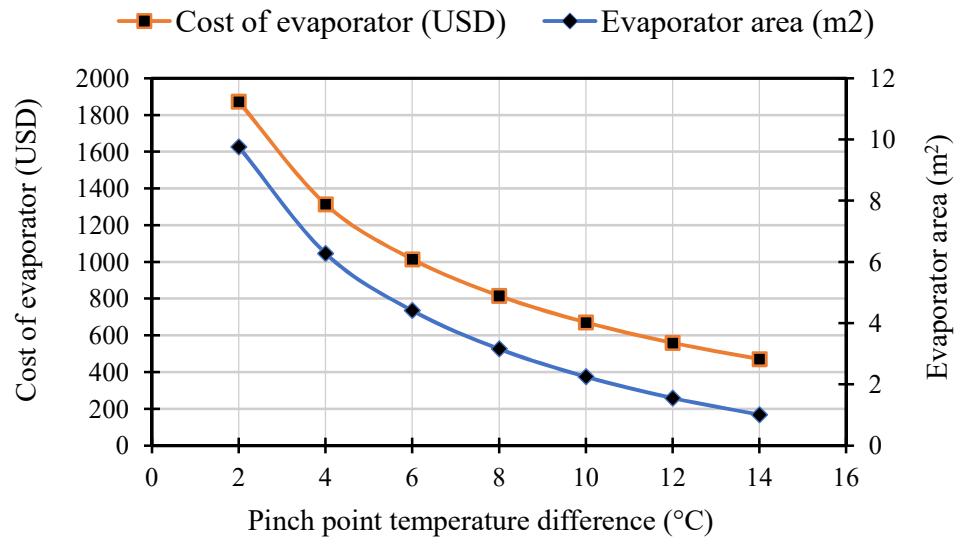


**Figure 4.6:** Effect of pinch point temperature difference on evaporator area and cost

### 4.3.3 Expander inlet temperature

**Table 4.4:** Effect of expander inlet temperature

SI No	Symbol	Parameter	Value	Unit
1	$T_{hf,in}$	Temperature of heat source	100	°C
2	$T_{wf,in}$	Condensation temperature	40	°C
3	P	Evaporation pressure	6.96	bar
4	PPTD	Pinch point temperature difference	5	°C

The operational parameters are tabulated in Table 4.4. The heat source temperature and the condensation temperature were set to 100 and 40 °C respectively. Pinch point temperature difference was set to 5 °C. Evaporator pressure was kept constant at 6.96 bar (corresponding to saturation temperature of 75 °C). Degree of superheat was then increased up to 20 °C. Figure 4.7 indicates the reduction in net power output. This is because; the marginal gain in enthalpy drop across the expander is lesser than the rate of decrease of mass flow rate. Figure 4.8 shows the variation of evaporator surface area and its cost with respect to expander inlet temperature. With increase in expander inlet temperature, the area reduces initially till the value reaches 6.59 m<sup>2</sup> at expander inlet temperature of 83 °C, and then increases again. Due to the constraint of PPTD, the mass flow rate decreases by energy balance. Hence, there is a significant reduction in heat transfer rate in the evaporation section. This effect is predominant at lower expander inlet temperatures. As the inlet temperature is increased further, the log mean temperature difference in the superheat zone also decreases. This results in the increase in area of the superheated zone. This phenomenon explains the increase in evaporator area at higher expander inlet temperatures. The evaporator cost also exhibits the same trend as that of evaporator area. It can be seen that, for dry fluids such as R245fa, increasing expander

inlet temperature by more than 7 °C, will not yield any positive results as surface area requirement of the evaporator and cost increases.

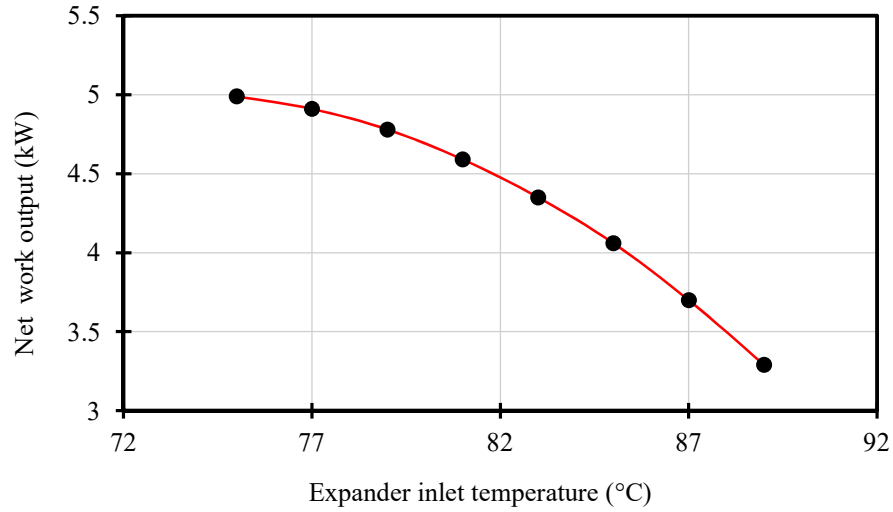


**Figure 4.7:** Effect of expander inlet temperature on net work output

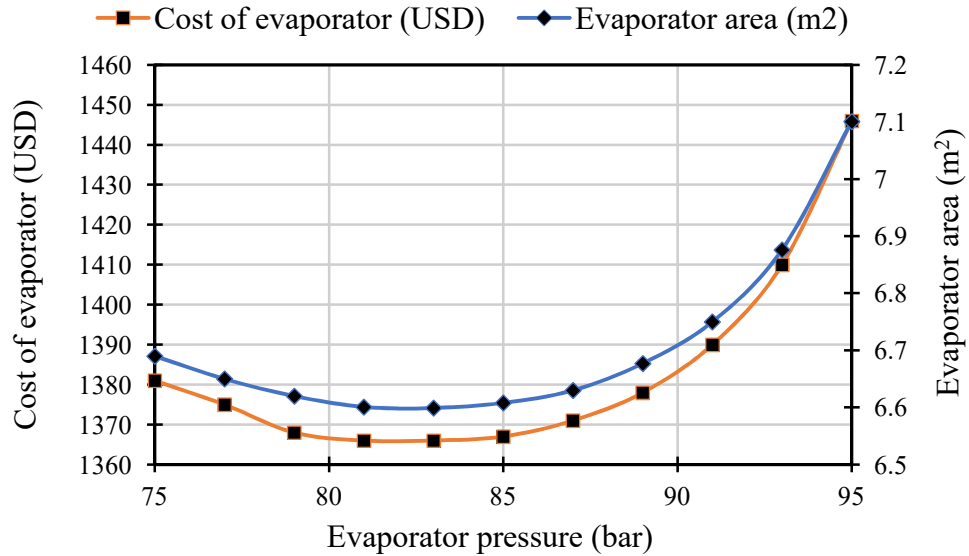
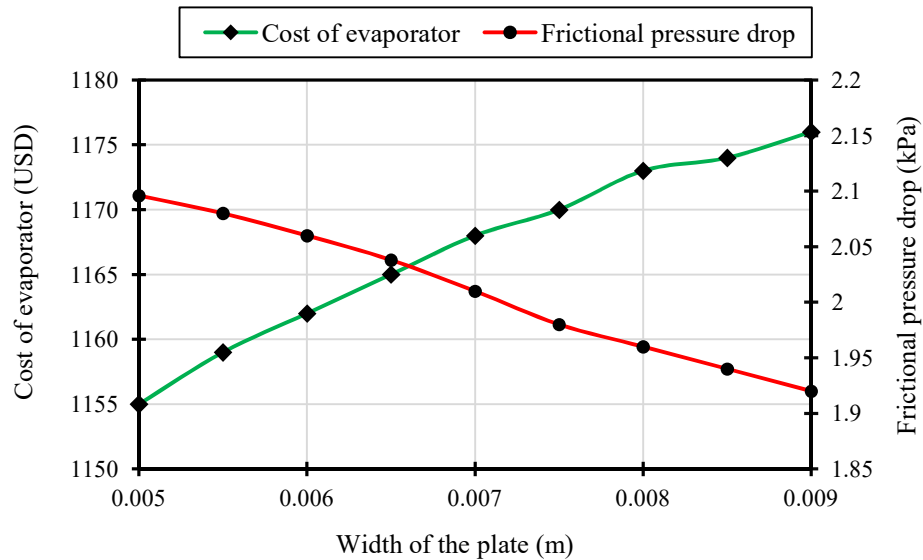


**Figure 4.8:** Effect of expander inlet temperature on evaporator area and cost

#### 4.4 Effect of geometrical parameters on pressure drop and evaporator cost

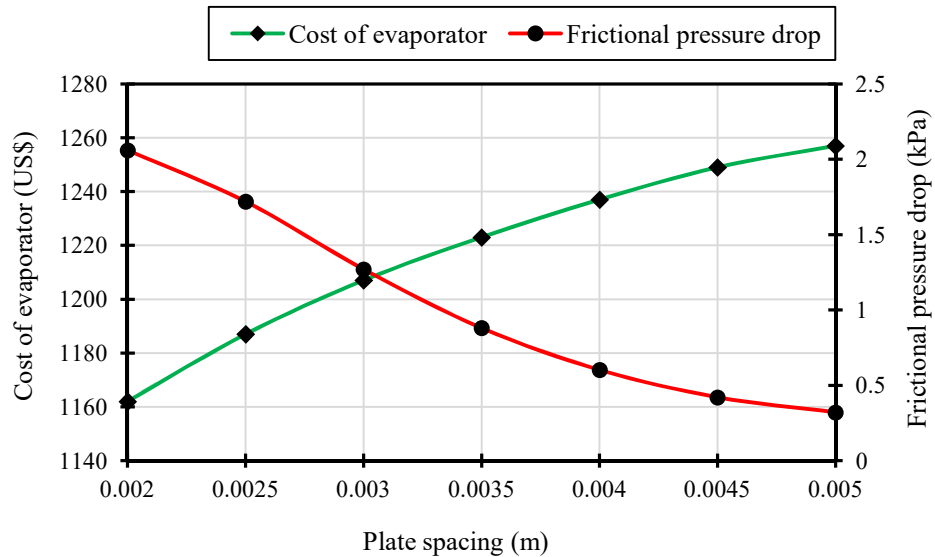
Plate spacing was kept constant at 0.003 m and the width of the plate was varied from 0.005 to 0.009 m. Hydraulic diameter was calculated based on Equation (4.14).

Figure 4.9 shows the effect of plate width on the cost of the evaporator and frictional pressure drop. As the width of the plate increases, the area increases slightly. This results in the marginal increase in the evaporator cost. Increase in plate width also causes Reynolds number to increase. The frictional pressure drop is related to Reynolds number as shown in Equation (4.16). Therefore, total pressure drop in the plate heat exchanger reduces. In this study, the trade-off point for plate width was at 0.0065 m, where the evaporator cost was found to be 1166 USD (Rs 87,450) and frictional pressure drop was 2.03 kPa.



**Figure 4.9:** Effect of plate width on evaporator cost and frictional pressure drop

The variation of evaporator cost and frictional pressure drop with plate spacing is presented in Figure 4.10. In this case, plate width was fixed at 0.5 m and plate spacing was varied from 0.002 to 0.005 m.



**Figure 4.10:** Effect of plate spacing on evaporator cost and frictional pressure drop

The increase in plate spacing creates more space for indirect contact between the heat source and the working fluid. This leads to reduced heat transfer. To maintain constant heat transfer, additional plates has to be added, which leads to the increase in the evaporator area. Therefore, cost of the evaporator increases. When plate spacing is increased, the hydraulic diameter & Reynolds number increases. This directly impacts the frictional pressure drop. Frictional pressure drop reduces with increase in plate spacing. The optimum point for plate spacing was at 0.003 m, where the evaporator cost was 1210 USD (Rs 90,750) and frictional pressure drop was 1.27 kPa.

#### 4.5 Chapter closure

Effect of evaporator pressure, expander inlet temperature and pinch point temperature difference on the size and cost of the plate heat exchanger was analyzed using a three zone thermo-hydraulic steady state model. Moreover, the effect of geometrical parameters such as plate spacing and plate width on the cost and pressure drop was also studied.



## CHAPTER 5

### PARAMETRIC INVESTIGATION OF OPEN-DRIVE SCROLL EXPANDER FOR ORGANIC RANKINE CYCLE SYSTEMS

The most important component in ORC is the expansion device which converts the available thermal energy into mechanical work. The choice of expander depends mainly on the operating conditions and the capacity of the system. They are broadly classified into dynamic and volumetric expanders. Volumetric (or positive displacement) expanders are more suitable for small scale power generation (Lemort et al. 2009). Moreover, these expanders can tolerate wet expansion. Among the positive displacement expanders, scroll expanders are a good choice for ORC systems because of lesser number of moving parts, lower rotational speeds compared to other expanders, high reliability and robustness and low noise and vibration (Ma et al. 2017). Scroll expanders of small capacities are not readily available in open market. Therefore, scroll compressors, which are extensively used in refrigeration and air conditioning industry, are modified to work as an expander.

In this study, parametric investigation of scroll expander is carried out using a validated semi-empirical model to study the effect of expansion ratio, rotational speed of the shaft and inlet temperature on mass flow rate, work output and efficiency of the scroll expander. The semi-empirical model helps in giving a better insight into the performance of the scroll expander in off-design conditions.

#### 5.1 Semi-empirical model description

A 5 kW<sub>e</sub> scroll expander used in experimental study was used for this analysis (Ziviani et al. 2018). The expander built-in volume ratio was 3.5 and it had a displacement volume of 73.6 cm<sup>3</sup> per revolution. Due to design constraints, the operating conditions of expander were limited to

- a) Maximum inlet pressure: 13.8 bar
- b) Maximum temperature: 175 °C

c) Rotational speed: 500 – 3600 rpm

In this study, a semi-empirical model developed by Lemort et al. (2009) has been used. Some researchers developed deterministic models which predict the behaviour of the machine based on their geometry and configuration (Garg et al. 2016; Ma et al. 2017; Oralli et al. 2011). But the geometric models has to be combined with other sub-models such as valve model, internal leakage model, motion equation, heat transfer equation etc. to complete the scroll expander modelling. Hence, it becomes more complicated and cannot be integrated into cycle models. Therefore, empirical and semi-empirical models are preferred.

Unlike deterministic models, semi-empirical simulation model does not need exact knowledge of the geometry of the machine. The proposed model involves only a limited number of parameters. The parameters are then identified using experimental data (Ziviani et al. 2018).

The input variables of the model are the supply pressure, the supply temperature, the exhaust pressure and the rotational speed of the expander. The model calculates the mass flow rate displaced by the expander, the delivered mechanical power and the exhaust temperature. The parameters of the model are identified by minimizing a global error function accounting for the errors on the prediction of the mass flow rate, shaft power and exhaust temperature which are the main output variables of the model.

$$\text{error} = \frac{1}{3} \left( \sqrt{\sum_1^{N_{\text{tests}}} \left( \frac{\dot{M}_{\text{calc}} - \dot{M}_{\text{meas}}}{\dot{M}_{\text{calc}}} \right)^2} \right) + \frac{1}{3} \left( \sqrt{\sum_1^{N_{\text{tests}}} \left( \frac{\dot{W}_{\text{sh,calc}} - \dot{W}_{\text{sh,meas}}}{\dot{W}_{\text{sh,calc}}} \right)^2} \right) + \frac{1}{3} \left( \sqrt{\sum_1^{N_{\text{tests}}} \left( \frac{T_{\text{ex,calc}} - T_{\text{ex,meas}}}{T_{\text{ex,meas,max}} - T_{\text{ex,meas,min}}} \right)^2} \right) \quad (5.1)$$

The semi empirical model describes the expansion process within the scroll expander which also consists of related equations. The entire expansion process is divided into 7 stages as shown in the Figure 5.1. The processes are as follows:

- a) Adiabatic supply pressure drop (su to su,1)
- b) Constant pressure supply cooling down (su,1 to su,2)
- c) Internal leakage (su,2 to ex,2)
- d) Adiabatic and reversible expansion to the adapted pressure which is forced upon by the built-in volume ratio of the machine (su,2 to ad)
- e) Adiabatic expansion at constant volume (ad to ex,2)
- f) Adiabatic fluid mixing between supply and leakage flows (ex,2 to ex,1)
- g) Constant pressure heating up or cooling down (ex,1 to ex)

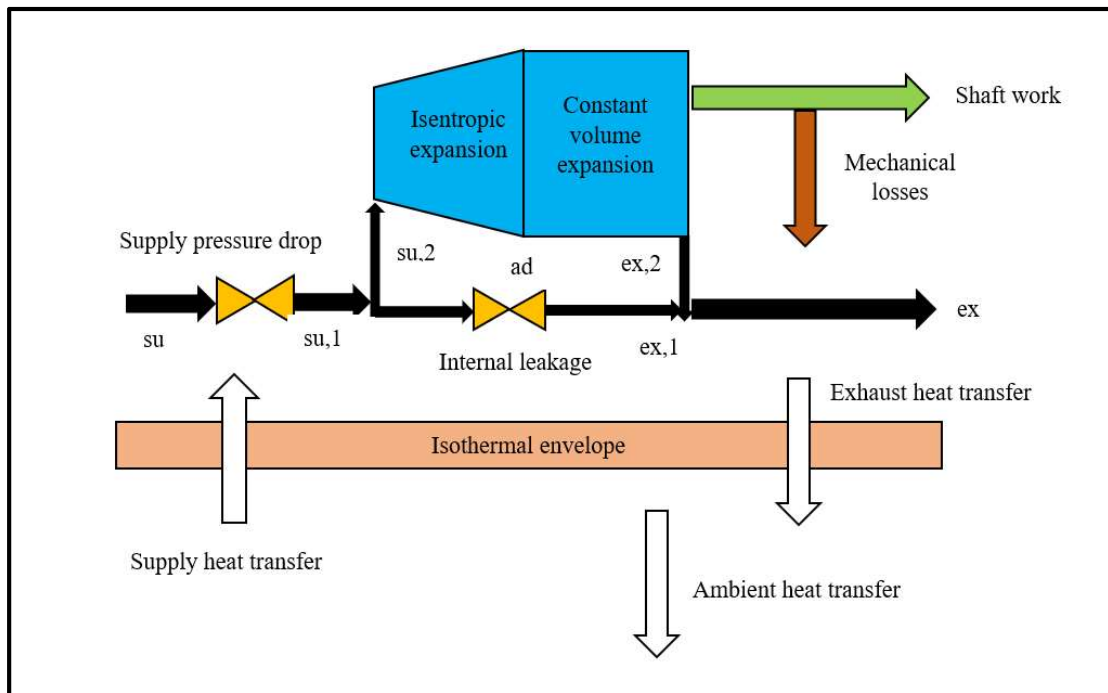


**Figure 5.1:** Conceptual diagram of scroll expander model

**a) Adiabatic supply pressure drop (su to su,1)**

This process accounts for the pressure losses occurring between the inlet of the expander and the suction chamber. The pressure drop occurs mainly due to two reasons. The

primary reason is that, during the suction process, the expander suction port is blocked by the tip of the orbiting scroll which reduces the effective suction port area. In addition to this, the flow passage is progressively reduced between the chamber and along the length of the scroll.

This process is modelled as isentropic flow through a converging nozzle whose cross sectional area is  $A_{su}$ .  $A_{su}$  represents the average inlet port effective area during the suction process. Mass flow rate of the fluid entering the expander can be expressed as

$$\dot{m} = \rho_{su,1} \times A_{su} \times \sqrt{2 \times (h_{su} - h_{su,1})} \quad (5.2)$$

### **b) Isobaric supply cooling down (su,1 to su,2)**

Supply heat transfer is simulated using a fictitious envelope with uniform temperature  $T_w$ . This envelope represents the outer shell of the expander and the scrolls. Heat transfer occurs between the supply chamber and this envelope. This can be modelled as,

$$\dot{Q}_{su} = \dot{m} \times (h_{su,1} - h_{su,2}) \quad (5.3)$$

$$\dot{Q}_{su} = \left[ 1 - e^{\frac{-AU_{su}}{\dot{m}C_p}} \right] \times \dot{m} \times C_p \times (T_{su,1} - T_w) \quad (5.4)$$

The relationship between supply heat transfer coefficient,  $AU_{su}$  and mass flow rate is defined by,

$$AU_{su} = AU_{su,nom} \times \left( \frac{\dot{m}}{\dot{m}_{nom}} \right)^{0.8} \quad (5.5)$$

Where,  $AU_{su,nom}$  is the nominal supply heat transfer coefficient corresponding to the nominal mass flow rate.

The supply heat transfer coefficient,  $AU_{su}$  is supposed to vary with the mass flow rate and takes into account only the convective heat transfer coefficient of the working fluid as the conductive thermal resistance of the scroll wraps is negligible due to the high metal

thermal conductivity and small thicknesses. Equation 5.5 is derived from Dittus-Boelter correlation valid for turbulent flow in pipes and it is further simplified using Reynolds analogy for a fully-developed turbulent flow.

**c) Internal leakage (su,2 to ex,2)**

Internal leakage is an irreversible loss which occurs along two paths in a scroll machine. The first leakage path occurs in the axial clearance between the scrolls and the bottom. This results in radial leakage. The second path is the clearance between the fixed and the orbiting scroll, which leads to tangential leakage. This internal leakage is modeled similar to the supply pressure drop. It is modeled as a lumped nozzle whose cross sectional area is  $A_{leak}$ . Critical pressure of the lumped nozzle is defined as (Yang et al. 2018),

$$P_{cr} = P_{su,2} \times \left( \left( \frac{2}{\gamma + 1} \right)^{\frac{\gamma}{\gamma - 1}} \right) \quad (5.6)$$

$$P_{thr} = \text{Max} (P_{ex,2}, P_{cr}) \quad (5.7)$$

The critical pressure is evaluated by considering the working fluid as a perfect gas.  $\gamma$  indicates the ratio of specific heats  $C_p$  and  $C_v$ .

The mass flow rate entering the expander can be divided into two parts. The first facilitates the rotation of the shaft at a particular speed, 'N'. The second part is the leakage mass flow rate.

Total mass flow rate is given by (Giuffrida 2014),

$$\dot{m} = \rho_{su,2} \times \left( \frac{N \times v_s}{r_{v,in}} \right) + \dot{m}_{leak} \quad (5.8)$$

where,  $v_s$  is the swept volume and  $r_{v,in}$  is built-in volume ratio of the expander

Leakage mass flow rate is calculated as,

$$\dot{m}_{\text{leak}} = \rho_{\text{leak}} \times A_{\text{leak}} \times \sqrt{2 \times (h_{\text{su},2} - h_{\text{leak}})} \quad (5.9)$$

**d) Adiabatic and reversible expansion to the adapted pressure (su,2 to ad)**

After the initial cooling down, the working fluid undergoes isentropic expansion. The pressure is reduced from  $P_{\text{su},2}$  to  $P_{\text{ad}}$ . This adapted pressure is decided by the built-in volume ratio,  $r_{v,\text{in}}$  of the expander. This is a geometric parameter of the scroll expander which is designed and fixed by the manufacturers.

$$V_{\text{ad}} = r_{v,\text{in}} \times V_{\text{su},2} \quad (5.10)$$

**e) Adiabatic expansion at constant volume (ad to ex,2)**

Most of the scroll expanders that are used in organic Rankine cycle systems are modified from a commercially available scroll compressor. The operating pressure of ORC system does not necessarily match with that of the built-in volume ratio of the expander. This leads to under or over expansion losses. Under expansion occurs when the adapted pressure,  $P_{\text{ad}}$  exceeds the exhaust pressure,  $P_{\text{ex},2}$ . Model assumes there is no pressure drop through the discharge port. Hence, in order to equalize the pressures in the exhaust chamber and the discharge line, the model assumes that, some fluid flows out of or into the expander chamber (under/over expansion) instantaneously after the chamber opens to the outlet line.

**f) Adiabatic fluid mixing between supply and leakage flows (ex,2 to ex,1)**

The mass flow rate responsible for shaft rotation and leakage mass flow rate mix together. This results in the increase in the specific enthalpy of the working fluid ( $h_{\text{ex},1} > h_{\text{ex},2}$ ).

**g) Constant pressure heating up or cooling down (ex,1 to ex)**

Isobaric exhaust heat transfer is modeled similar to isobaric supply cooling down. Heat is exchanged between the fluid leaving the expander and the metal envelope.

Internal expansion work can be calculated as (Giuffrida 2018),

$$\dot{W}_{\text{int}} = \dot{m}_{\text{int}} \times \left[ (h_{\text{su},2} - h_{\text{ad}}) - v_{\text{ad}} (P_{\text{ad}} - P_{\text{ex},2}) \right] \quad (5.11)$$

Net power output or shaft power is the difference between the internal expansion work and the mechanical losses associated with the expander. In this case, all mechanical losses are lumped into a constant parameter called loss torque. This is expressed as,

$$\dot{W}_{\text{sh}} = \dot{W}_{\text{int}} - \dot{W}_{\text{loss}} \quad (5.12)$$

$$\dot{W}_{\text{loss}} = \frac{2 \times \pi \times N \times \tau_{\text{loss}}}{60} \quad (5.13)$$

Expander isentropic effectiveness or expander efficiency is defined as the ratio of net output power to isentropic expansion power (Lemort et al. 2009).

$$\epsilon_{\text{is}} = \frac{\dot{W}_{\text{sh}}}{\dot{m} \times (h_{\text{su}} - h_{\text{is}})} \quad (5.14)$$

Thermal losses towards the ambient are evaluated as,

$$\dot{Q}_{\text{amb}} = AU_{\text{amb}} \times (T_w - T_{\text{amb}}) \quad (5.15)$$

where,  $AU_{\text{amb}}$  is the global heat transfer coefficient between the envelope and the ambient.

The metal wall temperature is calculated by applying the global heat balance equation which is given by,

$$\dot{W}_{\text{loss}} - \dot{Q}_{\text{ex}} + \dot{Q}_{\text{su}} - \dot{Q}_{\text{amb}} = 0 \quad (5.16)$$

The inputs to the semi empirical scroll expander are listed in Table 5.1. The parameters of the model were identified by minimizing a global error function accounting for the errors on the prediction of the mass flow rate, shaft power and exhaust temperature (Ziviani et al. 2018).

**Table 5.1:** Inputs to the semi empirical model

Parameter	Value	Unit
$\dot{m}_{nom}$	0.1384	kg/s
$AU_{su,nom}$	28.39	W/°C
$AU_{ex,nom}$	11.71	W/°C
$AU_{amb}$	6.17	W/°C
$V_s$	$8.1 \times 10^{-5}$	$m^3$
$r_{v,in}$	3.31	-
$A_{su}$	$4.01 \times 10^{-5}$	$m^2$
$A_{leak}$	$7.43 \times 10^{-6}$	$m^2$
$\tau_{loss}$	2.97	Nm

## 5.2 Parametric analysis

Using the semi empirical model, this study is performed to examine a specific parameter by varying it, while keeping the other parameters constant. The monitored parameters are the expansion ratio, the rotational speed of the shaft and the inlet temperature of the expander. The outputs to be assessed are mainly the mass flow rate, work output and efficiency of the expander.

### 5.2.1 Effect of expansion ratio

Two inlet pressures of 10 bar and 14 bar are considered. Inlet temperature is fixed at 110 °C. Expansion ratio is varied by varying the condensation pressure from 3 to 1.2 bar. The shaft power and expander efficiency are evaluated for different expansion ratios. The simulation is carried out for rotational speeds of 1500 and 2000 rpm.



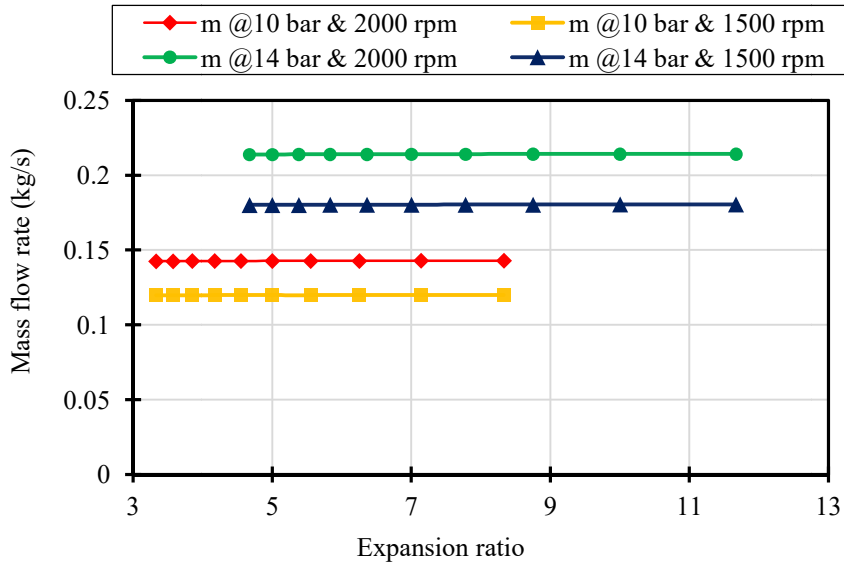


**Figure 5.2:** Effect of expansion ratio on mass flow rate of the working fluid

It is seen from Figure 5.3 that the shaft power increases with decreasing condensation pressure or increasing expansion ratio. However, the power curve is shifted downwards at lower shaft speeds at same inlet pressures. This is due to the decrease in mass flow rate of the working fluid as shown in Figure 5.2. In addition to this, the two cases with inlet pressure at 10 bar has lower mass flow rate compared to the two cases with 14 bar inlet pressure. This is because, at higher pressure, the fluid density is also high. When the inlet pressure is lowered to 10 bar, the power curve shifts downwards and towards the left, with respect to the cases with increased expansion ratios. Extraction of work from the expander also increases at higher expansion ratios which lead to higher power output.

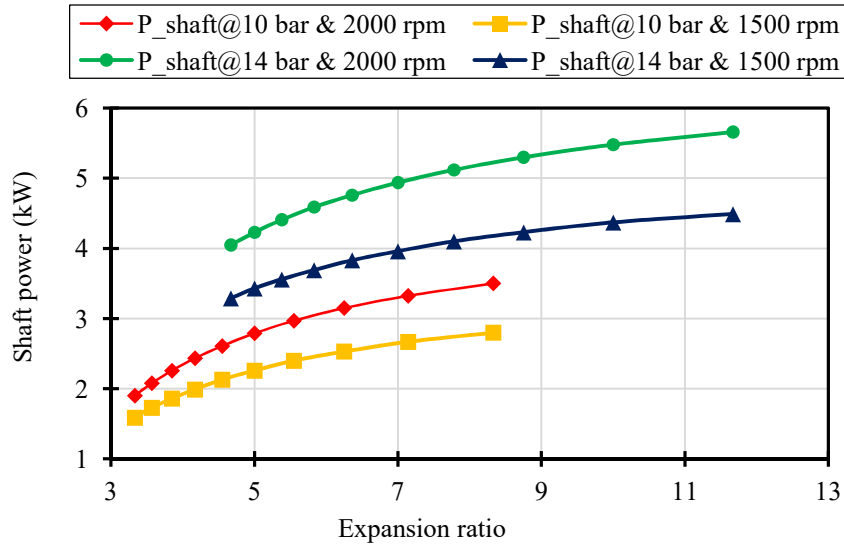


**Figure 5.3:** Effect of expansion ratio on shaft power

Figure 5.4 shows the variation of expander efficiency with expansion ratio. Expansion process is divided into two parts. The initial part is the isentropic expansion till the adapted pressure and the second part is the constant volume expansion. In the first part, the pressure of the working fluid is reduced from  $P_{su,2}$  to adapted pressure  $P_{ad}$  imposed by the built-in volume ratio of the expander. The built-in volume ratio is an intrinsic geometric parameter of the scroll expander. Under-expansion occurs when the internal pressure ratio imposed by the expander ( $P_{su,2}/P_{ad}$ ) is lower than the system pressure ratio ( $P_{su,2}/P_{ex,2}$ ).

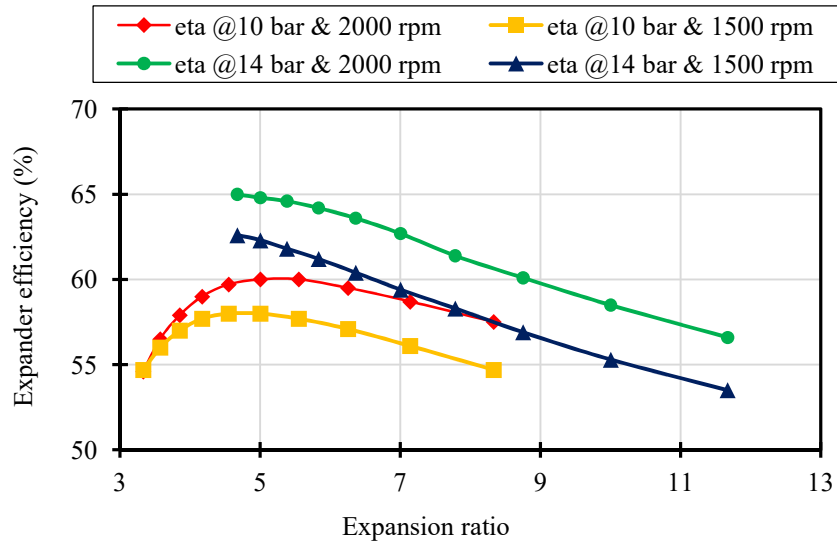


**Figure 5.4:** Effect of expansion ratio on expander efficiency

In cases when the inlet pressure is fixed at 14 bar and the expansion ratio is varied from 4.67 to 11.67, all condensation pressures (3 to 1.2 bar) leads to the condition of under expansion. The expander efficiency drops when under expansion takes place. The efficiency decreases by 12.92% for shaft speed of 2000 rpm and 14.53% for shaft speed of 1500 rpm. At inlet pressure of 10 bar, a peak is observed in efficiency curve for expansion ratio of 4.55 and 5 at shaft speeds of 1500 & 2000 rpm respectively. This is due to the fact that the condensation pressures passes through the adapted condition of the expander, where the efficiency is maximum.

### 5.2.2 Effect of shaft speed

Four different combinations (inlet pressure at 10 bar and condensation pressure of 3 bar; inlet pressure at 10 bar and condensation pressure of 1.2 bar; inlet pressure at 14 bar and condensation pressure of 3 bar; inlet pressure at 14 bar and condensation pressure of 1.2 bar) are used to study the effect of shaft speed on mass flow rate, work output and expander efficiency. Inlet temperature is fixed at 110 °C. The shaft speed is varied from 800 to 2600 rpm.

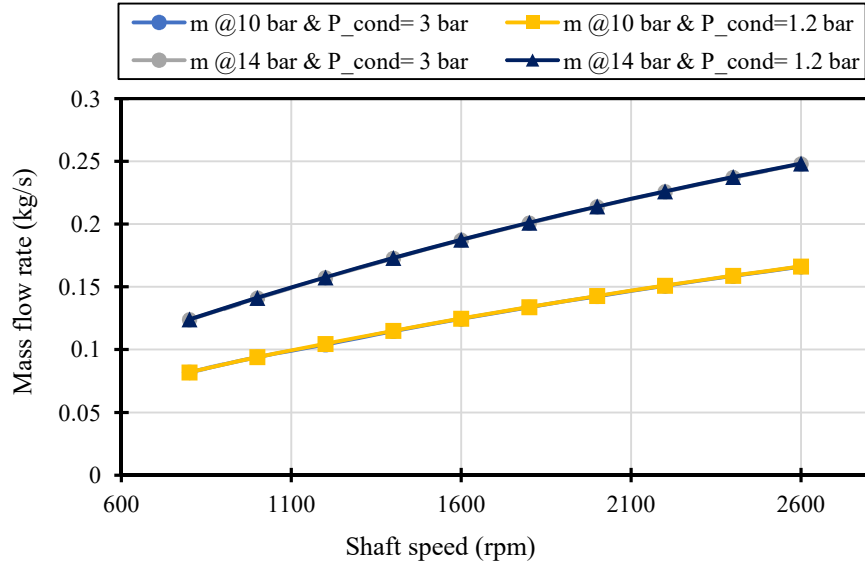


**Figure 5.5:** Effect of shaft speed on mass flow rate of the working fluid

Figure 5.5 shows the variation of mass flow rate of the fluid with shaft speed. The variation is almost linear with respect to shaft speed. Theoretically higher expansion ratio should lead to increase in leakage mass flow rate. However, the vapor is already in choked condition in the case of lowest expansion ratio (inlet pressure of 10 bar and condensation pressure of 3 bar). Therefore, the curves are superimposed. It is observed that the shaft power increases with increase in shaft speed as shown in Figure 5.6. However, the increase in mass flow rate due to increasing shaft speed is not enough to counter the losses occurring within the expander. Mechanical losses occur mainly within the scroll expander due to friction between the fixed and orbiting scroll. However, in this study, all losses are lumped into one mechanical loss torque,  $\tau_{loss}$ . The effect of increasing shaft speed beyond a certain point can be seen in Figure 5.7, when the expander efficiency witnesses a marginal drop. The trend is similar for all curves. But, the expander efficiency curve for inlet pressure of 10 bar and condensation pressure of 3 bar shows that the curve peaks (54.9%) at shaft speed of 1600 rpm. In other cases, the peak has shifted towards the extreme right (2400-2600 rpm). Power output is reduced due to increase in the losses. Therefore, the expander efficiency decreases.

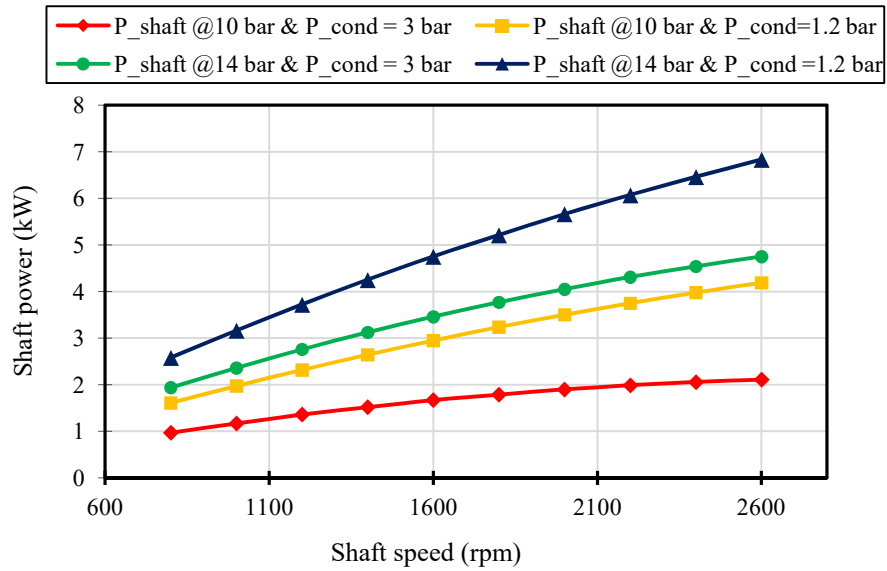


**Figure 5.6:** Effect of shaft speed on shaft power

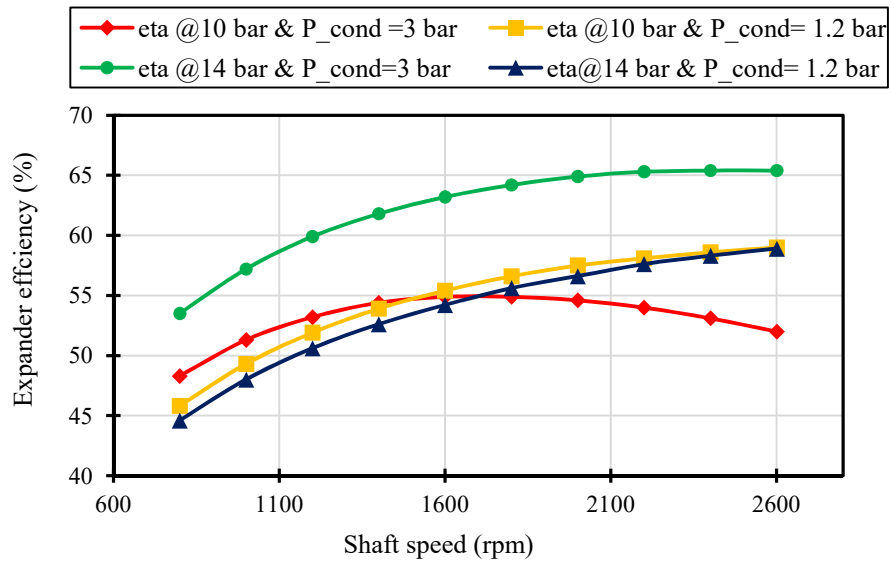


**Figure 5.7:** Effect of shaft speed on expander efficiency

### 5.2.3 Effect of inlet temperature

In this case, the fixed parameters are the expander inlet pressures of 10 and 14 bar, condensation pressure of 1.2 bar and shaft speeds of 1500 and 2000 rpm. The inlet temperature is varied from 90 to 120 °C at 10 bar and 105 to 135 °C at 14 bar.

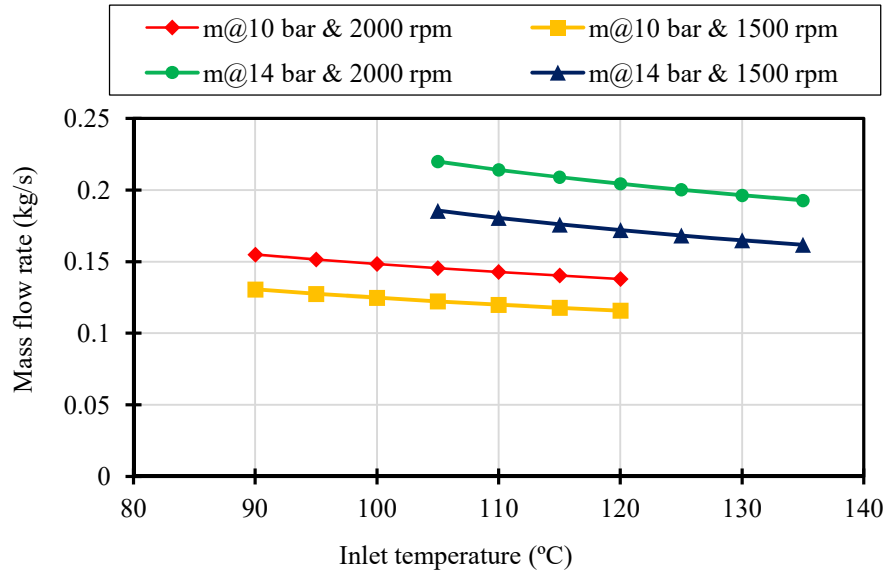


**Figure 5.8:** Effect of inlet temperature on mass flow rate

Figure 5.8 shows the trend of mass flow rate when inlet temperature (degree of superheat) is increased. It is seen that the mass flow rate of the working fluid decreases slightly, as the density of the fluid decreases. The mass flow rate is high in the case where inlet pressure is at 14 bar and shaft speed is at 2000 rpm. From Figure 5.9, it can be observed that the shaft power remains nearly constant when inlet temperature is increased. Therefore, it can be inferred that, the enthalpy gain across the expander is nullified due to the decrease in the mass flow rate. Superheating does not benefit in increasing the power output from the expander.

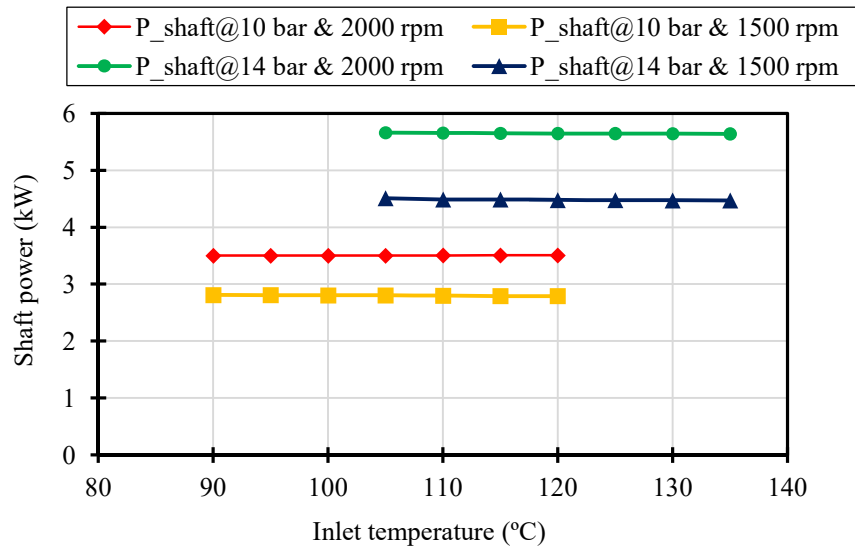


**Figure 5.9:** Effect of inlet temperature on shaft power

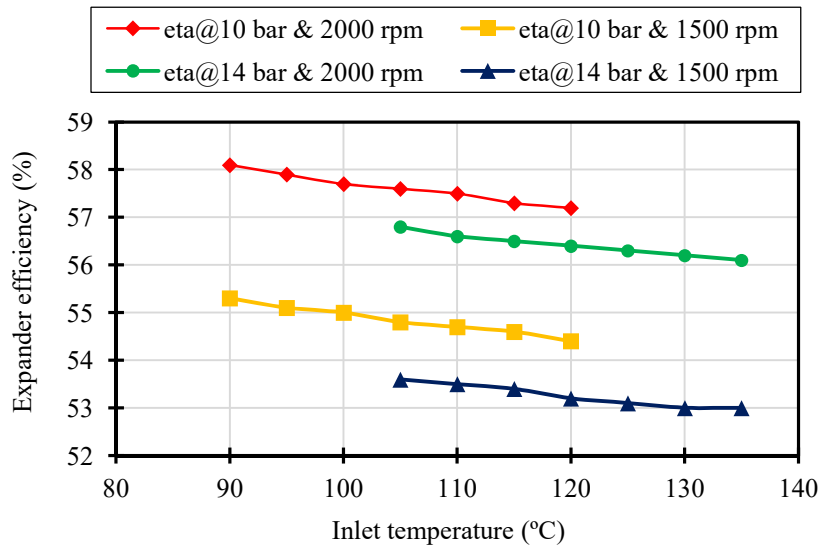


**Figure 5.10:** Effect of inlet temperature on expander efficiency

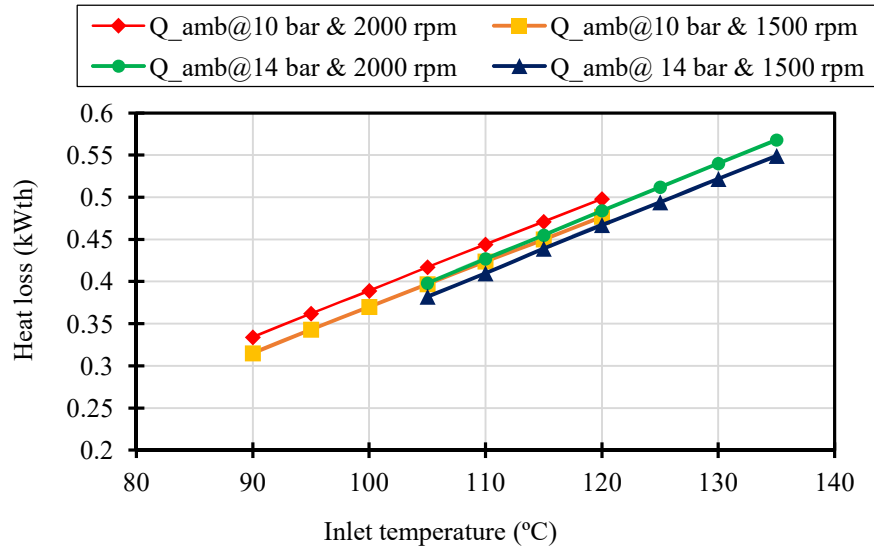


**Figure 5.11:** Effect of inlet temperature on heat loss to ambient

However, degree of superheat of the fluid determines the quantum of heat exchange with the wall in the isobaric cooling process, modelled at the inlet. This thermal energy which is exchanged is an important component similar to the power loss. This will decide how much heat is vented out to the environment. Increasing inlet temperature leads to increases in the wall temperature. This results in thermal energy dissipation. Thermal energy dissipation increases with inlet temperature for all curves as shown in Figure 5.11. This also leads to the deterioration in efficiency of the expander as shown in Figure 5.10. The curves with higher shaft speeds dissipate more heat. Higher shaft speed increases the wall temperature, as high shaft speeds leads to more frictional power loss.

### 5.3 Chapter closure

This chapter focuses on the parametric investigation of open-drive scroll expander used for micro organic Rankine cycle. A 5 kW<sub>e</sub> expander was used and its built-in volume ratio was 3.5. R245fa was used as the working fluid. Effect of key parameters such as expansion ratio, shaft speed and expander inlet temperature on power output and expander efficiency was evaluated for four different cases.



## CHAPTER 6

### COST ANALYSIS AND EXERGO-ECONOMIC OPTIMIZATION OF SOLAR DRIVEN ORGANIC RANKINE CYCLE SYSTEM

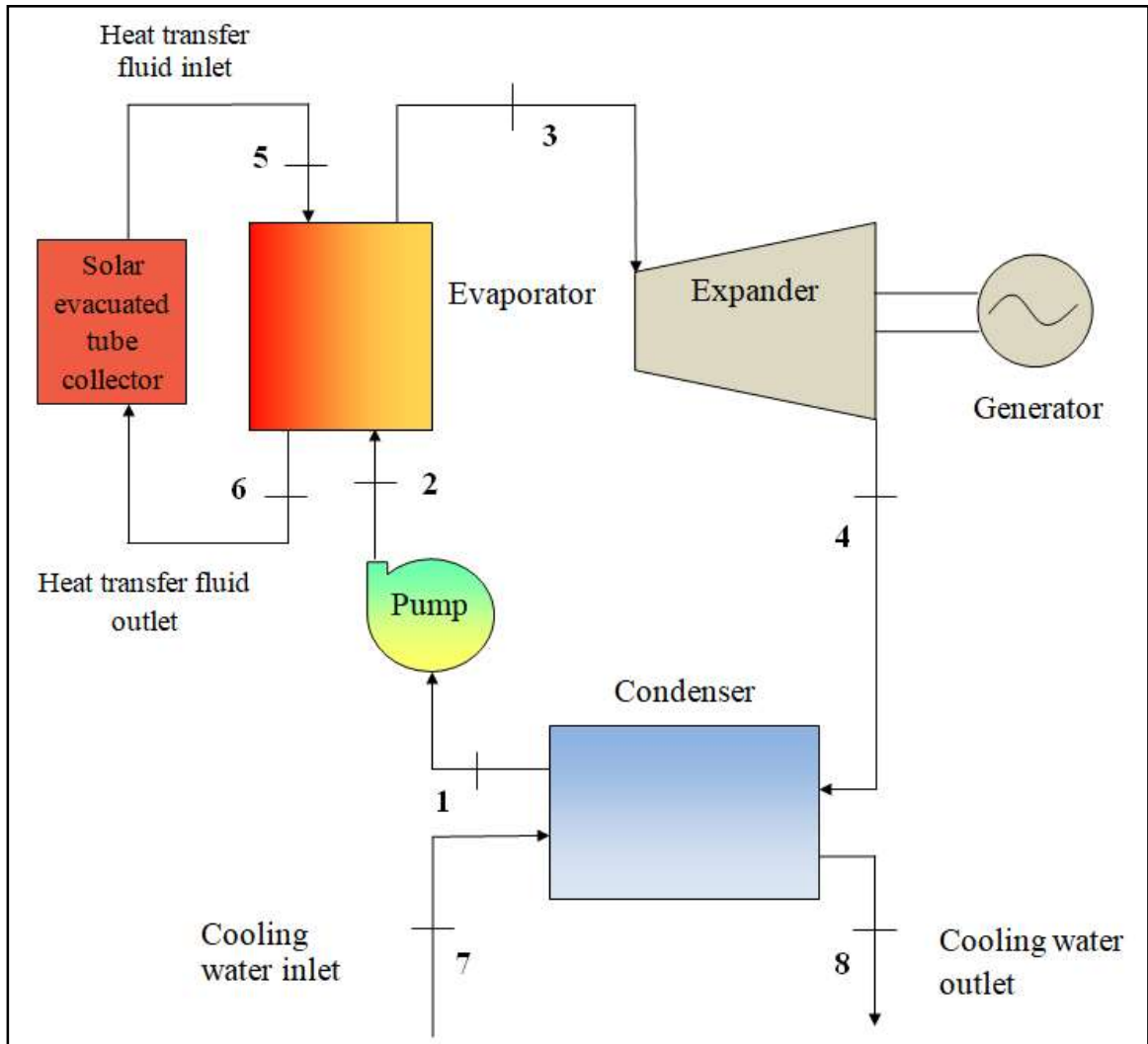
#### 6.1 Economic analysis of solar ORC system

Table 6.1 shows the cost estimation of major parts of solar driven organic Rankine cycle system. Schematic setup of ORC system driven by evacuated tube collectors is depicted in Figure 6.1. The total cost of the solar ORC system of 1 kW<sub>e</sub> is estimated to be Rs 7,42,500. This type of system can be used in India widely as an off grid power generation system. Heat source (Solar flat plate collector) and scroll expander forms the major portion of the cost. Cost of solar collector system is around 27% of the total cost. Presently, commercial expanders of 1 kW<sub>e</sub> capacity are not available in India. For research work, scroll expanders are used by modifying the available scroll compressors which is not very efficient. In this analysis, imported scroll expander (Air squared; Model: E15H022-SH) is considered and its cost constitutes around 55.5% of the total cost.

**Table 6.1:** Cost of major components of the solar ORC plant in India as per price quotations

Parameter	ICC (Rs)
Solar field (Evacuated tube collector cost calculated as Rs 10,000/m <sup>2</sup> for collector area of 20 m <sup>2</sup> )	2,00,000
Expander (Air-squared 1 kW <sub>e</sub> semi hermetic scroll expander)	4,12,500
Pump	30,000
Heat exchangers (Plate type)	1,00,000
<b>Total cost (Rs)</b>	<b>7,42,500</b>

\*Cost of air squared 1 kW scroll expander is 5500 USD which is approximately Rs 4,12,500 (calculated as 1 USD = Rs 75)



**Figure 6.1:** Schematic diagram of solar driven ORC system

**Table 6.2:** Cost of 1 kW<sub>p</sub> solar PV system (Ahsan et al. 2016)

Particulars	Investment (Rs)
PV Modules	50000
Batteries	25000
Inverter	10000

<b>Total Cost (Rs)</b>	<b>85000</b>
------------------------	--------------

Table 6.2 shows the cost of 1 kW<sub>e</sub> off-grid solar photovoltaic system. Total cost of the system is estimated to be around Rs 85,000 which is very competitive. Increasing the manufacturing of ORC systems will help reduce the cost of the system due to economies of scale. This will also help reduce import dependency. Various options have to be applied to finance off-grid solar ORC system in rural areas. Some of the options currently available are private financing, financing through power utilities, government financing and public private partnership. Since, the capital cost of solar ORC is significantly higher than other renewable energy technologies; Government of India needs to provide subsidies to promote solar ORC systems in India. The Government has to support the ORC developers and investors by ensuring financial viability to them and help them to develop a market. Financial assistance should be provided to them in the form of start up and working capital loans. At the same time, they need to ensure rural customers get ORC systems at affordable cost. Presently, for solar PV systems in India, there is an upper limit on the amount of subsidy provided per installed kW capacity. 30% capital subsidy is provided to residential consumers (upto 10 kW capacity). Similar approach can be adopted in case of solar ORC systems also. Therefore, by promoting domestic manufacturing of solar ORC systems, mainly expanders, and providing subsidy grants to consumers, off-grid solar ORC systems can be adopted on a large scale in rural India.

### **6.1.1 Exergoeconomic optimization of 1 kW<sub>e</sub> ORC system**

The exergo-economics is a powerful tool to study and optimize an energy system. The exergoeconomic analysis method combines exergy analysis with economic analysis. It is a method to evaluate the cost of inefficiencies or the costs of individual process streams, including intermediate and final products.

In exergoeconomic analysis, a specific cost is put on the exergy streams in an exergy balance on a component. After the cost is associated with the exergy streams,

capital and running costs are taken into account. Exergy cost for the streams in any cost rate balance is given as,

$$\dot{C} = c \times E\dot{x} \quad (6.1)$$

where,  $c$  is in Rs/kWh and  $E\dot{x}$  is given in kW. The capital and running costs for the components is given as  $\dot{Z}$  with units as Rs/h.

Typical cost rate balance for a component is given below:

$$\sum \dot{C}_{in} + \dot{W} \times c_{e,in} + \dot{Z} = \sum \dot{C}_{out} + \dot{W} \times c_{e,out} \quad (6.2)$$

For this system a costing analysis is done to estimate the initial capital costs (ICC) and the operating and maintenance costs (OM). An amortization factor is used to amortize the cost of the sum of ICC and OM over 20 years at 5% interest rate. This is given in the equation below (Nafey et al., 2010).

$$A_f = \frac{i(i+1)^n}{(1+i)^{n-1}} \quad (6.3)$$

Total costs for each of the components in the system are needed in Rs/h in order to use them in cost rate balance equations. The initial capital cost and the operating and maintenance costs are added and amortized. The total costs are then divided by the number of hours in a year to get a cost in Rs/h. Operating and maintenance costs are assumed to be a percentage of the initial capital costs. The general equations are as follows,

$$TCC_x = A_f \times (ICC_x + OM_x) \quad (6.4)$$

where  $OM_x$  is given below:

$$OM_x = ICC_x \times OM\% \quad (6.5)$$

Here  $OM\%$  is the percentage of operating and maintenance costs associated with initial capital cost.

$$\dot{Z}_x = \frac{TCC_x}{t_x} \quad (6.6)$$

Costing values and equations of major components of the solar ORC plant are as follows:

**a) Solar field**

Operating & maintenance costs are calculated as,

$$(OM)_{col} = 15\% \times ICC_{col} \quad (6.7)$$

Total capital costs are then evaluated as,

$$TCC_{col} = A_f \times (ICC + OM)_{col} \quad (6.8)$$

$$\dot{Z}_{col} = \frac{(TCC_{col})}{8760} \quad (6.9)$$

**b) Expander**

$$(OM)_{exp} = 25\% \times ICC_{exp} \quad (6.10)$$

$$TCC_{exp} = A_f \times (ICC + OM)_{exp} \quad (6.11)$$

$$\dot{Z}_{exp} = \frac{(TCC)_{exp}}{8760} \quad (6.12)$$

**c) Condenser**

$$(OM)_{cond} = 25\% \times ICC_{cond} \quad (6.13)$$

$$(TCC)_{cond} = A_f \times (ICC + OM)_{cond} \quad (6.14)$$

$$\dot{Z}_{cond} = \frac{(TCC)_{cond}}{8760} \quad (6.15)$$

**d) Pump**

$$(OM)_{pump} = 25\% \times ICC_{pump} \quad (6.16)$$

$$TCC_{pump} = A_f \times (ICC + OM)_{pump} \quad (6.17)$$

$$\dot{Z}_{\text{pump}} = \frac{(\text{TCC})_{\text{pump}}}{8760} \quad (6.18)$$

Exergo-economic optimization of 1 kW<sub>e</sub> solar driven ORC system is performed to determine the minimum cost rate of electricity. Genetic algorithm tool is used to perform the optimization.

The percentages for operating and maintenance costs are taken from Nafey and Sharaf (2010). The initial capital costs (ICC) are calculated and tabulated in Table 14. The cost rate balances for each of the components are done to complete the exergoeconomic analysis.

#### **Solar flat plate collector**

Input fuel cost  $C_f$  is considered as zero for solar flat plate collector. Therefore,  $C_f = 0.0$ .

$$(\text{E}\dot{x}_{\text{in}} \times \dot{C}_f) + (\text{E}\dot{x}_2 \times C_2) + \dot{Z}_{\text{col}} = (\text{E}\dot{x}_3 \times C_3) \quad (6.19)$$

#### **Expander**

$$C_4 = C_3 \times 0.5 \quad (6.20)$$

$$(\text{E}\dot{x}_3 \times C_3) + \dot{Z}_{\text{exp}} = (\dot{W}_e \times C_e) + (\text{E}\dot{x}_4 \times C_4) \quad (6.21)$$

where,  $C_e$  is the electricity cost rate.

The objective function for the exergoeconomic analysis is the electricity cost rate. Evaporator pressure, condensation pressure, hot fluid inlet temperature and degree of superheat are chosen as the independent variables. Bounds for independent variables are selected based on expander limitations and atmospheric constraints. The upper and lower bounds for independent variables involved in genetic algorithm optimization are as follows,

Minimize  $C_e$

Subjected to constraints,

$$5 \leq P \leq 14 \text{ bar for R245fa}$$

$$2 \leq P_{\text{cond}} \leq 4 \text{ bar}$$

$$80 \leq T_i \leq 120 \text{ }^\circ\text{C}$$

$$5 \leq DT_{\text{sup}} \leq 20 \text{ }^\circ\text{C}$$

The input operating conditions and constraints for optimization for each working fluid are mentioned in Table 6.3. GA optimization is carried out using EES. After the constraints and the objective function are defined, the GA tool evaluates the objective function. The iterations continue till it finds the optimal solution.

**Table 6.3:** Upper and lower bounds for GA optimization

<b>Working fluid</b>	<b>R245fa</b>
Population size	64
Stop generation	128
Mutation probability	0.18
Range of evaporator pressure (bar)	5-14
Range of degree of superheat ( $^\circ\text{C}$ )	5-20
Hot water inlet temperature ( $^\circ\text{C}$ )	80-120
Condensation pressure (bar)	2-4

**Table 6.4:** Exergoeconomic optimization results

<b>Parameter</b>	<b>Value</b>	<b>Unit</b>
Electricity cost rate	3.9	Rs/kWh
Degree of superheat	19.6	$^\circ\text{C}$
Evaporator pressure	13.9	bar
Hot water inlet temperature	112	$^\circ\text{C}$
Condensation pressure	2.06	bar
Net work output	1.02	kW
Exergy efficiency	51.08	%
Thermal efficiency	11.54	%

Table 6.4 shows the results of the optimization process. For the given operating range, electricity cost rate of 3.9 Rs/kWh is achieved for an ORC system of 1.02 kW<sub>e</sub> capacity. The results also indicate that, the cost of electricity decreases with increase in evaporator pressure. Minimum electricity cost of Rs 3.9/ kWh was attained at maximum evaporator pressure of 13.9 bar. This is a very competitive price as per the benchmark tariff costs set by the Karnataka electricity board (Rs 3.7/kWh upto 30 kWh, Rs 5.2/kWh for 31-100 kWh, Rs 6.75/kWh for 101-200 kWh and Rs 7.8/kWh above 200 kWh).

## **6.2 Chapter closure**

In this chapter, simple cost analysis was carried out for 1 kW<sub>e</sub> solar ORC system in India based on the market survey and compared with equivalent capacity solar PV system. Moreover, exergo-economic optimization of 1 kW<sub>e</sub> solar ORC system was carried out and optimal parameters for this system were determined at minimum cost of electricity.



## CHAPTER 7

### CONCLUSIONS AND SCOPE OF FUTURE WORK

#### 7.1 Conclusions

This research work mainly focussed on the parametric investigation and off-design simulation of small scale ORC system driven by low grade heat source. A thermodynamic model for ORC system was developed based on laws of mass and energy conservation. Using this model, ORC thermal and exergy efficiencies were evaluated for four different working fluids; R245fa, R123, Isobutane and R134a. Sensitivity analysis was performed using key thermodynamic parameters including expander inlet temperature, expander inlet pressure, condensation temperature and pinch point temperature difference to study its effect on net work output, mass flow rate, thermal and exergy efficiencies. Optimization of the system was also performed using genetic algorithm. The system was optimized to maximize cycle exergy efficiency. This was followed by detailed exergy analysis of ORC components. This analysis identified the location and assessed the magnitude of exergy losses occurring within the ORC power block. Parametric analysis was carried out to investigate the impact of evaporator pressure, condensation pressure, superheat, dead state temperature and pinch point temperature difference on exergy efficiency and irreversibilities in ORC components. Thermo-hydraulic model of plate heat exchanger evaporator was used to study the effect of key thermodynamic and geometric parameters on the size and cost of the evaporator. The model was used to estimate the evaporator area using heat transfer correlations. Parametric investigation of open-drive scroll expander used for micro organic Rankine cycle was carried out using a validated semi-empirical model. A 5 kW<sub>e</sub> expander was used and its built-in volume ratio was 3.5. R245fa was used as the working fluid. Effect of key parameters such as expansion ratio, shaft speed and expander inlet temperature on power output and expander efficiency was evaluated for four different cases. Finally, cost analysis and exergoeconomic optimization of 1 kW<sub>e</sub> driven solar ORC system was

performed to compare the cost of solar ORC with solar PV in India and to determine the minimum electricity cost of solar ORC respectively.

The following conclusions may be drawn from this study.

- Optimization results showed that, expander inlet temperature is close to the upper limit value (75 °C) which was set before the start of GA. Optimized inlet pressure values for each working fluid is the saturation pressure corresponding to expander inlet temperature of 75 °C for all working fluids. The optimal heat source temperature was 90 °C approximately for all working fluids.
- Optimization results also showed that the highest thermal efficiency (7.1%) and exergy efficiency (45.53%) at lowest expander inlet pressure (3.66 bar) was attained with R123. This was followed by R245fa with thermal efficiency of 7.04%, exergy efficiency of 44.98% at expander inlet pressure of 6.07 bar. From the optimization results, it can be inferred that R245fa and R123 are better suited for low temperature ORC applications compared to R134a and Isobutane because of its efficient system performance at lower operating pressures and temperatures. However, R245fa was preferred for this study as it is a zero ODP, non-corrosive, non-flammable fluid and also has a lower specific volume (higher density) compared to R123.
- Sensitivity analysis showed that, expander inlet pressure showed the highest degree of sensitiveness for all working fluids. In the case of R245fa, this was about 70 times greater than that of expander inlet temperature, 3 to 4 times greater than that of condensation temperature and pinch point temperature difference.
- Exergy analysis of 1 kW<sub>e</sub> ORC system showed that, evaporator accounted for the maximum exergy loss which is around 0.446 kW or 19.6% of the inlet exergy. 41% of the total exergy loss occurred in the evaporator followed by expander (26%), exergy rejection to cooling water (24%), condenser (8%) and pump (0.33%). Component exergy analysis showed that evaporator pressure has significant effect on both energy and exergy efficiencies of the ORC. The thermal

efficiency of the cycle increased by 35.71% and the cycle exergy efficiency by 21.86% when evaporator pressure was increased from 7 to 10 bar.

- Thermo-hydraulic model of plate heat exchanger evaporator was used to study the effect of evaporator pressure, pinch point temperature difference and superheat on evaporator area. A reduction of 75.87% in evaporator surface area and decrease of 63.59% in its cost was observed as evaporator pressure was increased from 4 to 10 bar. The maximum net work output of 5 kW was obtained at 6 bar whereas minimum evaporator area of 2.42 m<sup>2</sup> was achieved at evaporator pressure of 10 bar. Heat exchanger area decreased by 89.65% and evaporator cost was reduced by 74.86% when PPTD was increased from 2 to 14 °C. With increase in expander inlet temperature, the area reduced to a minimum value of 6.59 m<sup>2</sup> at expander inlet temperature of 83 °C, and then increased again. Increasing expander inlet temperature by more than 7 °C did not yield any positive results as surface area requirement of the evaporator and cost increases.
- Parametric investigation was performed to study the effect of geometrical parameters including plate width and plate spacing on evaporator area and cost. The trade-off point for plate width was at 0.0065 m, where the evaporator cost was found to be 1166 USD (Rs 87,450) and frictional pressure drop was 2.03 kPa. In case of plate spacing, it was at 0.003 m, where the evaporator cost was 1210 USD (Rs 90,750) and frictional pressure drop was 1.27 kPa.
- At inlet pressure of 14 bar, the efficiency decreased by 12.92% for shaft speed of 2000 rpm and 14.53% for shaft speed of 1500 rpm. At inlet pressure of 10 bar, a peak was observed in efficiency curve for expansion ratio of 4.55 (58%) and 5 (60%) at shaft speeds of 1500 & 2000 rpm respectively. This effect is observed because of under-expansion losses occurring within the expander. Therefore, it can be concluded that, scroll expander should be operated in a range close to its adapted expansion ratio to achieve maximum efficiency.
- Mechanical losses occur mainly within the scroll expander due to friction between the fixed and orbiting scroll. The increase in mass flow rate is not enough to

counter the losses occurring at higher shaft speeds. It was observed from the study that, the expander efficiency witnesses a marginal drop with increase in shaft speed. Power output is reduced due to increase in the losses. Therefore, the expander efficiency decreases. The trend is similar for all curves. The expander efficiency curve for inlet pressure of 10 bar and condensation pressure of 3 bar shows that the curve peaks (54.9%) at shaft speed of 1600 rpm. In other cases, the peak occurs around 2400-2600 rpm.

- Increasing inlet temperature results in the increase in wall temperature. This leads to thermal energy dissipation and deterioration in efficiency of the expander.
- The total cost of 1 kW<sub>e</sub> solar ORC system was estimated at Rs 7,42,500 as per the market survey. However, cost of 1 kW<sub>e</sub> solar PV system costs Rs 85,000 in India which is very competitive. Cost of solar flat plate collector system is around 27% of the total cost and expander cost constitutes around 55.5% of the total cost. Presently, small scale or low capacity expanders are not readily available in India. Therefore, indigenization or local manufacturing of small scale expanders is necessary to achieve economies of scale and reduction in cost.
- Exergo-economic optimization of solar driven ORC system showed that minimum electricity cost (3.9 Rs/kWhr) was attained at maximum evaporator pressure of 13.9 bar.

## 7.2 Scope of future work

- Global model of the organic Rankine cycle should be constructed by interconnecting the various sub-models presented in this work. This can be used to predict the system power output and cycle efficiency.
- Performance investigation of a 1 kW<sub>e</sub> solar driven ORC system should be carried out with experimental trials.

## REFERENCES

- Aboelwafa, O., Fateen, S. K., Soliman, A., and Ismail, I. M. (2018). "A review on solar Rankine cycles : Working fluids , applications , and cycle modifications." 82(July 2017), 868–885.
- Ackermann, T. (2001). "Distributed generation : a definition." 57, 195–204.
- Ahn, Y., Bae, S. J., Kim, M., Cho, S. K., Baik, S., Lee, J. I., and Cha, J. E. (2015). "Review of supercritical CO<sub>2</sub> power cycle technology and current status of research and development." *Nucl. Eng. Technol.*, 47(6), 647–661.
- Ahsan, S., Javed, K., Rana, A. S., and Zeeshan, M. (2016). "Design and cost analysis of 1kW photovoltaic system based on actual performance in Indian scenario." *Perspect. Sci.*, 8, 642–644.
- Al-Sulaiman, F. A., Dincer, I., and Hamdullahpur, F. (2012). "Energy and exergy analyses of a biomass trigeneration system using an organic Rankine cycle." *Energy*, 45(1), 975–985.
- Alshammari, F., Karvountzis-Kontakiotis, A., Pesyridis, A., and Usman, M. (2018). "Expander technologies for automotive engine organic rankine cycle applications." *Energies*, 11(7).
- Altun, A. F., and Kilic, M. (2020). "Thermodynamic performance evaluation of a geothermal ORC power plant." *Renew. Energy*, 148, 261–274.
- Ameri, M., and Jorjani, M. (2016). "Performance assessment and multi-objective optimization of an integrated organic Rankine cycle and multi-effect desalination system." *Desalination*, 392, 34–45.
- Ashouri, M., Ahmadi, M. H., Feidt, M., and Astaraei, F. R. (2017). "Exergy and energy analysis of a regenerative organic Rankine cycle based on flat plate solar collectors." *Mech. Ind.*, 18(2).
- Baldi, F., Larsen, U., and Gabriellii, C. (2015). "Comparison of different procedures for the optimisation of a combined Diesel engine and organic Rankine cycle system based on

ship operational profile.” *Ocean Eng.*, 110(2012), 85–93.

Bao, J., and Zhao, L. (2013). “A review of working fluid and expander selections for organic Rankine cycle.” *Renew. Sustain. Energy Rev.*, 24, 325–342.

Baral, S., and Kim, K. C. (2014). “Thermodynamic Modeling of the Solar Organic Rankine Cycle with Selected Organic Working Fluids for Cogeneration Thermodynamic Modeling of the Solar Organic Rankine Cycle with Selected Organic Working Fluids for Cogeneration.” 3306.

Barse, K. A., and Mann, M. D. (2016). “Maximizing ORC performance with optimal match of working fluid with system design.” *Appl. Therm. Eng.*, 100, 11–19.

Bellos, E., and Tzivanidis, C. (2018). “Investigation of a hybrid ORC driven by waste heat and solar energy.” *Energy Convers. Manag.*, 156(July 2017), 427–439.

Bianchi, M., and Pascale, A. De. (2011). “Bottoming cycles for electric energy generation: Parametric investigation of available and innovative solutions for the exploitation of low and medium temperature heat sources.” *Appl. Energy*, 88(5), 1500–1509.

Boyaghchi, F. A., and Heidarnajad, P. (2015). “Thermoeconomic assessment and multi objective optimization of a solar micro CCHP based on Organic Rankine Cycle for domestic application.” *Energy Convers. Manag.*, 97, 224–234.

Campana, C., Cioccolanti, L., Renzi, M., and Caresana, F. (2019). “Experimental analysis of a small-scale scroll expander for low-temperature waste heat recovery in Organic Rankine Cycle.” *Energy*, 187, 115929.

Chen, H., Goswami, D. Y., and Stefanakos, E. K. (2010). “A review of thermodynamic cycles and working fluids for the conversion of low-grade heat.” *Renew. Sustain. Energy Rev.*, 14(9), 3059–3067.

Cihan, E., and Kavasogullari, B. (2017). “Energy and exergy analysis of a combined refrigeration and waste heat driven organic Rankine cycle system.” *Therm. Sci.*, 21(6), 2621–2631.

- Cioccolanti, L., Tascioni, R., Bocci, E., and Villarini, M. (2018). "Parametric analysis of a solar Organic Rankine Cycle trigeneration system for residential applications." *Energy Convers. Manag.*, 163(March), 407–419.
- Darvish, K., Ehyaei, M. A., Atabi, F., and Rosen, M. A. (2015). "Selection of Optimum Working Fluid for Organic Rankine Cycles by Exergy and Exergy-Economic Analyses." 15362–15383.
- Dewallef, P., Lemort, V., Quoilin, S., and Broek, M. Van Den. (2013). "Techno-economic survey of Organic Rankine Cycle ( ORC ) systems." 22, 168–186.
- Dumont, O. (2017). "Modelling of organic Rankine cycle power systems in off-design conditions : An experimentally-validated comparative study." 123.
- El-Emam, R. S., and Dincer, I. (2013). "Exergy and exergoeconomic analyses and optimization of geothermal organic Rankine cycle." *Appl. Therm. Eng.*, 59(1–2), 435–444.
- Feng, Y., Zhang, Y., Li, B., Yang, J., and Shi, Y. (2015). "Sensitivity analysis and thermoeconomic comparison of ORCs ( organic Rankine cycles ) for low temperature waste heat recovery." *Energy*, 82, 664–677.
- Galloni, E., Fontana, G., and Staccone, S. (2015). "Design and experimental analysis of a mini ORC ( organic Rankine cycle ) power plant based on R245fa working fluid." *Energy*, 90, 768–775.
- Garg, P., Karthik, G. M., Kumar, P., and Kumar, P. (2016). "Development of a generic tool to design scroll expanders for ORC applications." *Appl. Therm. Eng.*, 109, 878–888.
- Garg, P., Kumar, P., and Srinivasan, K. (2013). "Supercritical carbon dioxide Brayton cycle for concentrated solar power." *J. Supercrit. Fluids*, 76, 54–60.
- Ge, Z., Wang, H., Wang, H. T., Wang, J. J., Li, M., Wu, F. Z., and Zhang, S. Y. (2015). "Main parameters optimization of regenerative organic Rankine cycle driven by low-temperature flue gas waste heat." *Energy*, 93, 1886–1895.
- Giuffrida, A. (2014). "Modelling the performance of a scroll expander for small organic

Rankine cycles when changing the working fluid.” *Appl. Therm. Eng.*, 70(1), 1040–1049.

Giuffrida, A. (2018). “A theoretical study on the performance of a scroll expander in an organic Rankine cycle with hydrofluoroolefins (HFOs) in place of R245fa.” *Energy*, 161, 1172–1180.

Han, D. H., Lee, K. J., and Kim, Y. H. (2003). “Experiments on the characteristics of evaporation of R410A in brazed plate heat exchangers with different geometric configurations.” *Appl. Therm. Eng.*, 23(10), 1209–1225.

He, Z., Zhang, Y., Dong, S., Ma, H., Yu, X., and Zhang, Y. (2017). “Thermodynamic analysis of a low-temperature organic Rankine cycle power plant operating at off-design conditions.” *Appl. Therm. Eng.*, 113, 937–951.

Hsieh, Y. Y., and Lin, T. F. (2002). “Saturated flow boiling heat transfer and pressure drop of refrigerant R-410A in a vertical plate heat exchanger.” *Int. J. Heat Mass Transf.*, 45(5), 1033–1044.

Huang, X. Y., Wang, H. Y., Wu, Z., Zhu, T., and Wu, J. Z. (2013). “Selection of working fluids for organic rankine cycle (ORC) in waste heat power generation system.” *ICMREE 2013 - Proc. 2013 Int. Conf. Mater. Renew. Energy Environ.*, 3, 774–779.

IEA, International Renewable Energy Agency, United Nations Statistics Division, The World Bank, and World Health Organization. (2019). “The Energy Progress Report.” *IEA, IRENA, UNSD, WB, WHO (2019), Track. SDG 7 Energy Prog. Rep. 2019, Washingt. DC*, 176.

Imran, M., Agung, N., and Farooq, M. (2017). “Case Studies in Thermal Engineering Thermal and hydraulic optimization of plate heat exchanger using multi objective genetic algorithm.” *Case Stud. Therm. Eng.*, 10(August), 570–578.

Imran, M., Sik, B., Ju, H., Hyun, D., Usman, M., and Heo, M. (2014). “Thermo-economic optimization of Regenerative Organic Rankine Cycle for waste heat recovery applications.” *Energy Convers. Manag.*, 87, 107–118.



- Imran, M., Usman, M., Park, B., Kim, H., and Lee, D. (2015). “Multi-objective optimization of evaporator of organic Rankine cycle ( ORC ) for low temperature geothermal heat source.” *Appl. Therm. Eng.*, 80, 1–9.
- Invernizzi, C., Iora, P., and Silva, P. (2007). “Bottoming micro-Rankine cycles for micro-gas turbines.” *Appl. Therm. Eng.*, 27(1), 100–110.
- Jiang, L., Lu, H. T., Wang, L. W., Gao, P., Zhu, F. Q., Wang, R. Z., and Roskilly, A. P. (2017). “Investigation on a small-scale pumpless Organic Rankine Cycle (ORC) system driven by the low temperature heat source.” *Appl. Energy*, 195, 478–486.
- KAHRAMAN, A., ŞAHİN, R., and ATA, S. (2018). “Energy and exergy analysis of an organic Rankine cycle under different heat source and turbine inlet temperature conditions.” *Int. J. Energy Appl. Technol.*, 5(3), 140–146.
- Karellas, S., and Braimakis, K. (2016). “Energy – exergy analysis and economic investigation of a cogeneration and trigeneration ORC – VCC hybrid system utilizing biomass fuel and solar power.” *Energy Convers. Manag.*, 107, 103–113.
- Kas, Ö. (2014). “Energy and exergy analysis of an organic Rankine for power generation from waste heat recovery in steel industry.” 77, 108–117.
- Kuo, C. R., Hsu, S. W., Chang, K. H., and Wang, C. C. (2011). “Analysis of a 50kW organic Rankine cycle system.” *Energy*, 36(10), 5877–5885.
- Landelle, A., Tauveron, N., Haberschill, P., Revellin, R., and Colasson, S. (2017). “Organic Rankine cycle design and performance comparison based on experimental database.” *Appl. Energy*, 204, 1172–1187.
- Le, V. L., Kheiri, A., Feidt, M., and Pelloux-Prayer, S. (2014). “Thermodynamic and economic optimizations of a waste heat to power plant driven by a subcritical ORC (Organic Rankine Cycle) using pure or zeotropic working fluid.” *Energy*, 78, 622–638.
- Lecompte, S., Oyewunmi, O. A., Markides, C. N., Lazova, M., Kaya, A., Broek, M. Van Den, and Paepe, M. De. (2017). “Case study of an organic Rankine cycle (ORC) for waste heat recovery from an electric arc furnace (EAF).” *Energies*, 10(5), 1–16.

- Lemort, V., Declaye, S., and Quoilin, S. (2011). "Experimental characterization of a hermetic scroll expander for use in a micro-scale Rankine cycle." 126–136.
- Lemort, V., Quoilin, S., Cuevas, C., and Lebrun, J. (2009). "Testing and modeling a scroll expander integrated into an Organic Rankine Cycle." *Appl. Therm. Eng.*, 29(14–15), 3094–3102.
- Li, J., Pei, G., Li, Y., Wang, D., and Ji, J. (2012). "Energetic and exergetic investigation of an organic Rankine cycle at different heat source temperatures." *Energy*, 38(1), 85–95.
- Lin, D., Zhu, Q., and Li, X. (2015). "Thermodynamic Comparative Analyses between (organic) Rankine Cycle and Kalina Cycle." *Energy Procedia*, 75, 1618–1623.
- Liu, H., Shao, Y., and Li, J. (2011). "A biomass-fired micro-scale CHP system with organic Rankine cycle ( ORC ) e Thermodynamic modelling studies." *Biomass and Bioenergy*, 35(9), 3985–3994.
- Ma, Z., Bao, H., and Roskilly, A. P. (2017). "Dynamic modelling and experimental validation of scroll expander for small scale power generation system." *Appl. Energy*, 186, 262–281.
- Maizza, V., and Maizza, A. (2001). "Unconventional working fluids in organic Rankine-cycles for waste energy recovery systems." *Appl. Therm. Eng.*, 21(3), 381–390.
- Mikielewicz, D., and Mikielewicz, J. (2016). "Criteria for selection of working fluid in low-temperature ORC." *Chem. Process Eng. - Inz. Chem. i Proces.*, 37(3), 429–440.
- Mohammadi, A., Ashjari, M. A., and Sadreddini, A. (2018). "Exergy analysis and optimisation of waste heat recovery systems for cement plants." 6451.
- Mohammadi, A., Kasaeian, A., Pourfayaz, F., and Ahmadi, M. H. (2017). "Thermodynamic analysis of a combined gas turbine , ORC cycle and absorption refrigeration for a CCHP system." *Appl. Therm. Eng.*, 111, 397–406.
- Montenegro, G., Torre, A. Della, Fiocco, M., Onorati, A., Benatzky, C., and Schlager, G. (2014). "Evaluating the performance of a rotary vane expander for small scale organic rankine cycles using CFD tools." *Energy Procedia*, 45, 1136–1145.

- Mudasar, R., Aziz, F., and Kim, M. H. (2017). "Thermodynamic analysis of organic Rankine cycle used for flue gases from biogas combustion." *Energy Convers. Manag.*, 153(June), 627–640.
- Muhammad, U., Imran, M., Lee, D. H., and Park, B. S. (2015). "Design and experimental investigation of a 1 kW organic Rankine cycle system using R245fa as working fluid for low-grade waste heat recovery from steam." *Energy Convers. Manag.*, 103, 1089–1100.
- Nafey, A. S., and Sharaf, M. A. (2010). "Combined solar organic Rankine cycle with reverse osmosis desalination process : Energy , exergy , and cost evaluations." *Renew. Energy*, 35(11), 2571–2580.
- Nazari, N., Heidarnejad, P., and Porkhial, S. (2016). "Multi-objective optimization of a combined steam-organic Rankine cycle based on exergy and exergo-economic analysis for waste heat recovery application." *Energy Convers. Manag.*, 127, 366–379.
- Nemati, A., Nami, H., Ranjbar, F., and Yari, M. (2017). "A comparative thermodynamic analysis of ORC and Kalina cycles for waste heat recovery: A case study for CGAM cogeneration system." *Case Stud. Therm. Eng.*, 9, 1–13.
- OECD/IEA. (2018). "Global Energy & CO2 Status Report." *Glob. Energy CO2 Status Rep.*, (March), 1–15.
- Ogriseck, S. (2009). "Integration of Kalina cycle in a combined heat and power plant, a case study." *Appl. Therm. Eng.*, 29(14–15), 2843–2848.
- Oralli, E., Engineering, B., Zamfirescu, C., and Dincer, I. (2011). "A study on scroll compressor conversion into expander for Rankine cycles." (August).
- Oudkerk, J. F., Dickes, R., Dumont, O., and Lemort, V. (2015). "Experimental performance of a piston expander in a small- scale organic Rankine cycle." *IOP Conf. Ser. Mater. Sci. Eng.*, 90(1).
- Papes, I., Degroote, J., and Vierendeels, J. (2015). "New insights in twin screw expander performance for small scale ORC systems from 3D CFD analysis." *Appl. Therm. Eng.*, 91, 535–546.

- Pei, G., Li, J., and Ji, J. (2010). "Analysis of low temperature solar thermal electric generation using regenerative Organic Rankine Cycle." *Appl. Therm. Eng.*, 30(8–9), 998–1004.
- Qiu, G., Liu, H., and Riffat, S. (2011). "Expanders for micro-CHP systems with organic Rankine cycle." *Appl. Therm. Eng.*, 31(16), 3301–3307.
- Qiu, G., Shao, Y., Li, J., Liu, H., and Riffat, S. B. (2012). "Experimental investigation of a biomass-fired ORC-based micro-CHP for domestic applications." *Fuel*, 96, 374–382.
- Quoilin, S., Broek, M. Van Den, Declaye, S., Dewallef, P., and Lemort, V. (2013). "Techno-economic survey of organic rankine cycle (ORC) systems." *Renew. Sustain. Energy Rev.*, 22(October 2014), 168–186.
- Quoilin, S., Declaye, S., Tchanche, B. F., and Lemort, V. (2011). "Thermo-economic optimization of waste heat recovery Organic Rankine Cycles." *Appl. Therm. Eng.*, 31(14–15), 2885–2893.
- Rahbar, K., Mahmoud, S., Al-dadah, R. K., Moazami, N., and Mirhadizadeh, S. A. (2017). "Review of organic Rankine cycle for small-scale applications." *Energy Convers. Manag.*, 134, 135–155.
- Rohmah, N., Pikra, G., Purwanto, A. J., and Pramana, R. I. (2015). "The effect of plate spacing in plate heat exchanger design as a condenser in organic Rankine cycle for low temperature heat source." *Energy Procedia*, 68, 87–96.
- Safarian, S., and Aramoun, F. (2015). "Energy and exergy assessments of modified Organic Rankine Cycles ( ORCs )." *Energy Reports*, 1, 1–7.
- Saleh, B., Koglbauer, G., Wendland, M., and Fischer, J. (2007). "Working fluids for low-temperature organic Rankine cycles." *Energy*, 32(7), 1210–1221.
- Schuster, A., Karellas, S., Kakaras, E., and Spliethoff, H. (2009). "Energetic and economic investigation of Organic Rankine Cycle applications." *Appl. Therm. Eng.*, 29(8–9), 1809–1817.
- Selbas, R., and Yilmaz, F. (2016). "Thermodynamic analyses and sustainability

- assessment of solar-based organic Rankine cycle.” *Int. J. Exergy*, 19(1), 91–109.
- Senturk Acar, M., and Arslan, O. (2019). “Energy and exergy analysis of solar energy-integrated, geothermal energy-powered Organic Rankine Cycle.” *J. Therm. Anal. Calorim.*, 137(2), 659–666.
- Seyedkavoosi, S., Javan, S., and Kota, K. (2017a). “Exergy-based optimization of an organic Rankine cycle ( ORC ) for waste heat recovery from an internal combustion engine ( ICE ).” *Appl. Therm. Eng.*, 126, 447–457.
- Seyedkavoosi, S., Javan, S., and Kota, K. (2017b). “Exergy-based optimization of an organic Rankine cycle (ORC) for waste heat recovery from an internal combustion engine (ICE).” *Appl. Therm. Eng.*, 126, 447–457.
- Shah, R. K. (1983). “Classification of heat exchangers.” ((eds.), Washington, U.S.A., Hemisphere Publishing Corp., 1983, pp.9-14. (ISBN 0-89116-254-2)), 1–77.
- Shen, L., Wang, W., Wu, Y., Lei, B., Zhi, R., Lu, Y., Wang, J., and Ma, C. (2018). “A study of clearance height on the performance of single-screw expanders in small-scale organic Rankine cycles.” *Energy*, 153, 45–55.
- Tchanche, B. F., Lambrinos, G., Frangoudakis, A., and Papadakis, G. (2011). “Low-grade heat conversion into power using organic Rankine cycles – A review of various applications.” *Renew. Sustain. Energy Rev.*, 15(8), 3963–3979.
- United Nations Framework Convention on Climate Change (UNFCCC). (2016). “Report of the Conference of the Parties on COP 21.” *Conf. Parties its twenty-first Sess. (COP 21)*, 01192(January), 1.
- Walraven, D., Laenen, B., and D’Haeseleer, W. (2014). “Comparison of shell-and-tube with plate heat exchangers for the use in low-temperature organic Rankine cycles.” *Energy Convers. Manag.*, 87, 227–237.
- Wang, J., Yan, Z., Wang, M., Ma, S., and Dai, Y. (2013a). “Thermodynamic analysis and optimization of an ( organic Rankine cycle ) ORC using low grade heat source.” *Energy*, 49, 356–365.

- Wang, J., Yan, Z., Zhao, P., and Dai, Y. (2014). "Off-design performance analysis of a solar-powered organic Rankine cycle." *Energy Convers. Manag.*, 80, 150–157.
- Wang, M., Wang, J., Zhao, Y., Zhao, P., and Dai, Y. (2013b). "Thermodynamic analysis and optimization of a solar-driven regenerative organic Rankine cycle (ORC) based on flat-plate solar collectors." *Appl. Therm. Eng.*, 50(1), 816–825.
- Wang, M., Wang, J., Zhao, Y., Zhao, P., and Dai, Y. (2013c). "Thermodynamic analysis and optimization of a solar-driven regenerative organic Rankine cycle ( ORC ) based on flat-plate solar collectors." *Appl. Therm. Eng.*, 50(1), 816–825.
- Wang, Q., Wu, W., and He, Z. (2019). "Thermodynamic analysis and optimization of a novel organic Rankine cycle-based micro-scale cogeneration system using biomass fuel." *Energy Convers. Manag.*, 198(July), 111803.
- Wei, D., Lu, X., Lu, Z., and Gu, J. (2007). "Performance analysis and optimization of organic Rankine cycle (ORC) for waste heat recovery." *Energy Convers. Manag.*, 48(4), 1113–1119.
- Wu, Z., Pan, D., Gao, N., Zhu, T., and Xie, F. (2015). "Experimental testing and numerical simulation of scroll expander in a small scale organic Rankine cycle system." *Appl. Therm. Eng.*, 87, 529–537.
- Xi, H., Li, M. J., Xu, C., and He, Y. L. (2013). "Parametric optimization of regenerative organic Rankine cycle (ORC) for low grade waste heat recovery using genetic algorithm." *Energy*, 58, 473–482.
- Yang, J., Sun, Z., Yu, B., and Chen, J. (2018). "Modeling and optimization criteria of scroll expander integrated into organic Rankine cycle for comparison of R1233zd ( E ) as an alternative to." 141(June), 386–393.
- Zhang, X., Wu, L., Wang, X., and Ju, G. (2016). "Comparative study of waste heat steam SRC, ORC and S-ORC power generation systems in medium-low temperature." *Appl. Therm. Eng.*, 106, 1427–1439.
- Zhao, Y., Liu, G., Li, L., Yang, Q., Tang, B., and Liu, Y. (2019). "Expansion devices for

organic Rankine cycle (ORC) using in low temperature heat recovery: A review.” *Energy Convers. Manag.*, 199(April), 111944.

Ziviani, D., James, N. A., Accorsi, F. A., Braun, J. E., and Groll, E. A. (2018).

“Experimental and numerical analyses of a 5 kWe oil-free open-drive scroll expander for small-scale organic Rankine cycle ( ORC ) applications.” *Appl. Energy*, 230(January), 1140–1156.

## Appendix A

### MATHEMATICAL MODELLING CODE

#### A.1 Mathematical code to calculate energy and exergy efficiency of the ORC cycle using R245fa as the working fluid

##### Inputs

WF1\$ = 'R245fa'

WF2\$ = 'water'

P1 = 400000

P2 = 300000

P3 = 120000

PP<sub>cd</sub> = 5

PP<sub>ev</sub> = 5

DT<sub>sup</sub> = 5

M<sub>3</sub> = 0.248

T<sub>wf, in</sub> = 40

T<sub>cw, in</sub> = 27

T<sub>hf, in</sub> = 100

M<sub>2</sub> = 0.7

##### Thermodynamic properties

T<sub>wf, in</sub> = T [WF1\$, P = P<sub>cd</sub>, x = 0]

T<sub>sup</sub> = T<sub>sat, v</sub> + DT<sub>sup</sub>

T<sub>wf, out</sub> = T<sub>sup</sub>

T<sub>sat, v</sub> = T [WF1\$, P = P1, x = 1]

T<sub>sat, l</sub> = T [WF1\$, P = P1, x = 0]

h<sub>sat, l</sub> = h [WF1\$, T = T<sub>sat, l</sub>, x = 0]

h<sub>sat, v</sub> = h [WF1\$, T = T<sub>sat, v</sub>, x = 1]

h<sub>sup, v</sub> = h [WF1\$, T = T<sub>sup</sub>, P = P1]



$$h_{wf,in} = h [\text{WF1}\$, P = P_1, T = T_{wf,in}]$$

$$CP_{hf} = C_p [\text{WF2}\$, P = P_2, T = T_{hf,in}]$$

### Energy balance in evaporator

$$[T_{cor,sat,l} - T_{hf,out}] \cdot CP_{hf} \cdot M_2 = [h_{sat,l} - h_{wf,in}] \cdot M_1$$

$$[T_{hf,in} - T_{hf,out}] \cdot CP_{hf} \cdot M_2 = [h_{sup,v} - h_{wf,in}] \cdot M_1$$

$$[T_{hf,in} - T_{cor,sat,v}] \cdot CP_{hf} \cdot M_2 = [h_{sup,v} - h_{sat,v}] \cdot M_1$$

### Evaporator & Condenser pinch point temperature difference

$$PP_{ev} = T_{cor,sat,l} - T_{sat,l}$$

$$PP_{cd} = T_{wf,in} - T_{cor,sat,cd}$$

### Energy balance in condenser

$$CP_{cw} = CP(\text{WF2}\$, T = T_{cw,in}, P = P_3)$$

$$[T_{cw,out} - T_{cw,in}] \cdot CP_{cw} \cdot M_3 = [h_4 - h_1] \cdot M_1$$

### ORC efficiency calculations

#### Parameters

$$\eta_t = 0.8$$

$$\eta_p = 0.8$$

#### Evaporator

$$h_3 = h_{sup,v}$$

$$s_3 = s [\text{WF1}\$, T = T_{sup}, P = P_1]$$

#### Expander

$$s_{4id} = s_3$$

$$h_{4id} = h [\text{WF1}\$, P = P_{cd}, s = s_{4id}]$$

$$h_4 = h_3 - [h_3 - h_{4id}] \cdot \eta_t$$

$$s_4 = s [\text{WF1}\$, h = h_4, P = P_{cd}]$$

#### Condenser

$$h_1 = h [\text{WF1}\$, P = P_{cd}, x = 0]$$

$$s_1 = s [\text{WF1}\$, P = P_{cd}, x = 0]$$

## Pump

$$s_{2id} = s_1$$

$$h_{2id} = h [\text{WF1\$}, P = P_1, s = s_{2id}]$$

$$h_2 = h_1 + [(h_{2id} - h_1) / \eta_p]$$

$$s_2 = s [\text{WF1\$}, h = h_2, P = P_1]$$

## Thermal Efficiency

$$w_t = h_3 - h_4$$

$$w_p = h_2 - h_1$$

$$w_{net} = M_1 \cdot [w_t - w_p]$$

$$q_{in} = M_1 \cdot [h_3 - h_2]$$

$$\eta_{th} = w_{net} / q_{in}$$

## Inputs for exergy analysis

$$T_o = 25$$

$$T = T_o + 273$$

$$P_o = 101300$$

$$h_{o,orc} = h [\text{WF1\$}, T = T_o, P = P_o]$$

$$s_{o,orc} = s [\text{WF1\$}, T = T_o, P = P_o]$$

$$h_o = h [\text{WF2\$}, T = T_o, P = P_o]$$

$$s_o = s [\text{WF2\$}, T = T_o, P = P_o]$$

## Evaporator exergy analysis

$$E_3 = M_1 \cdot [h_3 - h_{o,orc} - T \cdot (s_3 - s_{o,orc})]$$

$$E_2 = M_1 \cdot [h_2 - h_{o,orc} - T \cdot (s_2 - s_{o,orc})]$$

$$h_5 = h [\text{WF2\$}, T = T_{hf,in}, P = P_2]$$

$$s_5 = s [\text{WF2\$}, T = T_{hf,in}, P = P_2]$$

$$h_6 = h [\text{WF2\$}, T = T_{hf,out}, P = 120000]$$

$$s_6 = s [\text{WF2\$}, T = T_{hf,out}, P = 120000]$$

$$E_5 = M_2 \cdot [h_5 - h_o - T \cdot (s_5 - s_o)]$$

$$E_6 = M_2 \cdot [h_6 - h_o - T \cdot (s_6 - s_o)]$$

$$\eta_{\text{exg, evp}} = (E_3 - E_2) / (E_5 - E_6)$$

### **Working fluid pump exergy analysis**

$$E_1 = M_1 \cdot [h_1 - h_{o, \text{orc}} - T \cdot (s_1 - s_{o, \text{orc}})]$$

$$\eta_{\text{exg, pump}} = (E_2 - E_1) / (M_1 \cdot w_p)$$

### **Expander exergy analysis**

$$E_4 = M_1 \cdot [h_4 - h_{o, \text{orc}} - T \cdot (s_4 - s_{o, \text{orc}})]$$

$$\eta_{\text{exg, t}} = (M_1 \cdot w_t) / (E_3 - E_4)$$

### **Condenser exergy analysis**

$$M_1 \cdot [h_4 - h_1] = M_3 \cdot [h_8 - h_7]$$

$$h_7 = h [\text{WF2\$}, T = T_{\text{cw, in}}, P = P_3]$$

$$s_7 = s [\text{WF2\$}, T = T_{\text{cw, in}}, P = P_3]$$

$$s_8 = s [\text{WF2\$}, h = h_8, P = 120000]$$

$$E_7 = M_3 \cdot [h_7 - h_o - T \cdot (s_7 - s_o)]$$

$$E_8 = M_3 \cdot [h_8 - h_o - T \cdot (s_8 - s_o)]$$

$$\eta_{\text{exg, cond}} = (E_8 - E_7) / (E_4 - E_1)$$

### **Irreversibility/exergy destruction**

$$I_{\text{evp}} = (E_5 - E_6) - (E_3 - E_2)$$

$$I_{\text{cond}} = (E_7 - E_8) - (E_1 - E_4)$$

$$I_{\text{pump}} = E_1 + (M_1 \cdot w_p) - E_2$$

$$I_{\text{expander}} = E_3 - E_4 + M_1 \cdot w_t$$

$$I_{\text{total}} = I_{\text{evp}} + I_{\text{cond}} + I_{\text{pump}} + I_{\text{expander}}$$

### **Overall exergy efficiency**

$$E_{\text{in}} = M_2 \cdot [h_5 - h_6 - T \cdot (s_5 - s_6)]$$

$$\eta_{\text{exg}} = w_{\text{net}} / E_{\text{in}}$$

## **A.2 Mathematical code of plate heat exchanger evaporator to estimate the surface area of the heat exchanger using Han Lee Kim correlations**

Procedure evaporatorpd (WF\_1\$, WF\_2\$, T\_wf\_in, T\_hf\_in, P1, P2, PP, DT\_sup, M[2], G[1] : A\_ev, M[1], T\_wf\_out, T\_hf\_out, DP[1..2], M)

### **"Initialize pressure drop"**

Duplicate i= 1, 20

DP\_in[i] =0

End

### **"Iterate till pressure drops converge"**

Call evaporator (WF\_1\$, WF\_2\$, DP\_in[1..20], T\_wf\_in, T\_hf\_in, P1, P2, PP, DT\_sup, M[2], G[1] : A\_ev, M[1], T\_wf\_out,

T\_hf\_out, DP[1], DP[2], DP\_II[1..20,1], M)

{Repeat

DP\_ev\_old [1] = DP [1]

CALL evaporator (WF\_1\$, WF\_2\$, DP\_II[1..20,1], T\_wf\_in, T\_hf\_in, P1, P2, PP, DT\_sup, M[2] : A\_ev, M[1], T\_wf\_out,

T\_hf\_out, DP [1], DP [2], DP\_II [1...20, 1])

until (abs(DP\_ev\_old[1]-DP[1])<100)}

End

Subprogram evaporator (WF\_1\$, WF\_2\$, DP\_in[1..20,1], T\_wf\_in, T\_hf\_in, P1, P2, PP, DT\_sup[2], G[1] : A\_tot, M[1],

T\_wf\_out, T\_hf\_out, DP\_tot [1], DP\_tot [2], DP\_cum[1..20,1], M)

### **"Input model parameters"**

#### **"Width of heat exchanger"**

n[2]\*j[2]=n[1]\*j[1]

#### **"Hydraulic diameter"**

b = 0.007

w = 0.5

$$D_h = (2 * b * w) / (w + b)$$

**"Geometric parameters"**

$$\text{Beta} = \pi/4$$

$$p_{\text{co}} = 0.007$$

**"Number of paths and passes of plate heat exchanger"**

$$n [1] = 1$$

$$n [2] = 1$$

$$j [1] = 1$$

$$M = n [2]$$

$$j [2] = 1$$

**"Thickness of plate"**

$$\text{delta} = 0.0005$$

**"Thermal conductivity of plate"**

$$\text{lambda}_p = 13.56$$

**"Fouling factors"**

$$Rf_1 = 0$$

$$Rf_2 = 0$$

**"Number of segments in evaporation zone"**

$$N = 20$$

**"Overall heat transfer coefficient in zone I and zone III"**

$$1/U_1 = 1/\alpha_{1\_I} [2] + 1/\alpha_{1\_I} [1] + \text{delta}/\text{lambda}_p + Rf_1 + Rf_2$$

$$1/U_{III} = 1/\alpha_{1\_III} [2] + 1/\alpha_{1\_III} [1] + \text{delta}/\text{lambda}_p + Rf_1 + Rf_2$$

**"Temperature and enthalpy ZONE I and ZONE III"**

$$T_{\text{sup}} = T_{\text{sat\_v}} + DT_{\text{sup}}$$

$$T_{\text{wf\_out}} = T_{\text{sup}}$$

$$T_{\text{sat\_1}} = \text{temperature} (\text{WF}_1, P=P1, x=0)$$

$$T_{\text{sat\_v}} = T_{\text{out}} [1]$$

$h_{sat\_l} = \text{enthalpy}(\text{WF\_1}, T=T_{sat\_l}, x=0)$   
 $h_{sat\_v} = \text{enthalpy}(\text{WF\_1}, T=T_{sat\_v}, x=1)$   
 $h_{sup\_v} = \text{enthalpy}(\text{WF\_1}, T=T_{sup}, P=P1-DP\_in[N,1])$   
 $h_{wf\_in} = \text{enthalpy}(\text{WF\_1}, P=P1, T=T_{wf\_in})$   
 $CP\_hf = \text{cp}(\text{WF\_2}, P=P2, T=T_{hf\_in})$

**"Energy balance in zone I and zone III"**

$(T_{corresp\_sat\_l}-T_{hf\_out}) * CP\_hf * M[2] = (h_{sat\_l}-h_{wf\_in}) * M[1]$   
 $(T_{hf\_in}-T_{corresp\_sat\_v}) * CP\_hf * M[2] = (h_{sup\_v}-h_{sat\_v}) * M[1]$   
 $(T_{hf\_in}-T_{hf\_out}) * CP\_hf * M[2] = (h_{sup\_v}-h_{wf\_in}) * M[1]$

**"LMTD zone I and zone III"**

$Arg\_I * (T_{corresp\_sat\_l}-T_{sat\_l}) = (T_{hf\_out}-T_{wf\_in})$   
 $Q\_I = (T_{corresp\_sat\_l}-T_{hf\_out}) * CP\_hf * M[2]$   
 $Q\_I = U\_I * A\_I * ((T_{hf\_out}-T_{wf\_in}) - (T_{corresp\_sat\_l}-T_{sat\_l})) / \ln(Arg\_I)$   
 $Arg\_III * (T_{hf\_in}-T_{sup}) = (T_{corresp\_sat\_v}-T_{sat\_v})$   
 $Q\_III = (T_{hf\_in}-T_{corresp\_sat\_v}) * CP\_hf * M[2]$   
 $Q\_III = U\_III * A\_III * ((T_{corresp\_sat\_v}-T_{sat\_v}) - (T_{hf\_in}-T_{sup})) / \ln(Arg\_III)$

**"Velocities zone I"**

$u_{I[1]} = M[1] / \rho_{I[1]} / (n[1] * w * De/2)$   
 $G_{I[1]} = u_{I[1]} * \rho_{I[1]}$   
 $Re_{I[1]} = De * u_{I[1]} / \nu_{I[1]}$   
 $u_{I[2]} = M[2] / \rho_{I[2]} / (n[2] * w * De/2)$   
 $G_{I[2]} = u_{I[2]} * \rho_{I[2]}$   
 $Re_{I[2]} = De * u_{I[2]} / \nu_{I[2]}$

**"Correlations of heat transfer fluid and working fluid in zone I"**

**"Properties of working fluid"**

$T_{avg\_I[1]} = (T_{wf\_in} + T_{sat\_l}) / 2$   
 $P_{avg\_I[1]} = P1$

**"Thermal conductivity"**

$$\lambda_{I[1]} = \text{conductivity}(\text{WF}_1, T=T_{\text{avg}_I[1]}, P=P_{\text{avg}_I[1]})$$

**"Dynamic viscosity"**

$$\mu_{I[1]} = \text{viscosity}(\text{WF}_1, T=T_{\text{avg}_I[1]}, P=P_{\text{avg}_I[1]})$$

$$\mu_{w_I[1]} = \mu_{I[1]}$$

**"Density"**

$$\rho_{I[1]} = \text{density}(\text{WF}_1, T=T_{\text{avg}_I[1]}, P=P_{\text{avg}_I[1]})$$

**"Heat capacity"**

$$c_{p_I[1]} = \text{cp}(\text{WF}_1, T=T_{\text{avg}_I[1]}, P=P_{\text{avg}_I[1]})$$

**"Kinematic viscosity"**

$$\nu_{I[1]} = \mu_{I[1]}/\rho_{I[1]}$$

**"Prandtl number"**

$$\text{Pr}_{I[1]} = c_{p_I[1]}*\mu_{I[1]}/\lambda_{I[1]}$$

**"Properties of heating fluid"**

$$T_{\text{avg}_I[2]} = (T_{\text{hf\_out}} + T_{\text{corresp\_sat}_1})/2$$

$$P_{\text{avg}_I[2]} = P_2$$

**"Thermal conductivity"**

$$\lambda_{I[2]} = \text{conductivity}(\text{WF}_2, T=T_{\text{avg}_I[2]}, P=P_{\text{avg}_I[2]})$$

**"Dynamic viscosity"**

$$\mu_{I[2]} = \text{viscosity}(\text{WF}_2, T=T_{\text{avg}_I[2]}, P=P_{\text{avg}_I[2]})$$

$$\mu_{w_I[2]} = \mu_{I[1]}$$

**"Density"**

$$\rho_{I[2]} = \text{density}(\text{WF}_2, T=T_{\text{avg}_I[2]}, P=P_{\text{avg}_I[2]})$$

**"Heat capacity"**

$$c_{p_I[2]} = \text{cp}(\text{WF}_2, T=T_{\text{avg}_I[2]}, P=P_{\text{avg}_I[2]})$$

### **"Kinematic viscosity"**

$$\nu_{I[2]} = \mu_{I[2]}/\rho_{I[2]}$$

### **"Prandtl number"**

$$\text{Pr}_{I[2]} = c_{p_{I[2]}}*\mu_{I[2]}/\lambda_{I[2]}$$

$$f_{I[1]} = 0.572*\text{Re}_{I[1]}^{(-0.217)}$$

$$\text{DP}_{I[1]} = 2*f_{I[1]}*l_{I[1]}*G_{I[1]}^2/(De*\rho_{I[1]})$$

$$\alpha_{1_{I[1]}}=0.2092*(\lambda_{I[1]}/De)*\text{Re}_{I[1]}^{0.78}*\text{Pr}_{I[1]}^{(1/3)}*(\mu_{I[1]}/\mu_{w_{I[1]}})^{(0.14)}$$

$$l_{I[1]} = A_{I[1]}/(n_{I[1]}*w)$$

$$f_{I[2]} = 0.572*\text{Re}_{I[2]}^{(-0.217)}$$

$$\text{DP}_{I[2]} = 2*f_{I[2]}*l_{I[2]}*G_{I[2]}^2/(De*\rho_{I[2]})$$

$$\alpha_{1_{I[2]}}=0.1876*(\lambda_{I[2]}/De)*\text{Re}_{I[2]}^{0.7179}*\text{Pr}_{I[2]}^{(1/3)}*(\mu_{I[2]}/\mu_{w_{I[2]}})^{(0.17)}$$

$$l_{I[2]} = A_{I[2]}/(n_{I[2]}*w)$$

### **"Velocities zone III"**

$$u_{III[1]} = M_{I[1]}/\rho_{III[1]}/(n_{I[1]}*w*De/2)$$

$$G_{III[1]} = u_{III[1]}*\rho_{III[1]}$$

$$\text{Re}_{III[1]} = De*u_{III[1]}/\nu_{III[1]}$$

$$u_{III[2]} = M_{I[2]}/\rho_{III[2]}/(n_{I[2]}*w*De/2)$$

$$G_{III[2]} = u_{III[2]}*\rho_{III[2]}$$

$$\text{Re}_{III[2]} = De*u_{III[2]}/\nu_{III[2]}$$

### **"Correlations of heat transfer fluid and working fluid in zone III"**

#### **"Properties of working fluid"**

$$T_{\text{avg}_{III[1]}} = (T_{\text{sup}} + T_{\text{sat}_v})/2$$

$$P_{\text{avg}_{III[1]}} = P_1$$

#### **"Conductivity"**

$$\lambda_{III[1]} = \text{conductivity}(\text{WF}_1, T=T_{\text{avg}_{III[1]}}, P=P_{\text{avg}_{III[1]}})$$



**"Dynamic viscosity"**

$$\mu_{III}[1] = \text{viscosity}(\text{WF}_1, T=T_{\text{avg\_III}}[1], P=P_{\text{avg\_III}}[1])$$

$$\mu_{w\_III}[1] = \mu_{III}[1]$$

**"Density"**

$$\rho_{III}[1] = \text{density}(\text{WF}_1, T=T_{\text{avg\_III}}[1], P=P_{\text{avg\_III}}[1])$$

**"Heat capacity"**

$$c_{p\_III}[1] = \text{cp}(\text{WF}_1, T=T_{\text{avg\_III}}[1], P=P_{\text{avg\_III}}[1])$$

**"Kinematic viscosity"**

$$\nu_{III}[1] = \mu_{III}[1]/\rho_{III}[1]$$

**"Prandtl number"**

$$\text{Pr}_{III}[1] = c_{p\_III}[1]*\mu_{III}[1]/\lambda_{III}[1]$$

**"Properties of heating fluid"**

$$T_{\text{avg\_III}}[2] = (T_{\text{hf\_in}}+T_{\text{corresp\_sat\_v}})/2$$

$$P_{\text{avg\_III}}[2] = P_2$$

**"Thermal conductivity"**

$$\lambda_{III}[2] = \text{conductivity}(\text{WF}_2, T=T_{\text{avg\_III}}[2], P=P_{\text{avg\_III}}[2])$$

**"Dynamic viscosity"**

$$\mu_{III}[2] = \text{viscosity}(\text{WF}_2, T=T_{\text{avg\_III}}[2], P=P_{\text{avg\_III}}[2])$$

$$\mu_{w\_III}[2] = \mu_{III}[2]$$

**"Density"**

$$\rho_{III}[2] = \text{density}(\text{WF}_2, T=T_{\text{avg\_III}}[2], P=P_{\text{avg\_III}}[2])$$

**"Heat capacity"**

$$c_{p\_III}[2] = \text{cp}(\text{WF}_2, T=T_{\text{avg\_III}}[2], P=P_{\text{avg\_III}}[2])$$

**"Kinematic viscosity"**

$$\nu_{III}[2] = \mu_{III}[2]/\rho_{III}[2]$$

**"Prandtl number"**

$$\text{Pr\_III [2]} = \text{cp\_III [2]} * \text{mu\_III [2]} / \text{lambda\_III [2]}$$

$$\text{f\_III [1]} = 0.572 * \text{Re\_III [1]}^{(-0.217)}$$

$$\text{DP\_III [1]} = 2 * \text{f\_III [1]} * \text{l\_III [1]} * \text{G\_III [1]}^2 / (\text{De} * \text{rho\_III [1]})$$

$$\text{alpha\_1\_III [1]} = 0.2092 * (\text{lambda\_III [1]} / \text{De}) * \text{Re\_III [1]}^{0.78} * \text{Pr\_III [1]}^{(1/3)} * (\text{mu\_III [1]} / \text{mu\_w\_III [1]})^{(0.14)}$$

$$\text{l\_III [1]} = \text{A\_III} / (\text{n [1]} * \text{w})$$

$$\text{f\_III [2]} = 0.572 * \text{Re\_III [2]}^{(-0.217)}$$

$$\text{DP\_III [2]} = 2 * \text{f\_III [2]} * \text{l\_III [2]} * \text{G\_III [2]}^2 / (\text{De} * \text{rho\_III [2]})$$

$$\text{alpha\_1\_III [2]} = 0.1876 * (\text{lambda\_III [2]} / \text{De}) * \text{Re\_III [2]}^{0.7179} * \text{Pr\_III [2]}^{(1/3)} * (\text{mu\_III [2]} / \text{mu\_w\_III [2]})^{(0.17)}$$

$$\text{l\_III [2]} = \text{A\_III} / (\text{n [2]} * \text{w})$$

### **"Discretized model in zone II"**

#### **"Inlet and outlet temperatures"**

$$\text{T\_in [1]} = \text{temperature (WF\_1$, P=P1, x=0)}$$

$$\text{T\_out [1]} = \text{temperature (WF\_1$, P=P1-DP\_in[N,1], x=1)}$$

$$\text{T\_avg [1]} = (\text{T\_in [1]} + \text{T\_out [1]}) / 2$$

$$\text{T\_in [2]} = \text{T\_corresp\_sat\_v}$$

#### **"Pinch point temperature difference"**

$$\text{PP} = \text{T\_out [2]} - \text{T\_in [1]}$$

#### **"Calculation of enthalpy"**

$$\text{h[N,1]} = \text{enthalpy(WF\_1$, P=P1-DP\_in[N,1], x=1)}$$

$$\text{h[1,1]} = \text{enthalpy(WF\_1$, P=P1, x=0)}$$

$$\text{h[1,2]} = \text{enthalpy(WF\_2$, T=T\_in[2], P=P2)}$$

$$\text{h[N,2]} = \text{enthalpy(WF\_2$, T=T\_out[2], P=P2)}$$

$$\text{i\_fg} = \text{h[N,1]} - \text{h[1,1]}$$

$$\text{Q\_II} = \text{i\_fg} * \text{M [1]}$$

$$\text{Q\_II} = (\text{h[1,2]} - \text{h[N,2]}) * \text{M [2]}$$

### **"Discretization"**

$DH = (h[N,1] - h[1,1]) / (N-1)$   $T[1,1] = T\_in[1]$   
 $T[N,1] = T\_out[1]$   
 $T[1,2] = T\_in[2]$   
 $T[N,2] = T\_out[2]$   
 $x[1,1] = 0$   
 $x[N,1] = 1$   
 $x[1,2] = \text{quality}(\text{WF\_2\$}, h=h[1,2], P=P2)$   
 $x[N,2] = \text{quality}(\text{WF\_2\$}, h=h[N,2], P=P2)$   
 $s[1,1] = \text{entropy}(\text{WF\_1\$}, p = P1, x=0)$   
 $s[N,1] = \text{entropy}(\text{WF\_1\$}, P=P1-DP\_in[N,1], x=1)$   
 $s[1,2] = \text{entropy}(\text{WF\_2\$}, p = P1, h=h[1,2])$   
 $s[N,2] = \text{entropy}(\text{WF\_2\$}, P=P1, h=h[N,2])$   
Duplicate l=1, N-2  
 $h[l+1,1] = h[l,1] + DH$  "calculation of enthalpy in the next segment"  
 $T[l+1,1] = \text{temperature}(\text{WF\_1\$}, h=h[l+1,1], P=P1-DP\_in[l+1,1])$   
 $T[l+1,2] = \text{temperature}(\text{WF\_2\$}, h=h[l+1,2], P=P2)$   
 $s[l+1,1] = \text{entropy}(\text{WF\_1\$}, h=h[l+1,1], P=P1-DP\_in[l+1,1])$   
 $h[l+1,2] = h[l,2] - (Q[l] / M[2])$   
 $s[l+1,2] = \text{entropy}(\text{WF\_2\$}, h=h[l+1,2], P=P2)$   
 $x[l+1,1] = \text{quality}(\text{WF\_1\$}, h=h[l+1,1], P=P1-DP\_in[l+1,1])$   
 $x[l+1,2] = \text{quality}(\text{WF\_2\$}, h=h[l+1,2], P=P2)$   
End  
 $Q\_cum [1] = 0$   
Duplicate i=1, N-1  
 $Q[i] = (h[i+1,1] - h[i,1]) * M[1]$   
 $Q\_cum [i+1] = Q[i] + Q\_cum[i]$   
**"Calculation of LMTD"**  
 $Argg[i] = (T [i+1, 2] - T [N-i, 1])$   
 $Arg[i] = (T [i, 2] - T [N-i+1, 1]) / Argg[i]$

$$\text{LMTD}[i] = ((T[i,2]-T[N-i+1,1])-(T[i+1,2]-T[N-i,1]))/\ln(\text{Arg}[i])$$

End

$$\text{Arg} = (T[1,2]-T[N,1])/(T[N,2]-T[1,1])$$

$$\text{LMTD\_overall} = ((T[1,2]-T[N,1])-(T[N,2]-T[1,1]))/\ln(\text{Arg})$$

### **"Correlations and properties"**

$$u [1] = M [1]/\rho_{f[1,1]}/(n[1]*w*D_h/2)$$

$$G [1] = u[1]*\rho_{f[1,1]}$$

$$u [2] = M[2]/\rho_{\text{avg}[1,2]}/(n[2]*w*D_h/2)$$

$$G [2] = u[2]*\rho_{\text{avg}[1,2]}$$

### **"Evaporation heat transfer and pressure drop: Han, Lee and Kim correlation"**

$$Ge\_1[1] = 2.81*(p\_co/De)^{-0.041}*(\pi/2-\beta)^{-2.83}$$

$$Ge\_2[1] = 0.746*(p\_co/De)^{-0.082}*(\pi/2-\beta)^{0.61}$$

$$Ge\_3[1] = 64710*(p\_co/De)^{-5.27}*(\pi/2-\beta)^{-3.03}$$

$$Ge\_4[1] = -1.314*(p\_co/De)^{-0.62}*(\pi/2-\beta)^{-0.47}$$

### **"Segment length and heat transfer surface area"**

$$A\_cum [1] = 0$$

$$jl\_cum [1, 1] = 0$$

$$jl\_cum [1, 2] = 0$$

$$DP\_cum [1, 1] = 0$$

$$DP\_cum[1, 2] = 0$$

Duplicate i=1, N-1

### **"Properties of heat transfer fluid"**

#### **"Thermal conductivity"**

$$\lambda_{\text{avg}} [i, 2] = \text{conductivity} (\text{WF\_2}, T=(T[i,2]+T[i+1,2])/2, P=P2)$$

#### **"Dynamic viscosity"**

$$\mu_{\text{avg}} [i, 2] = \text{viscosity} (\text{WF\_2}, T= (T[i,2]+T[i+1,2])/2, P=P2)$$

$$\mu_{w\_avg} [i, 2] = \mu_{\text{avg}} [i,2]$$

**"Density"**

$$\rho_{\text{avg}} [i, 2] = \text{density} (\text{WF\_2\$}, T = (T [i, 2] + T [i+1, 2]) / 2, P = P2)$$

**"Heat capacity"**

$$c_{p, \text{avg}} [i, 2] = \text{cp} (\text{WF\_2\$}, T = (T [i, 2] + T [i+1, 2]) / 2, P = P2)$$

**"Kinematic viscosity"**

$$\nu_{\text{avg}} [i, 2] = \mu_{\text{avg}} [i, 2] / \rho_{\text{avg}} [i, 2]$$

**"Prandtl number"**

$$Pr_{\text{avg}} [i, 2] = c_{p, \text{avg}} [i, 2] * \mu_{\text{avg}} [i, 2] / \lambda_{\text{avg}} [i, 2]$$

$$Re [i, 2] = De * u [2] / \nu_{\text{avg}} [i, 2]$$

$$\alpha_l [i, 2] = 0.1876 * (\lambda_{\text{avg}} [i, 2] / De) * Re [i, 2]^{0.7179} * Pr_{\text{avg}} [i, 2]^{(1/3)} * (\mu_{\text{avg}} [i, 2] / \mu_{w, \text{avg}} [i, 2])^{(0.17)}$$

$$f [i, 2] = 0.572 * Re [i, 2]^{(-0.217)}$$

$$DP [i, 2] = 2 * f [i, 2] * l [i, 2] * G [2]^2 / (De * \rho_{\text{avg}} [i, 2])$$

$$DP_{\text{cum}} [i+1, 2] = DP_{\text{cum}} [i, 2] + DP [i, 2]$$

**"Properties of working fluid"****"Density"**

$$\rho_f [i, 1] = \text{density} (\text{WF\_1\$}, P = P1, x = 0)$$

$$\rho_g [i, 1] = \text{density} (\text{WF\_1\$}, P = P1, x = 1)$$

**"Equivalent mass velocity"**

$$x_{\text{avg}} [i, 1] = (x [i, 1] + x [i+1, 1]) / 2$$

$$G_{\text{eq}} [i, 1] = G [1] * (1 - x_{\text{avg}} [i, 1] + x_{\text{avg}} [i, 1] * (\rho_f [i, 1] / \rho_g [i, 1])^{(1/2)})$$

**"Dynamic viscosity"**

$$\mu_1 [i, 1] = \text{viscosity} (\text{WF\_1\$}, P = P1, x = 0)$$

**"Heat capacity"**

$$c_{p, I} [i, 1] = \text{cp} (\text{WF\_1\$}, P = P1, x = 0)$$

**"Equivalent Reynolds number"**

$$Re_{\text{eq}} [i, 1] = G_{\text{eq}} [i, 1] * De / \mu_1 [i, 1]$$

**"Equivalent Boiling number"**

$$Bo\_eq [i, 1] = (Q[i]/A[i]) / (i\_fg * G\_eq [i, 1])$$

**"Conductivity"**

$$lambda\_l [i, 1] = \text{conductivity (WF\_1$, P=P1, x=0)}$$

**"Prandtl number"**

$$Pr [i,1] = cp\_l[i,1] * mu\_l[i,1] / lambda\_l[i,1]$$

**"Evaporation heat transfer and pressure drop correlation: Han, Lee and Kim"**

$$Nu[i,1] = Ge\_1[1] * Re\_eq[i,1]^{(Ge\_2[1])} * Bo\_eq[i,1]^{(0.3)} * Pr[i,1]^{(0.4)}$$

$$alpha\_t\_HLK [i, 1] = Nu [i, 1] * lambda\_l[i,1] / De$$

**"Local heat transfer, LMTD correlation"**

$$A[i] = (Q[i] / (LMTD[i] * Fc)) * (1 / alpha\_t\_HLK[i,1] + 1 / alpha\_l[i,2] + delta / lambda\_p + Rf\_1 + Rf\_2)$$

**"Calculate heat flux"**

$$\text{heatflux [i]} = Q[i] / A[i]$$

**"Calculate cumulative area"**

$$A\_cum [i+1] = A[i] + A\_cum[i]$$

**"Calculate section length"**

$$j[1] * l[i,1] = A[i] / (n[1] * w)$$

$$jl\_cum [i+1,1] = j[1] * l[i,1] + jl\_cum[i,1]$$

$$j [2] * l[i,2] = A[i] / (n[2] * w)$$

$$jl\_cum [i+1, 2] = j[2] * l[i,2] + jl\_cum[i,2]$$

**"Pressure drop correlation: Han, Lee, Kim"**

$$f [i,1] = Ge\_3[1] * Re\_eq[i,1]^{Ge\_4[1]}$$

$$DP[i,1] = f[i,1] * j[1] * l[i,1] * G\_eq[i,1]^2 / (De * rho\_f[i,1])$$

$$DP\_cum [i+1, 1] = DP\_cum [i, 1] + DP [i, 1]$$

End

$$A\_II = A\_cum [N]$$

DP\_II [1] = DP\_cum [N, 1]

DP\_II [2] = DP\_cum [N, 2]

**"Calculate total heat transfer area and pressure drops"**

A\_tot = A\_I + A\_II + A\_III

Q\_tot = Q\_I + Q\_II + Q\_III

DP\_tot [1] = DP\_I [1] + DP\_II [1] + DP\_III [1]

DP\_tot [2] = DP\_I [2] + DP\_II [2] + DP\_III[2]

Evp\_cost = 310 + (160 \* A\_tot) **"USD"**

**"Inputs"**

WF\_1\$ = 'R245fa'

WF\_2\$ = 'water'

P1=5.77e5

P2 = 3e5

PP=5

M [2] = 0.7

T\_hf\_in = 100

T\_wf\_in = 40

G [1] =20

**"Call model"**

Call evaporatorpd(WF\_1\$, WF\_2\$,T\_wf\_in, T\_hf\_in, P1, P2, PP, 5, M[2], G[1] : A\_ev,

M[1],T\_wf\_out, T\_hf\_out, DP[1..2],M)

### A.3 Mathematical code for semi-empirical model of open-drive scroll expander

#### MODULE

Expander(fluid\$,V\_s\_cp,r\_v\_in,A\_leak,AU\_su\_exp\_n,AU\_ex\_exp\_n,M\_dot\_r\_nom,T\_m,AU\_amb\_exp,d\_thr\_su,M\_dot\_r\_exp,N\_rot\_exp,t\_amb\_exp,t\_amb,p\_r\_ex\_exp,t\_r\_su\_exp,t\_r\_ex\_exp,p\_r\_su\_exp,W\_dot\_sh\_exp,epsilon\_s\_exp)

#### "Expander characteristics"

$V_{s\_exp} = V_{s\_cp} / r_{v\_in}$

#### "Supply expander"

$t_{r\_sat\_su\_exp} = T_{sat}(fluid$, P=P_{r\_su\_exp})$

$DELTA T_{oh\_su\_exp} = T_{r\_su\_exp} - T_{r\_sat\_su\_exp}$

$r_{p\_exp} = P_{r\_su\_exp} / P_{r\_ex\_exp}$

$h_{r\_su\_exp} = enthalpy(fluid$, P=P_{r\_su\_exp}, T=t_{r\_su\_exp})$

$s_{r\_su\_exp} = entropy(fluid$, P=P_{r\_su\_exp}, T=t_{r\_su\_exp})$

$v_{r\_su\_exp} = volume(fluid$, P=P_{r\_su\_exp}, T=t_{r\_su\_exp})$

#### "Supply pressure drop"

$A_{thr\_su} = PI * d_{thr\_su}^2 / 4$

$h_{r\_su\_exp} = h_{thr\_su} + C_{thr\_su}^2 / 2$

$V_{dot\_thr\_su} = A_{thr\_su} * C_{thr\_su}$

$M_{dot\_r\_exp} = V_{dot\_thr\_su} / v_{r\_su\_exp}$

$DELTA P_{r\_su\_exp} = C_{thr\_su}^2 / (v_{r\_su\_exp}^2)$

$P_{r\_su1\_exp} = P_{r\_su\_exp} - DELTA P_{r\_su\_exp}$

#### "Supply cooling down"

$C_{dot\_su\_exp} = M_{dot\_r\_exp} * cp_{r\_su\_exp}$

$cp_{r\_su\_exp} = CP(fluid$, P=P_{r\_su1\_exp}, T=t_{r\_su\_exp})$

$NTU_{su\_exp} = AU_{su\_exp} / C_{dot\_su\_exp}$

$AU_{su\_exp} = AU_{su\_exp\_n} * (M_{dot\_r\_exp} / M_{dot\_r\_nom})^{0.6}$

$epsilon_{su\_exp} = 1 - exp(-NTU_{su\_exp})$

$Q_{dot\_r\_wall\_su\_exp} = epsilon_{su\_exp} * C_{dot\_su\_exp} * (t_{r\_su\_exp} - t_{wall\_exp})$



$Q_{\dot{r}_{wall\_su\_exp}} = C_{\dot{su\_exp}} * (t_{r\_su\_exp} - t_{r\_su1\_exp})$   
 $h_{r\_su1\_exp} = \text{enthalpy}(\text{fluid}\$, P = P_{r\_su1\_exp}, T = t_{r\_su1\_exp})$   
 $s_{r\_su1\_exp} = \text{entropy}(\text{fluid}\$, P = P_{r\_su1\_exp}, T = t_{r\_su1\_exp})$   
 $v_{r\_su1\_exp} = \text{volume}(\text{fluid}\$, P = P_{r\_su1\_exp}, T = t_{r\_su1\_exp})$

**"Isentropic expansion up to the adapted pressure"**

$r_{v\_in} = v_{r\_in\_exp} / v_{r\_su1\_exp}$   
 $P_{r\_in\_exp} = \text{pressure}(\text{fluid}\$, v = v_{r\_in\_exp}, s = s_{r\_su1\_exp})$   
 $h_{r\_in\_exp} = \text{enthalpy}(\text{fluid}\$, v = v_{r\_in\_exp}, P = P_{r\_in\_exp})$   
 $w_{exp\_1} = h_{r\_su1\_exp} - h_{r\_in\_exp}$   
 $r_{p\_in} = P_{r\_su1\_exp} / P_{r\_in\_exp}$

**"Isochoric expansion from adapted pressure to exhaust pressure"**

$w_{exp\_2} = v_{r\_in\_exp} * (P_{r\_in\_exp} - P_{r\_ex\_exp})$

**"total work"**

$w_{in\_exp} = w_{exp\_1} + w_{exp\_2}$   
 $w_{in\_exp} = h_{r\_su1\_exp} - h_{r\_ex2\_exp}$

**"Power"**

$W_{\dot{in\_exp}} = M_{\dot{r\_in\_exp}} * w_{in\_exp}$

**"Leakage flow rate"**

$h_{r\_su1\_exp} = h_{r\_thr} + C_{thr}^2 / 2$   
 $P_{r\_su1\_exp} * v_{r\_su1\_exp}^{\gamma_r} = P_{r\_thr} * v_{r\_thr}^{\gamma_r}$   
 $r = 8314 / MM_r$   
 $MM_r = \text{molarmass}(\text{fluid}\$)$   
 $P_{r\_crit} = P_{r\_su1\_exp} * (2 / (\gamma_r + 1))^{\gamma_r / (\gamma_r - 1)}$   
 $P_{r\_thr} = P_{r\_crit}$   
 $h_{r\_thr} = \text{enthalpy}(\text{fluid}\$, P = P_{r\_thr}, s = s_{r\_su1\_exp})$   
 $t_{r\_thr} = \text{temperature}(\text{fluid}\$, h = h_{r\_thr}, P = P_{r\_thr})$   
 $C_{thr\_bis} = \sqrt{\gamma_r * r * (t_{r\_thr} + 273)}$   
 $t_{r\_thr\_bis} = t_{r\_su1\_exp} * 2 / (\gamma_r + 1)$

$$M_{\dot{r}_{leak\_exp}} = A_{leak} * C_{thr} / v_{r\_thr}$$

$$v_{r\_thr} = \text{volume}(\text{fluid}\$, P = P_{r\_thr}, h = h_{r\_thr})$$

**“Mass flow rate”**

$$V_{\dot{s}_{exp}} = N_{rot\_exp} / 60 * V_{s\_exp}$$

$$M_{\dot{r}_{in\_exp}} = V_{\dot{s}_{exp}} / v_{r\_sul\_exp}$$

$$M_{\dot{r}_{exp}} = M_{\dot{r}_{in\_exp}} + M_{\dot{r}_{leak\_exp}}$$

**“Mixing with leakage at exhaust”**

$$M_{\dot{r}_{in\_exp}} * h_{r\_ex2\_exp} + M_{\dot{r}_{leak\_exp}} * h_{r\_sul\_exp} = M_{\dot{r}_{exp}} * h_{r\_ex1\_exp}$$

$$h_{r\_ex1\_exp} = \text{enthalpy}(\text{fluid}\$, T = t_{r\_ex1\_exp}, P = P_{r\_ex\_exp})$$

**“Exhaust cooling down”**

$$cp_{r\_ex\_exp} = CP(\text{fluid}\$, P = P_{r\_ex\_exp}, T = t_{r\_ex1\_exp})$$

$$C_{\dot{ex\_exp}} = M_{\dot{r}_{exp}} * cp_{r\_ex\_exp}$$

$$NTU_{ex\_exp} = AU_{ex\_exp} / C_{\dot{ex\_exp}}$$

$$AU_{ex\_exp} = AU_{ex\_exp\_n} * (M_{\dot{r}_{exp}} / M_{\dot{r}_{nom}})^{0.6}$$

$$\epsilon_{ex\_exp} = 1 - \exp(-NTU_{ex\_exp})$$

$$Q_{\dot{r}_{wall\_ex\_exp}} = \epsilon_{ex\_exp} * C_{\dot{ex\_exp}} * (t_{r\_ex1\_exp} - t_{wall\_exp})$$

$$Q_{\dot{r}_{wall\_ex\_exp}} = C_{\dot{ex\_exp}} * (t_{r\_ex1\_exp} - t_{r\_ex\_exp})$$

$$h_{r\_ex\_exp} = \text{enthalpy}(\text{fluid}\$, P = P_{r\_ex\_exp}, T = t_{r\_ex\_exp})$$

**“Power”**

$$W_{\dot{sh\_exp}} = W_{\dot{in\_exp}} - W_{\dot{loss\_exp}}$$

$$W_{\dot{loss\_exp}} = 2 * \pi * N_{rot\_exp} / 60 * T$$

**“Heat balance over the expander”**

$$Q_{\dot{exp\_amb}} = AU_{amb\_exp} * (t_{wall\_exp} - t_{amb\_exp})$$

$$Q_{\dot{r}_{wall\_su\_exp}} + Q_{\dot{r}_{wall\_ex\_exp}} + W_{\dot{loss\_exp}} - Q_{\dot{exp\_amb}} = 0$$

**“Global isentropic effectiveness”**

$$W_{\dot{sh\_exp\_s}} = M_{\dot{r}_{exp}} * w_{in\_exp\_s}$$

```
w_in_exp_s=h_r_su_exp-h_r_ex_exp_s
h_r_ex_exp_s=enthalpy (fluid$,P=P_r_ex_exp,s=s_r_su_exp)
epsilon_s_exp=W_dot_sh_exp/W_dot_sh_exp_s

END "expander"
```

### **"Inputs"**

```
V_s_cp=V_s_cp_cm3/1000000
V_s_exp=V_s_cp/r_v_in
V_s_exp=V_s_exp_cm3/1000000
```

### **"Call Model"**

```
CALL
expander(fluid$,V_s_cp,r_v_in,A_leak,AU_su_exp_n,AU_ex_exp_n,M_dot_r_exp_n,T_
m,AU_amb_exp,d_su,M_dot_r_exp,N_rot_exp,t_amb_exp,t_amb_exp,p_r_ex_exp,t_r_s
u_exp,t_r_ex_exp,p_r_su_exp,W_dot_sh_exp,epsilon_s_exp)
```

#### A.4 Mathematical code for exergoeconomic optimization of solar driven ORC system

**// Inputs //**

WF\_1\$ = 'R245fa'

WF\_2\$ = 'water'

P2= 2e5

PP\_ev = 5

M[2] =0.3

**// Temperature and enthalpy ZONE I and ZONE III //**

T\_wf\_in = temperature(WF\_1\$, P=P\_cd, x=0)

T\_sup = T\_sat\_v + DT\_sup

T\_wf\_out = T\_sup

T\_sat\_v = temperature(WF\_1\$, P=P1, x=1)

T\_sat\_l = temperature(WF\_1\$, P=P1, x=0)

h\_sat\_l = enthalpy(WF\_1\$, T=T\_sat\_l, x=0)

h\_sat\_v = enthalpy(WF\_1\$, T=T\_sat\_v, x=1)

h\_sup\_v =enthalpy(WF\_1\$, T=T\_sup, P=P1)

h\_wf\_in = enthalpy(WF\_1\$, P=P1, T=T\_wf\_in)

CP\_hf = Cp(WF\_2\$, P=P2, T=T\_hf\_in)

**// Mass and energy balance//**

$(T\_corresp\_sat\_l - T\_hf\_out) * CP\_hf * M[2] = (h\_sat\_l - h\_wf\_in) * M[1]$

$(T\_hf\_in - T\_hf\_out) * CP\_hf * M[2] = (h\_sup\_v - h\_wf\_in) * M[1]$

$$(T_{hf\_in} - T_{corresp\_sat\_v}) * CP_{hf} * M[2] = (h_{sup\_v} - h_{sat\_v}) * M[1]$$

**// Evaporator & Condenser pinch //**

$$PP_{ev} = T_{corresp\_sat\_1} - T_{sat\_1}$$

**// ORC efficiency calculations //**

**// Parameters //**

$$\eta_t = 0.8$$

$$\eta_p = 0.8$$

**// Evaporator //**

$$h[3] = h_{sup\_v}$$

$$s[3] = \text{entropy}(\text{WF}_1, T=T_{sup}, P=P_1)$$

**// Expander //**

$$s_{4id} = s[3]$$

$$h_{4id} = \text{enthalpy}(\text{WF}_1, P=P_{cd}, s=s_{4id})$$

$$h[4] = h[3] - ((h[3] - h_{4id}) * \eta_t)$$

$$s[4] = \text{entropy}(\text{WF}_1, h=h[4], P=P_{cd})$$

**// Condenser //**

$$h[1] = \text{enthalpy}(\text{WF}_1, P=P_{cd}, x=0)$$

$$s[1] = \text{entropy}(\text{WF}_1, P=P_{cd}, x=0)$$

**// Pump //**

$$s_{2id} = s[1]$$

$$h_{2id} = \text{enthalpy}(\text{WF}_1, P=P_1, s=s_{2id})$$

$$h[2] = h[1] + ((h_{2id} - h[1]) / \eta_p)$$

```

s[2] = entropy(WF_1$, h=h[2], P= P1)

// Thermal Efficiency //

w_t= h[3] - h[4]

w_p= h[2] - h[1]

w_net= M[1] * (w_t - w_p)

q_in = M[1] * (h[3]- h[2])

eta_th= w_net/q_in

// Inputs for exergy analysis //

T_o = 25

T = T_o + 273

P_o = 1.013e5

h_o_orc = enthalpy (WF_1$, T=T_o, P = P_o)

s_o_orc = entropy (WF_1$, T=T_o, P = P_o)

h_o = enthalpy (WF_2$, T=T_o, P = P_o)

s_o = entropy (WF_2$, T=T_o, P = P_o)

Ex_dot_in = (1 - (T)/(T_hf_in+273)) * q_in

// Evp exergy analysis //

Ex_dot_2 + Ex_dot_in = Ex_dot_3 + Ex_dot_d_evap

ex_2 = (h[2] - h_o) - (T*(s[2] - s_o))

Ex_dot_2 = M[1] * ex_2

// Expander exergy analysis //

Ex_dot_3 = Ex_dot_4 + (M[1] * w_t) + Ex_dot_d_exp

```

```

ex_3 = (h[3] - h_o) - (T*(s[3] - s_o))

Ex_dot_3 = M[1] * ex_3

// Condenser exergy analysis //

Ex_dot_4 = Ex_dot_1 + Ex_dot_d_cond

ex_4 = (h[4] - h_o) - (T*(s[4] - s_o))

Ex_dot_4 = M[1] * ex_4

// Pump exergy analysis //

Ex_dot_1 + (M[1] * w_p) = Ex_dot_2 + Ex_dot_d_pump

ex_1 = (h[1] - h_o) - (T*(s[1] - s_o))

Ex_dot_1 = M[1] * ex_1

// Exergoeconomic Analysis //

n_sys = 20

i = 0.05

Am = (i*(1+i)^n_sys)/((1+i)^(n_sys-1))

// Expander Costs //

OM% = 0.25

ICC_exp = 412500

OM_exp = ICC_exp*OM%

TCC_exp = Am*(ICC_exp+OM_exp)

t_exp = 365*24

Z_dot_exp = (TCC_exp+TCC_cond+TCC_p)/t_exp

```

**// Heat Exchanger Costs //**

$$\text{ICC}_b = 250000$$

$$\text{OM\%}_b = 0.25$$

$$\text{OM}_b = \text{OM\%}_b * \text{ICC}_b$$

$$\text{TCC}_b = \text{Am} * (\text{ICC}_b + \text{OM}_b)$$

$$t_b = t_{\text{exp}}$$

$$Z_{\text{dot}}_b = \text{TCC}_b / t_b$$

**// Condenser Costs //**

$$t_{\text{cond}} = t_b$$

$$\text{ICC}_{\text{cond}} = 50000$$

$$\text{OM\%}_{\text{cond}} = 0.25$$

$$\text{OM}_{\text{cond}} = \text{OM\%}_{\text{cond}} * \text{ICC}_{\text{cond}}$$

$$\text{TCC}_{\text{cond}} = \text{Am} * (\text{ICC}_{\text{cond}} + \text{OM}_{\text{cond}})$$

$$Z_{\text{dot}}_{\text{cond}} = \text{TCC}_{\text{cond}} / t_{\text{cond}}$$

**// Pump Costs //**

$$t_p = t_b$$

$$\text{ICC}_p = 30000$$

$$\text{OM\%}_p = 0.25$$

$$\text{OM}_p = \text{OM\%}_p * \text{ICC}_p$$

$$\text{TCC}_p = \text{Am} * (\text{ICC}_p + \text{OM}_p)$$

$$Z_{\text{dot}}_p = \text{TCC}_p / t_p$$



**// Evaporator cost rate balance //**

$$c_f = 0$$

$$(Ex\_dot\_in * c_f) + (Ex\_dot\_2 * c_2) + Z\_dot\_b = Ex\_dot\_3 * c_3$$

**// Expander cost rate balance //**

$$c_4 = c_3 * 0.5$$

$$(Ex\_dot\_3 * c_3) + Z\_dot\_exp = C\_dot\_e + (c_4 * Ex\_dot\_4)$$

$$C\_dot\_e = ((M[1] * w_t) * c_e)$$

$$c_2 = 0$$

## LIST OF PUBLICATIONS

### 1. Journal publications

a) **Suhas Upadhyaya** and Veershetty Gumtapure (2019). “Parametric analysis and thermodynamic optimization of organic Rankine cycle for low grade waste heat recovery”, *Indian Journal of environment protection*, 39 (6): 556-567.

b) **Suhas Upadhyaya** and Veershetty Gumtapure (2019). “Parametric Investigation of Organic Rankine Evaporator for Low Temperature Applications”, *The Journal of Engineering Research (TJER)*, 16 (2): 130-141.

c) **Suhas Upadhyaya** and Veershetty Gumtapure (2021). “Parametric investigation of open-drive scroll expander for micro organic Rankine cycle applications”, *Journal of thermal engineering*. (Accepted for publication).

d) **Suhas Upadhyaya** and Veershetty Gumtapure (2021). “Exergoeconomic optimization of low temperature solar driven organic Rankine cycle”, *Thermal Engineering* (Accepted for publication).

e) **Suhas Upadhyaya** and Veershetty Gumtapure (2021). “Energy and Exergy analysis of a mini Organic Rankine Cycle system using R245fa as the working fluid”, *Energy sources, Part A: Recovery, Utilization and environmental effects* (Under review).

### 2. Conference proceedings/Symposium

a) **Suhas Upadhyaya** and Veershetty Gumtapure (2017). “Simulation of solar ORC system for small scale power generation”, *6<sup>th</sup> International Engineering Symposium - IES 2017 March 1-3, Kumamoto University, Japan*.

b) **Suhas Upadhyaya** and Veershetty Gumtapure. (2018). “Thermodynamic analysis of organic Rankine cycle with Hydrofluoroethers as working fluids”, *Proceedings of Icon MMEE, 2018, Mangalore Institute of Technology and Engineering, March 2-3, 2018, IOP Conf. Series: Materials Science and Engineering*, 376, 012026: 1-8.

## BIODATA

**NAME:** SUHAS UPADHYAYA

**DATE OF BIRTH:** 07-09-1987

**Mobile No.:** +91 8971269718

**Email:** suhas.upa@gmail.com

**ADDRESS:**

2-140/18, SUJAY, REGENT PARK, HOSABETTU,  
MANGALORE, KARNATAKA-575019



### EDUCATIONAL QUALIFICATION:

Examination	Board/Institute	Academic Year	Percentage/ CGPA
Ph. D (course work)	National Institute of Technology Karnataka, Surathkal	2015-2016	7.69
M. Tech (Thermal Engg.)	National Institute of Technology Karnataka, Surathkal	2010-2012	7.64
B.E. (Mechanical Engg)	National Institute of Engineering, Mysore	2005-2009	69%

### INDUSTRIAL EXPERIENCE:

Name of the company/industry	Designation	From	To
GMR Kamalanga Energy Ltd (GKEL), 3 x 350 MW thermal power plant, Angul, Odisha	Executive Engineer, Mechanical Maintenance dept	September 2012	March 2015